Photochemistry and diffusion in Jupiter's stratosphere: Constraints from ISO observations and comparisons with other giant planets

Julianne I. Moses, Thierry Fouchet, Bruno Bézard, G. Randall Gladstone, Emmanuel Lellouch, Helmut Feuchtgruber

Photochemistry and diffusion in Jupiter's stratosphere: Constraints from ISO observations and comparisons with other giant planets

J. I. Moses,[1] T. Fouchet,[2,3] B. Bézard,[2] G. R. Gladstone,[4] E. Lellouch,[2] and H. Feuchtgruber[5]

Received 1 February 2005; revised 9 May 2005; accepted 18 May 2005; published 4 August 2005.

[1] We have developed a one-dimensional, diurnally averaged, photochemical model for Jupiter's stratosphere that couples photodissociation, chemical kinetics, vertical diffusion, and radiative transport. The predictions regarding the abundances and vertical profiles of hydrocarbon compounds are compared with observations from the Infrared Space Observatory (ISO) to better constrain the atmospheric composition, to better define the eddy diffusion coefficient profile, and to better understand the chemical reaction schemes that produce and destroy the observed constituents. From model-data comparisons we determine that the C_2H_6 mole fraction on Jupiter is $(4.0 \pm 1.0) \times 10^{-6}$ at 3.5 mbar and $(2.7 \pm 0.7) \times 10^{-6}$ at 7 mbar, and the C_2H_2 mole fraction is $(1.4 \pm 0.8) \times 10^{-6}$ at 0.25 mbar and $(1.5 \pm 0.4) \times 10^{-7}$ at 2 mbar. The column densities of CH_3C_2H and C_6H_6 are $(1.5 \pm 0.4) \times 10^{15}$ cm^{-2} and $(8.0 \pm 2) \times 10^{14}$ cm^{-2}, respectively, above 30 mbar. Using identical reaction lists, we also have developed photochemical models for Saturn, Uranus, and Neptune. Although the models provide good first-order predictions of hydrocarbon abundances on the giant planets, our current chemical reaction schemes do not reproduce the relative abundances of C_2H_x hydrocarbons. Unsaturated hydrocarbons like C_2H_4 and C_2H_2 appear to be converted to saturated hydrocarbons like C_2H_6 more effectively on Jupiter than on the other giant planets, more effectively than is predicted by the models. Further progress in our understanding of photochemistry at low temperatures and low pressures in hydrogen-dominated atmospheres hinges on the acquisition of high-quality kinetics data.

Citation: Moses, J. I., T. Fouchet, B. Bézard, G. R. Gladstone, E. Lellouch, and H. Feuchtgruber (2005), Photochemistry and diffusion in Jupiter's stratosphere: Constraints from ISO observations and comparisons with other giant planets, *J. Geophys. Res.*, *110*, E08001, doi:10.1029/2005JE002411.

1. Introduction

[2] Although the Jovian stratosphere is composed largely of hydrogen, helium, and methane, infrared spectra from the planet exhibit numerous emission features due to higher-order hydrocarbons. Trace amounts of these heavier hydrocarbons are produced from the photolysis of methane in Jupiter's upper stratosphere. The hydrocarbon photochemical products eventually diffuse downward into the deep troposphere, where they encounter high temperatures and are converted back into methane. Although our qualitative understanding of Jovian hydrocarbon photochemistry goes back decades (see the reviews of *Strobel* [1975, 1983], *Atreya* [1986], *Yung and DeMore* [1999], and *Moses et al.* [2004]), a detailed quantitative understanding is lacking. Photochemical models to date have not always done a good job of reproducing all the observed hydrocarbon abundances [see *Lebonnois*, 2005; *Lee et al.*, 2000; *Wong et al.*, 2000; *Gladstone et al.*, 1996; *Romani*, 1996; *Allen et al.*, 1992; *Landry et al.*, 1991; *West et al.*, 1986; *Strobel*, 1969, 1973, 1983; *Yung and Strobel*, 1980; *Atreya and Donahue*, 1979; *Prasad et al.*, 1975; *Hunten*, 1969; C. A. Nixon et al., Meridional variations of C_2H_2 and C_2H_6 in Jupiter's atmosphere from Cassini CIRS infrared spectra, submitted to *Icarus*, 2005 (hereinafter referred to as Nixon et al., submitted manuscript, 2005)], especially if one takes into account the new high-quality observational constraints provided by ISO, the Infrared Space Observatory (ISO was an ESA project with instruments funded by ESA Member States (especially the PI countries: France, Germany, the Netherlands, and the United Kingdom) with the participation of NASA and ISAS.) [e.g., *Encrenaz et al.*, 1996, 1999; *Drossart et al.*, 1999; *Feuchtgruber et al.*, 1999; *Fouchet et al.*, 2000b; *Bézard et al.*, 2001b; *Lellouch et al.*, 2001; *Encrenaz*, 2003]. Information about the

[1]Lunar and Planetary Institute, Houston, Texas, USA.
[2]LESIA, Observatoire de Paris, Meudon, France.
[3]Université Paris 6, Paris, France.
[4]Space Sciences Department, Southwest Research Institute, San Antonio, Texas, USA.
[5]Max-Planck-Institut für Extraterrestrische Physik, Garching, Germany.

0148-0227/05/2005JE002411

latitudinal variation of C_2H_2 and C_2H_6 has now also been supplied by the Composite Infrared Spectrometer (CIRS) during the Cassini Jupiter flyby [*Kunde et al.*, 2004; Nixon et al., submitted manuscript, 2005]. Recent advances in our knowledge of the stratospheric temperature profile, stratospheric molecular abundances, species distribution with altitude and latitude, chemical reaction rate coefficients, ultraviolet absorption cross sections, and photolysis quantum yields have provided important new model constraints and input parameters, and updated models of Jovian stratospheric photochemistry are needed in order to explain the observed composition.

[3] Observations of stratospheric constituents generally have centered around ethane (C_2H_6) and acetylene (C_2H_2), the most abundant hydrocarbon photochemical products [e.g., *Moses et al.*, 2004]. Using ISO data, *Fouchet et al.* [2000b] were able to derive information about the altitude distribution of ethane and acetylene; such information is very useful for constraining photochemical reaction schemes and eddy diffusion coefficients in Jupiter's stratosphere. Along with these two species, observers using the Short-Wavelength Spectrometer (SWS) of the ISO satellite have detected methylacetylene (CH_3C_2H) [*Fouchet et al.*, 2000b] and benzene (C_6H_6) [*Bézard et al.*, 2001b] for the first time in non-auroral observations. ISO data also show evidence for stratospheric CO_2 and H_2O, indicating that oxygen is being introduced to Jupiter's upper atmosphere from external sources [*Feuchtgruber et al.*, 1997, 1999; *Moses et al.*, 2000b; *Lellouch et al.*, 2002] (see also the ground-based infrared CO observations of *Bézard et al.* [2002a]). The oxygen-bearing molecules can slightly influence hydrocarbon photochemistry [e.g., *Moses et al.*, 2000b] and can provide useful constraints on eddy diffusion coefficients in Jupiter's stratosphere [*Bézard et al.*, 2002a; *Lellouch et al.*, 2002; *Moreno et al.*, 2003]. In addition, the extensive wavelength coverage of the ISO-SWS data facilitates the derivation of stratospheric temperatures [*Drossart et al.*, 1999; *Fouchet et al.*, 2000b; *Lellouch et al.*, 2001], allowing a less ambiguous determination of molecular abundances.

[4] We use the observational constraints provided by ISO, along with recent C_2H_4 observations [*Bézard et al.*, 2001a, 2002b; P. N. Romani et al., Temporally varying ethylene on Jupiter, submitted to *Icarus*, 2005], to construct a new one-dimensional steady-state model of Jovian stratospheric photochemistry. The model includes coupled hydrocarbon and oxygen photochemistry, vertical eddy and molecular diffusion, and radiative transport (including multiple Rayleigh scattering by H_2, He, and CH_4). The comprehensive Jupiter study of *Gladstone et al.* [1996] and Saturn study of *Moses et al.* [2000a, 2000b] form the basis for our model, but the rate coefficients and some reaction pathways have been completely revamped on the basis of new laboratory and theoretical determinations. In the following sections, we discuss the details of the photochemical model, examine the previous observations that have been used to constrain the eddy diffusion coefficient profile in Jupiter's stratosphere, and compare the model results with ISO and other Earth-based and spacecraft data. Because the ISO-SWS observations do not provide information about hydrocarbon abundances at the methane homopause (with the exception of the CH_4 ν_3 band fluorescence analysis of *Drossart et al.* [1999]), we also examine how our models compare with H and He ultraviolet emission data [e.g., *Broadfoot et al.*, 1981; *McConnell et al.*, 1981; *Skinner et al.*, 1988; *Shemansky and Judge*, 1988; *Ben Jaffel et al.*, 1993; *Vervack et al.*, 1995; *Gladstone et al.*, 1995] and with the results from the α Leo occultation recorded by the Voyager Ultraviolet Spectrometer (UVS) [e.g., *Festou et al.*, 1981; *Yelle et al.*, 1996]. The implications of the model-data comparisons with respect to Jovian stratospheric chemistry and the eddy diffusion coefficient profile will be discussed in detail. The photochemical models will also be applied to Saturn, Uranus, and Neptune and the results compared with observations. Although we were successful in reproducing the observed abundances of C_2H_2, C_2H_6, and some of the other hydrocarbons for Jupiter with a single reaction list, not all the hydrocarbon abundances were well reproduced, and the same reaction list did not always provide the best fit to observations from the other giant planets. While the one-dimensional nature of the model and/or the spatial and temporal variability of the data sets may be partly at fault, it is clear from our comparisons of the model with observations from all the giant planets that our understanding of hydrocarbon photochemistry at conditions relevant to the outer planets is still incomplete. We will indicate what future observations, laboratory measurements, and/or theoretical calculations may be needed to improve our understanding of the chemical processes occurring in Jupiter's stratosphere.

2. Photochemical Model Inputs

[5] To determine the distribution of chemical constituents in Jupiter's atmosphere, we use the Caltech/JPL chemical kinetics and diffusion code [e.g., *Gladstone et al.*, 1996; *Yung et al.*, 1984; *Allen et al.*, 1981] to solve the coupled one-dimensional continuity equations. The solutions to the coupled equations are allowed to reach steady state, and the chemical production and loss terms are diurnally averaged. Eddy and molecular diffusion are considered in the transport terms. The temperature-pressure profile adopted for our 30°N latitude vernal equinox models is shown in Figure 1. At pressures greater than $\sim$1 mbar, the temperatures are derived from infrared observations from ISO [*Lellouch et al.*, 2001]. At pressures less than $\sim 10^{-3}$ mbar, the temperature profile is a smoothed version of that derived from the ASI experiment on the Galileo entry probe [*Seiff et al.*, 1998]. Between 1 mbar and 10^{-3} mbar, the temperatures are assumed to be roughly isothermal until they gradually connect with the smoothed ASI profile at high altitudes. Note that our resulting profile is warmer than the Galileo ASI profile in the upper stratosphere. We also assume that the atmosphere is in hydrostatic equilibrium, with pressure, temperature, altitude, density, mean molecular mass, and other atmospheric parameters of interest given in auxiliary material Table S1[1]. The molecular and thermal diffusion coefficients used in the model are described by *Moses et al.* [2000a]. The eddy diffusion coefficient profile is one of the

[1]Supporting material is available via Web browser or via Anonymous FTP from ftp://ftp.agu.org/apend/" (Username = "anonymous", Password = "guest"); subdirectories in the ftp site are arranged by journal and paper number. Information on searching and submitting electronic supplements is found at http://www.agu.org/pubs/esupp_about.html.

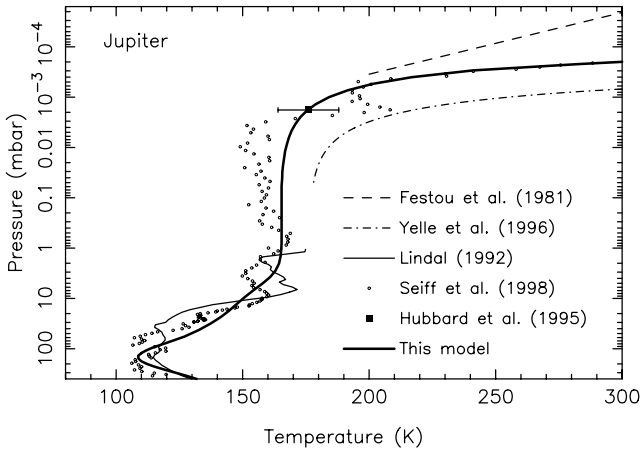

Figure 1. The temperature profile adopted for our Jupiter model (thick line), as compared with profiles derived from various observations. The dashed line represents the Voyager UVS occultation analysis of *Festou et al.* [1981], the dot-dashed line is Model C of *Yelle et al.* [1996] and is derived from a reanalysis of the UVS occultation data set in conjunction with various other ultraviolet and visible observations, the thin solid line represents the Voyager 1 egress radio occultation results from *Lindal* [1992] that have been rescaled by *Conrath and Gautier* [2000] for an updated helium abundance, the small circles represent the Galileo probe measurements from the ASI experiment [*Seiff et al.*, 1998], and the square with associated error bars represents the ground-based stellar occultation results of *Hubbard et al.* [1995]. Our profile is derived from ISO observations at pressures greater than $\sim$1 mbar [see *Lellouch et al.*, 2001, and references therein] and from the ASI measurements at pressures less than $\sim 10^{-3}$ mbar. As can be seen from the variations in the different measurements, determining an appropriate globally averaged stratospheric temperature profile is problematic (figure modified from *Moses et al.* [2004]; reprinted with permission).

main free parameters in the model, and our adopted profiles are discussed in section 3. Because of uncertainties in chemical reaction rate coefficients and in the location of the methane homopause, we create three distinct models (Models A, B, and C) that all provide a reasonable fit to the ISO data for the ν_5 band of C_2H_2 and the ν_9 band of C_2H_6. Models A and B have the same chemistry but different eddy diffusion coefficient profiles. Model C has different chemistry from Models A and B (see below).

[6] The continuity equations are solved using finite-difference techniques (Newton's method) with 111 atmospheric levels and a vertical resolution of at least three altitude levels per scale height. The lower boundary is located at 6.7 bar and the upper boundary at 7.4×10^{-8} mbar. Calculations are performed until successive iterations differ by no more than 0.1%. The model includes 66 different hydrocarbon and oxygen species that are allowed to vary with vertical transport and with 501 different chemical reactions. Of these 501 reactions, 120 involve photodissociation. Note that tropospheric photochemistry of nitrogen, phosphorus, and sulfur is not included, so the results for the troposphere are not accurate. Unlike the situation for the Saturn model of *Moses et al.* [2000a, 2000b], we now include multiple Rayleigh scattering by H_2, He, and CH_4 using a Feautrier radiative-transfer method [e.g., *Michelangeli et al.*, 1992]. Low-to-average solar ultraviolet flux values are used in our models [see *Moses et al.*, 2000a]. Calculations are performed for 30° latitude at equinox.

[7] The volume mixing ratios (mole fractions) of He, CH_4, and CO are assumed to be fixed at the lower boundary in the model. On the basis of the Galileo probe mass spectrometer and helium interferometer experiments, the mole fractions of He and CH_4 are assumed to be 0.136 and 1.81×10^{-3}, respectively, at 6.7 bar [*Niemann et al.*, 1998; *von Zahn et al.*, 1998]. The mole fraction of CO is assumed to be 8.0×10^{-10} on the basis of the high-resolution ground-based infrared observations of *Bézard et al.* [2002a]. All other species are assumed to have a zero concentration gradient at the lower boundary so that the species are transported through the boundary at a maximum possible velocity given by the eddy diffusion coefficient divided by the atmospheric scale height. Because our lower boundary is so far below the tropopause, our choice of the boundary condition has little effect on concentration profiles in the stratosphere.

[8] Zero flux is assumed as an upper boundary condition for most of the species in the model because the constituents are too heavy to escape thermally, and chemical sources and sinks are expected to be negligible. Atomic hydrogen, which is produced by photochemical processes at higher altitudes in the thermosphere, is the one exception to this rule. We assume a fixed downward flux for atomic hydrogen at the upper boundary. The magnitude of that flux is a free parameter in the model; our choice depends on the eddy diffusion coefficient profile and the adopted chemistry. For Models A, B, and C (see below), we consider a downward flux at the upper boundary of 1.5×10^9 H atoms cm^{-2} s^{-1}, 4.3×10^9 H atoms cm^{-2} s^{-1}, and 8.0×10^8 H atoms cm^{-2} s^{-1}, respectively. The photochemical model results are not particularly sensitive to the selected values; however, the assumptions regarding the H influx rate do affect the predicted Ly α brightness.

[9] Our models contain the list of species given by *Moses et al.* [2000a], along with C_5H_3, C_5H_4, C_6H_4, and C_6H_5. We also now distinguish between benzene (C_6H_6) and linear C_6H_6 molecules such as 1, 5-hexadiyne and 1, 2-hexadien-5-yne (hereafter all linear C_6H_6 molecules are designated as *l*-C_6H_6). Water and benzene molecules in the condensed phase are also included, following the procedure described by *Moses et al.* [2000b], but other condensed hydrocarbons are not, as condensation is not expected to be an important loss process for the major hydrocarbons on Jupiter. Meteoritic oxygen is introduced to the upper atmosphere in the form of H_2O, CO, and CO_2 in the 4×10^{-4} to 7×10^{-8} mbar region, with an ablation peak at 4×10^{-5} mbar. The total influx rate is assumed to be 4×10^4 H_2O molecules cm^{-2} s^{-1}, 4×10^6 CO molecules cm^{-2} s^{-1}, and 1×10^4 CO_2 molecules cm^{-2} s^{-1}; the low H_2O/CO ratio assumed for Jupiter as opposed to Saturn is based on observational constraints and likely reflects the importance of cometary impacts as a source of the external oxygen on Jupiter [*Bézard et al.*, 2002a; *Lellouch et al.*, 2002]. The ablation profiles were taken from *Moses* [2001].

[10] The photodissociation reactions included in our models, along with the photolysis rate coefficients at all altitudes, can be found in auxiliary material Table S2. The cross sections are taken from *Moses et al.* [2000a, 2000b] and references therein. The branching ratios for CH_4 photolysis are not well known. We use the recommendations of *J.-H. Wang et al.* [2000] for Ly α photolysis:

(R5) $CH_4 \xrightarrow{h\nu} CH_3 + H$ 0.291

(R6) $CH_4 \xrightarrow{h\nu} {}^1CH_2 + H_2$ 0.584

(R7) $CH_4 \xrightarrow{h\nu} {}^1CH_2 + 2H$ 0.055

(R8) $CH_4 \xrightarrow{h\nu} {}^3CH_2 + 2H$ 0

(R9) $CH_4 \xrightarrow{h\nu} CH + H + H_2$ 0.07

Although the branching ratios change at other wavelengths, Ly α dominates the UV flux at wavelengths that can dissociate CH_4, and the first two branches (R5 and R6) account for most of the photolysis of methane in our model Jovian stratosphere. The branch producing CH plays an important role in the production of unsaturated hydrocarbons like C_2H_2 and C_2H_4, and experiments that better define the CH quantum yield from Ly α photolysis of CH_4 are needed. We could not find cross sections for C_5H_4, C_6H_4, or C_6H_5 in the literature and have estimated that the photolysis rate (J_{81}) for reaction R81 ($C_5H_4 \xrightarrow{h\nu} C_3H_2 + C_2H_2$) is 10 times less than that for reaction R4 ($CH_3 \xrightarrow{h\nu} {}^1CH_2 + H$). Similarly, we have assumed that $J_{84} = J_{85} = J_{86} = J_{43}/300$, and $J_{87} = J_{88} = J_{43}/200$. The resulting J values allow photolysis to be an important loss process for C_5H_4, but other loss processes such as reaction with atomic H dominate for C_6H_4 and C_6H_5. We tested the influence of these estimated rates by dividing or multiplying the J values by 100. A change in J_{81}, J_{84}, J_{85}, J_{86}, J_{87}, and J_{88} by a factor of a hundred has no effect on the abundances of the observable hydrocarbons.

[11] Photoabsorption cross sections for benzene were taken from *Suto et al.* [1992] and *Pantos et al.* [1978]. Branching ratios were estimated from *Tsai et al.* [2001], *Mebel et al.* [1997], and *Yokoyama et al.* [1990]. However, the photolysis of benzene is complicated, and the photoproducts are not completely characterized. Absorption of ultraviolet photons can lead to "hot" benzene molecules that are in a transient highly excited state of the ground electronic state [e.g., *Nakashima and Yoshihara*, 1982; *Tsai et al.*, 2001; and references therein]. The dissociation lifetime of hot benzene is quite long, as much as 10^{-5} seconds according to *Tsai et al.* [2000]. Thus hot benzene can be collisionally stabilized without dissociating if the background atmospheric pressure is high enough, whereas dissociation can occur in collision-free conditions [e.g., *Yokoyama et al.*, 1990; *Tsai et al.*, 2001]. Given the long lifetime of hot benzene, absorption of a second photon is also possible, leading to different dissociation pathways from single-photon absorption. A full investigation of benzene photolysis is beyond the scope of this work. However, the long dissociation lifetime for benzene likely plays a role in its high observed abundance [*Bézard et al.*, 2001b] on Jupiter and Saturn. To simulate this process with a simple parameterization scheme, we assume that the photolysis rate is pressure dependent. We first note that at $\sim 7 \times 10^{-3}$ mbar on Jupiter, the lifetime against collisions is equal to the $\sim$10 μs dissociation lifetime. To calculate the photolysis lifetime of benzene in Jupiter's stratosphere, we then take the derived "instantaneous dissociation" J value (assuming 100% dissociation efficiency with cross sections from the sources mentioned above), and divide by $1 + (p/7 \times 10^{-3})$, for the atmospheric pressure p in mbar. The resulting J values tail off quickly at high pressures once C_6H_6 collisions with other atmospheric constituents become important. This parameterization scheme results in a benzene column abundance that is a factor of $\gtrsim$400 higher than would be the case assuming 100% dissociation efficiency and no pressure dependence; the large difference in the C_6H_6 abundance with these different assumptions is the result of relatively inefficient benzene recycling with our reaction schemes once photolysis takes place [cf. *Lebonnois*, 2005].

[12] As with the Saturn model of *Moses et al.* [2000a, 2000b], we consider a fairly complete set of bimolecular and termolecular chemical reactions for hydrocarbons containing from one to four carbon atoms and for oxygen-bearing species containing two or fewer oxygen atoms and two or fewer carbon atoms. Our list of hydrocarbon and oxygen reactions is shown in auxiliary material Table S3. Table 1 provides a subset of Table S3 to highlight the differences between Models A and B and Model C: Models A and B have the same reaction list but a different eddy diffusion coefficient profile, whereas the chemistry in Model C differs in several important ways from the chemistry in Models A and B. Reactions with total integrated column rates less than 1 cm^{-2} s^{-1} in the stratosphere (for Model A) are omitted from these tables. Our overall reaction list has its roots in the Titan investigation of *Yung et al.* [1984], the Jupiter investigation of *Gladstone et al.* [1996], and the Saturn investigation of *Moses et al.* [2000a, 2000b], but the rate coefficients have been extensively updated. Reactions whose rate constants have been updated from the *Moses et al.* [2000a, 2000b] studies have reaction numbers highlighted in bold. Other models of hydrocarbon photochemistry on the giant planets and Titan that have influenced our selection of reaction rates include *Allen et al.* [1992], *Romani et al.* [1993], *Toublanc et al.* [1995], *Romani* [1996], *Lara et al.* [1996], *Bishop et al.* [1998], *Lee et al.* [2000], *Lebonnois et al.* [2001, 2003], *Wilson et al.* [2003], *Wilson and Atreya* [2004], and *Lebonnois* [2005].

[13] For the three-body (termolecular) addition reactions, we assume that the rate constants (in cm^6 s^{-1}) obey the form

$$k = \left(\frac{k_0}{1 + \frac{k_0[M]}{k_\infty}} \right) F_c^\beta, \quad (1)$$

where k_0 is the low-pressure three-body limiting value in units of cm^6 s^{-1}, k_∞ is the high-pressure limiting value in

Table 1. Reaction Rate Differences Between Models A and B and Model C[a]

Reaction	Rate constant	Reference[b]
R186: $H + CH_3 \xrightarrow{M} CH_4$	$k_0 = 1.5 \times 10^{-24}\ T^{-1.8}$ $k_0 = 6.0 \times 10^{-29}$, $T \leq 277.5$ K $k_\infty = 1.92 \times 10^{-8}\ T^{-0.5}\ e^{(-400/T)}$ $k_\infty = 4.823 \times 10^{-11}$, $T \leq 110$ K $F_c = 0.3 + 0.58e^{(-T/800)}$	Models A and B; based on [1], [2], and [3]
	$k_0 = 7.81 \times 10^{-18}\ T^{-3.87}\ e^{(-1222/T)}$ $k_0 = 3.46 \times 10^{-29}$, $T \leq 316$ K $k_\infty = 4.6 \times 10^{-7}\ T^{-1}\ e^{(-474/T)}$ $k_\infty = 4.8 \times 10^{-11}$, $T \leq 105$ K $F_c = 0.31 + e^{(-T/425)}$ $F_c = 1.0$, for $T \leq 157.7$ K	Model C; based on [1] and [2]
R190: $H + C_2H_2 \xrightarrow{M} C_2H_3$	$k_0 = 3.3 \times 10^{-30}\ e^{(-740/T)}$ $k_\infty = 1.4 \times 10^{-11}\ e^{(-1300/T)}$ $F_c = 0.44$	Models A and B; [3]
	$k_0 = 3.34 \times 10^{-26}\ T^{-1.46}\ e^{(-1144/T)}$ $k_\infty = 2.3 \times 10^{-11}\ e^{(-1350/T)}$ $F_c = 0.6$	Model C; based on [4]
R191: $H + C_2H_3 \longrightarrow C_2H_2 + H_2$	$1.5 \times 10^{-12}\ T^{0.5}$	Models A and B; data compilation
	$k_{192,\infty} - k_{192}[M]$	Model C; estimate
R192: $H + C_2H_3 \xrightarrow{M} C_2H_4$	$k_0 = 2.3 \times 10^{-24}\ T^{-1}$ $k_\infty = 1.8 \times 10^{-10}$	Models A and B; based on [5], [6]
	$k_0 = 1.75 \times 10^{-27}\ T^{-0.3}$ $k_\infty = 7.0 \times 10^{-11}\ T^{0.18}$	Model C; based on [6], [7]
R194: $H + C_2H_4 \xrightarrow{M} C_2H_5$	$k_0 = 1.3 \times 10^{-29}\ e^{(-380/T)}$	Models A and B; [3]
	$k_0 = 3.7 \times 10^{-30}$, $T \leq 302.4$ K $k_\infty = 6.6 \times 10^{-15}\ T^{1.28}\ e^{(-650/T)}$ $F_c = 0.24e^{(-T/40)} + 0.76e^{(-T/1025)}$	estimate [3] [3]
	$k_0 = 1.68 \times 10^{-38}\ T^{2.87}\ e^{(923/T)}$ $k_\infty = 6.6 \times 10^{-15}\ T^{1.28}\ e^{(-650/T)}$ $F_c = 0.24e^{(-T/40)} + 0.76e^{(-T/1025)}$	Model C; from [8] [3] [3]
R294: $CH_3 + C_3H_2 \longrightarrow C_2H_2 + C_2H_3$	1.0×10^{-11}	Models A and B; estimate
	8.0×10^{-11}	Model C; estimate
R328: $C_2H_3 + H_2 \longrightarrow C_2H_4 + H$	$1.57 \times 10^{-20}\ T^{2.56}\ e^{(-2529/T)}$	Models A and B; [9]
	$5.23 \times 10^{-15}\ T^{0.7}\ e^{(-2574/T)}$	Model C; [10]

[a]M represents any third body. Two-body rate constants and high-pressure limiting rate constants for three-body reactions (k_∞) are in units of $cm^3\ s^{-1}$. Low-pressure limiting rate constants for three-body reactions (k_0) are in units of $cm^6\ s^{-1}$.

[b]References: 1, *Brouard et al.* [1989]; 2, *Seakins et al.* [1997]; 3, *Baulch et al.* [1994]; 4, *Payne and Stief* [1976]; 5, *Fahr* [1995]; 6, *Monks et al.* [1995]; 7, *Klippenstein and Harding* [1999b]; 8, *Lightfoot and Pilling* [1987]; 9, *Knyazev et al.* [1996]; 10, *Weissman and Benson* [1988].

units of $cm^3\ s^{-1}$, $[M]$ is the total atmospheric density (cm^{-3}), and the exponent β is

$$\beta = \left(\frac{1}{1 + \left[\log_{10} \left(\frac{k_0[M]}{k_\infty} \right) \right]^2} \right). \quad (2)$$

We assume $F_c \approx 0.6$ [*DeMore et al.*, 1992], unless otherwise noted.

[14] The important association reaction $H + CH_3 \xrightarrow{M} CH_4$ (R186) has been studied extensively at room temperature and higher, but low-temperature investigations are rare. We use the interpolation expression from equation (1) along with the rate measurements of *Brouard et al.* [1989] and *Seakins et al.* [1997] to derive the temperature-dependent low- and high-pressure limiting rate constants shown in Tables 1 and S3 and plotted in Figure 2. Our expression provides a reasonable fit to the 300–600 K data of *Brouard et al.* [1989] and to the k_∞ at 200 and 298 K inferred by *Seakins et al.* [1997]. The extrapolation to colder temperatures is not known, however. Because the relative effectiveness of R186 versus R287 ($CH_3 + CH_3 + M \rightarrow C_2H_6 + M$) helps control the C_2H_6 abundance in Jupiter's stratosphere, further low-temperature laboratory investigations or theoretical calculations regarding these two reactions are encouraged. Recently, *Smith* [2003] used a restricted Gorin RRKM model to calculate k_0 (in He) and k_∞ for R186 at 65–300 K. His derived expression produces k_0 and k_∞ values that are higher than ours at relevant Jovian stratospheric temperatures.

[15] As discussed by *Moses et al.* [2000a], *Romani* [1996], *Gladstone et al.* [1996], *Fahr et al.* [1995], and *Allen et al.* [1992], the C_2H_6/C_2H_2 ratio in Jupiter's lower stratosphere is sensitive to the atomic hydrogen reactions R189–R195 that affect the efficiency of C_2H_2 and C_2H_4 recycling. Although all these reactions have been studied in the laboratory, the investigated temperatures are generally higher than is relevant for giant-planet stratospheres and the low-pressure limiting rate constants are not always well determined. The reaction $H + C_2H_2 \xrightarrow{M} C_2H_3$ (R190) is important in controlling the atomic hydrogen abundance in outer-planetary stratospheres. Our expression for the rate constant of R190 was taken from *Baulch et al.* [1994] for our Models A and B. However, because this expression may underestimate k_∞ (see Figure 3) [*Payne and Stief*, 1976; *Sugawara et al.*, 1981; *Knyazev and Slagle*, 1996], we adopt an alternative expression for Model C (see Table 1

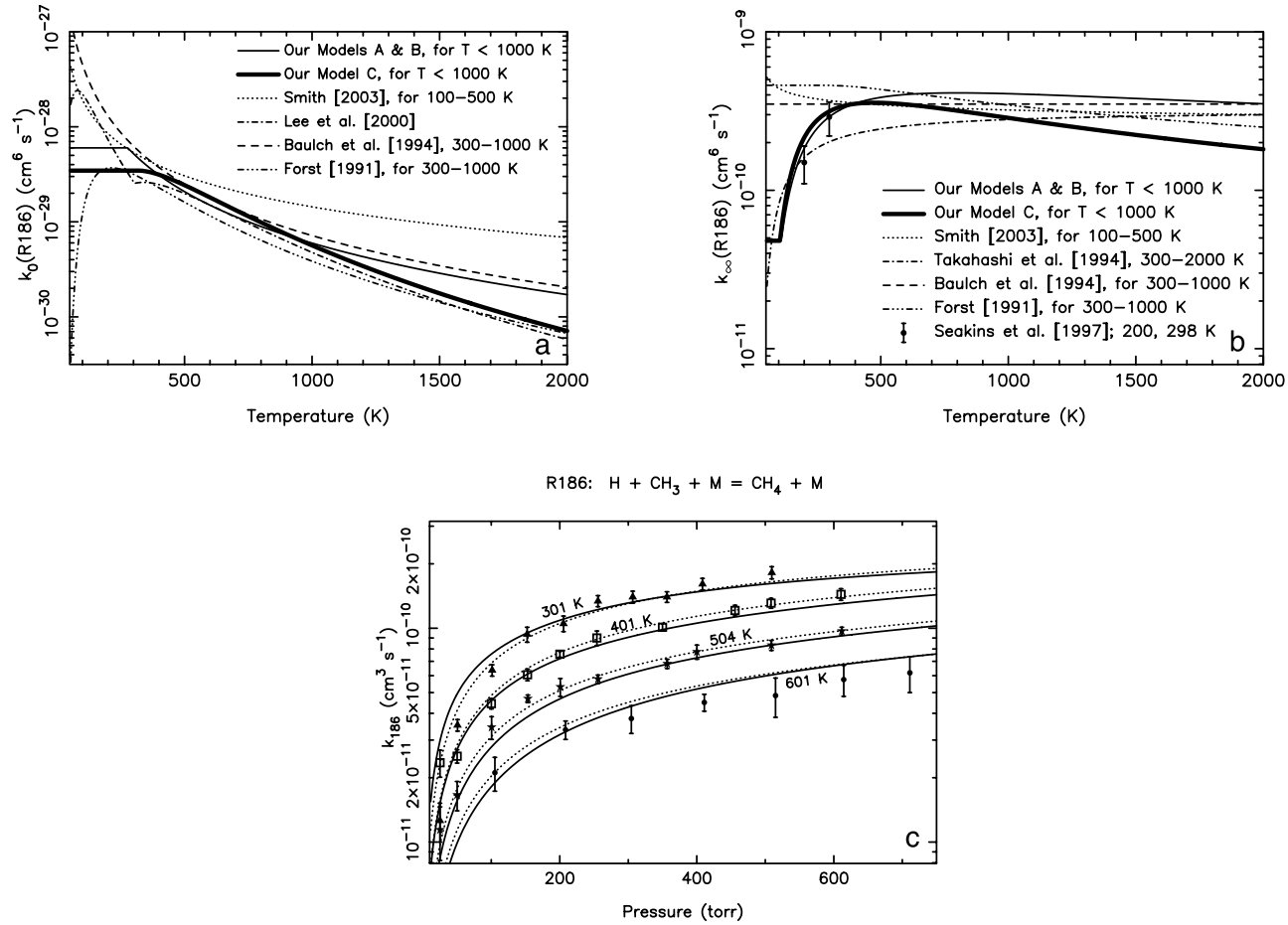

Figure 2. The rate constant for reaction R186 ($H + CH_3 \underset{\rightarrow}{M} CH_4$), as calculated or measured by various groups: (a) low-pressure limit, (b) high-pressure limit, and (c) the pressure-dependent rates as predicted from our expressions given in Table S3 and equation (1). Note that the rate constants shown in Figures 2a and 2b are extrapolated beyond the temperature ranges suggested by the various authors. In Figure 2c, our full rate-constant expressions from Models A and B (solid lines) and Model C (dotted lines) are compared with experimental data from *Brouard et al.* [1989] at 301 K (triangles), 401 K (squares), 504 K (stars), and 601 K (circles).

and auxiliary material Table S3). The fit of our two different expressions to the data of *Payne and Stief* [1976] is shown in Figure 3. New work by *Miller and Klippenstein* [2004] and their theoretical extrapolation to very low temperatures (G. P. Smith, personal communication, 2004) suggests that we may be underestimating k_0 at Jovian stratospheric temperatures as well. The sensitivity of our model results to the rate coefficients for R190 are discussed in section 4.4.

[16] The photochemistry of methylacetylene has not been extensively studied, especially at the low temperatures typical in Jupiter's stratosphere. Few data exist for the potentially important reactions of atomic H with C_3H_x radicals (e.g., reactions R199–R201, R207–R210). The reactions of atomic H with allene, methylacetylene, and propene have been studied in laboratory settings, but the reaction products are not well known, except for the case of CH_3C_2H [*B. Wang et al.*, 2000]. Our adopted expressions for R202, R203, and R204 compare well with the total rate for the $H + CH_3C_2H$ reaction as determined by *Whytock et al.* [1976] (see Figure 4). According to *Wagner and Zellner* [1972] and *B. Wang et al.* [2000], reaction of H with CH_3C_2H (R204) occurs by terminal addition to form CH_3CCH_2 (1-methylvinyl) radicals rather than CH_2CHCH_2 (allyl) radicals. Because R204 is the dominant mechanism for producing C_3H_5 in our model, we include reaction R209 ($H + C_3H_5 \rightarrow CH_3 + C_2H_3$), as suggested by *Wagner and Zellner* [1972], although the pathway would be endothermic with allyl as the C_3H_5 radical. Reaction R209 plays an important role in our model through its effect on the H atom abundance (i.e., the CH_3 and C_2H_3 products continue to scavenge hydrogen); therefore more studies of the reaction of atomic hydrogen with CH_3CCH_2 radicals are greatly needed.

[17] Reaction of CH with H_2 is an important loss process for CH in Jupiter's stratosphere. The abstraction pathway (reaction R241) dominates in the upper stratosphere, whereas the addition pathway becomes important in the lower stratosphere. Figure 5 shows how our adopted expressions for R242 compare with the experimental data of *Berman and Lin* [1984] and *Becker et al.* [1991].

[18] Excited singlet methylene ($^1CH_2$) is an important product of CH_4 photolysis at Ly α [see *J.-H. Wang et al.*, 2000]. The most likely fate of $^1CH_2$ in Jupiter's stratosphere is reaction with H_2 to form CH_3 (reaction R259) or collisional deactivation (reaction R258). Our adopted rate

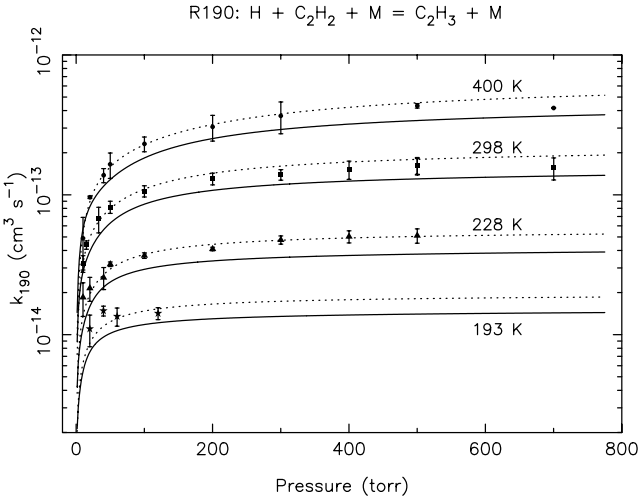

Figure 3. The rate constant for reaction R190 ($H + C_2H_2 \underset{\downarrow}{\overset{M}{\rightarrow}} C_2H_3$), as calculated from our expressions used in Models A and B (solid lines) and in Model C (dotted lines), compared with experimental data from *Payne and Stief* [1976] at 193 K (stars), 228 K (triangles), 298 K (squares), and 400 K (circles).

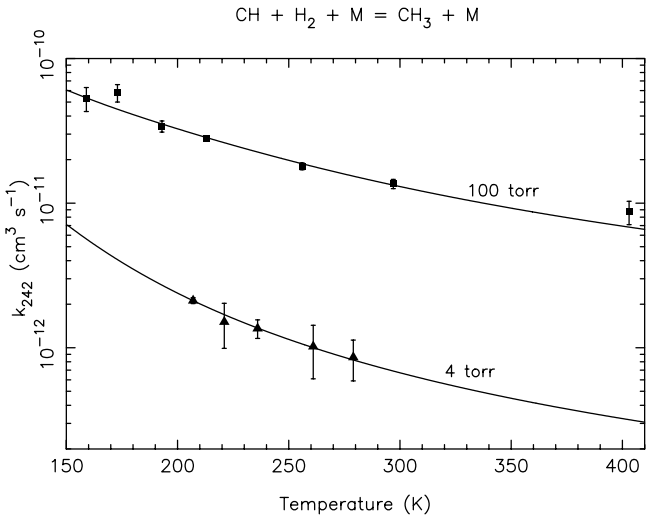

Figure 5. The rate constant for reaction R242 ($CH + H_2 \underset{\downarrow}{\overset{M}{\rightarrow}} CH_3$), as predicted from the expression given in Table S3 (solid lines), compared with experimental data from *Becker et al.* [1991] at a total pressure of 100 torr (squares) and with data from *Berman and Lin* [1984] at 4 torr (triangles).

constants for k_{258} and k_{259} use information on the relative importance of the two branches at 298 K from *Braun et al.* [1970] and the absolute rate constant derived by *Langford et al.* [1983]. Our expressions and the relative importance of R258 and R259 are roughly consistent with the recent derivations of *Blitz et al.* [2001]. We discuss the sensitivity of the results to k_{258} and k_{259} in section 4.4. Further investigations into the low-temperature behavior and pressure dependence of these reactions are warranted.

[19] Methyl-methyl recombination (reaction R287) is responsible for most of the production of C_2H_6 in Jupiter's stratosphere. The high-pressure limiting rate constant $k_{\infty,287}$ has been established in the 155–400 K temperature range [e.g., *Hippler et al.*, 1984; *Slagle et al.*, 1988; *Walter et al.*, 1990; *Cody et al.*, 2002, 2003]; however, obtaining rate-constant information in the falloff regime at temperatures relevant to the Jovian stratosphere poses experimental difficulties, and the low-pressure limiting rate constant $k_{0,287}$ is not well constrained for $T \leq 200$ K (and no data exist for H_2 as the bath gas). *Klippenstein and Harding* [1999a] have calculated the reaction rate using a variational transition-state-theory analysis, but the results are not presented for temperatures below 200 K, and their calculations tend to overpredict $k_{\infty,287}$ (as compared with experimental values) at temperatures above 298 K. Recently, *Smith* [2003] has used RRKM and master-equation calculations to derive rate-constant expressions for R287 at 65–300 K at any pressure. Our expression, which has somewhat lower values for $k_{0,287}$ than that of *Smith* [2003], was designed to fit the experimental data of *Walter et al.* [1990] at 200, 300, and 408 K with Ar as the bath gas (see Figure 6). The derived expression is also consistent with the He-bath-gas data of *Cody et al.* [2003] at 155 K, the He bath gas data of *Cody et al.* [2002] at 202 K, and the Ar-bath-gas data of *Slagle et al.* [1988] at 296 K; however, the expression overestimates the rate constant when compared with the 298-K He-bath-gas data of *Cody et al.* [2002] and the $T \geq 296$ He-bath-gas data of *Slagle et al.* [1988] and underestimates k_{287} when compared with the Ar-bath-gas data of *Slagle et al.* [1988] at 474 K. The extrapolation to temperatures below 200 K is very uncertain, and our expression assumes that both $k_{0,287}$ and $k_{\infty,287}$ increase with decreasing temperature.

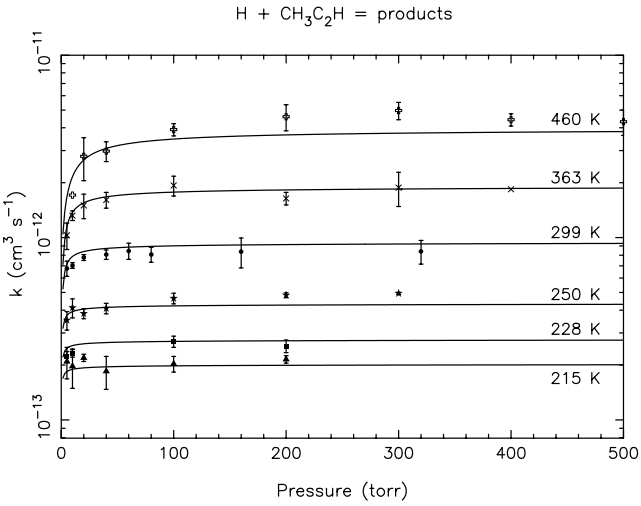

Figure 4. The rate constant for reaction R202 + R203 + R204 ($H + CH_3C_2H \rightarrow$ products), as predicted from the expression given in Table S3 (solid lines), compared with experimental data from *Whytock et al.* [1976] at various temperatures (as labeled).

[20] Reactions R295 and R296 that deal with the reaction of methyl radicals (CH_3) with propargyl radicals (C_3H_3) can influence not only the abundance of C_4H_6 but also that of CH_3C_2H, CH_2CCH_2, C_4H_2, and C_6H_6. The propargyl-methyl cross-combination reaction has recently been studied experimentally by *Fahr and Nayak* [2000], who determine a room-temperature rate constant at 50 torr of $(1.5 \pm 0.3) \times 10^{-10}$ cm^3 s^{-1}, and by *Knyazev and Slagle* [2001], who determine $k_{\infty,295+296} = 6.8 \times 10^{-11}$

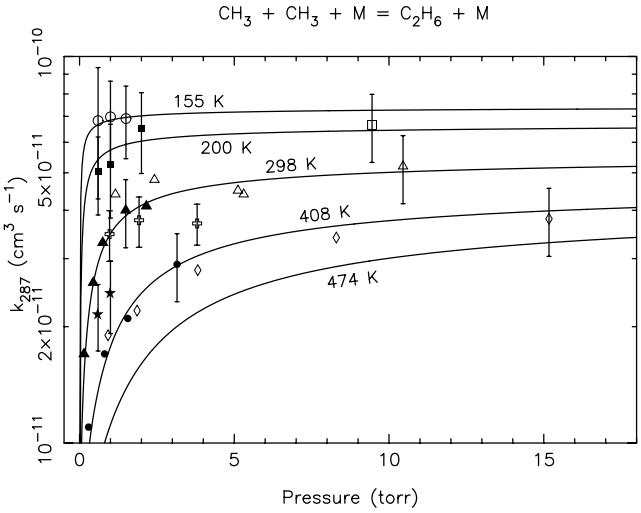

Figure 6. Our adopted rate constants (solid lines) for methyl-methyl recombination (reaction R287: 2 $CH_3 \rightleftarrows C_2H_6$) in the falloff regime at several temperatures, as compared with various experimental values (data points, some with typical error bars). The data of *Walter et al.* [1990] with Ar as the bath gas are represented by open squares (200 K), solid triangles (300 K), and solid circles (408 K), and the data of *Slagle et al.* [1988] with Ar as the bath gas are represented by open triangles (296 K) and diamonds (474 K). The data of *Stoliarov et al.* [2000] with He as the bath gas are represented by crosses (~310 K). The recent discharge-flow kinetic measurements of *Cody et al.* [2002, 2003] with He as the bath gas are marked with open circles (155 K), solid squares (202 K), and solid stars (298 K).

exp(130/*T*). To maintain high abundances of CH_3C_2H and C_6H_6 in our model, we use a lower rate constant $k_{\infty,295+296} = 1.66 \times 10^{-11}$ cm^3 s^{-1} that is more consistent with the high-temperature shock-tube study of *Wu and Kern* [1987]. The relative importance of the reaction products, however, is consistent with that determined by *Fahr and Nayak* [2000].

3. Previous Constraints on the Eddy Diffusion Coefficient Profile

[21] Although the decreasing atmospheric density with increasing altitude enables molecular diffusion to become important in the upper stratosphere, large- and small-scale atmospheric motions keep relatively stable chemical constituents like He and CH_4 uniformly mixed throughout Jupiter's lower stratosphere. The eddy diffusion coefficient K is commonly used as a means for parameterizing the strength of this atmospheric mixing in one-dimensional models. When molecular diffusion starts to dominate over eddy mixing, the concentration of each atmospheric constituent begins to fall off with its own scale height. Methane, which is heavier than the background atmospheric H_2, exhibits a pronounced concentration gradient in this "homopause" region (where the homopause is defined as the level where K equals the molecular diffusion coefficient of the species in question). Methane molecules are photolyzed just below their homopause level, and the pressure at which photolysis occurs can affect the resulting production and loss of various other hydrocarbons (including influencing the C_2H_6/C_2H_2 ratio, the effectiveness of CH_4 recycling, and the overall production rate of unsaturated hydrocarbons). The abundance of long-lived photochemical products is also strongly influenced by the magnitude of the eddy diffusion coefficient in the stagnant lower stratosphere and/or upper troposphere. Small minimum values of the eddy diffusion coefficient (K_{min}) in this region provide an efficient bottleneck to the flow of hydrocarbons into the troposphere and allow the stratospheric column abundances to build up to large values. High values of K_{min} increase the flow rate into the troposphere and reduce the stratospheric abundance of photochemical products.

[22] Because eddy diffusion coefficients cannot in general be derived from physical principles [cf. *Lindzen*, 1981; *Strobel et al.*, 1985; *West et al.*, 1986; *Medvedev and Klassen*, 1995], the eddy diffusion coefficient profile is one of the main free parameters of photochemical models. The presence of a stagnant lower stratosphere and upper troposphere on Jupiter (i.e., low value of K_{min} in this region) is indicated by numerous pieces of evidence (see Figure 7). *Conrath et al.* [1984] use Voyager Infrared Interferometric Spectrometer (IRIS)

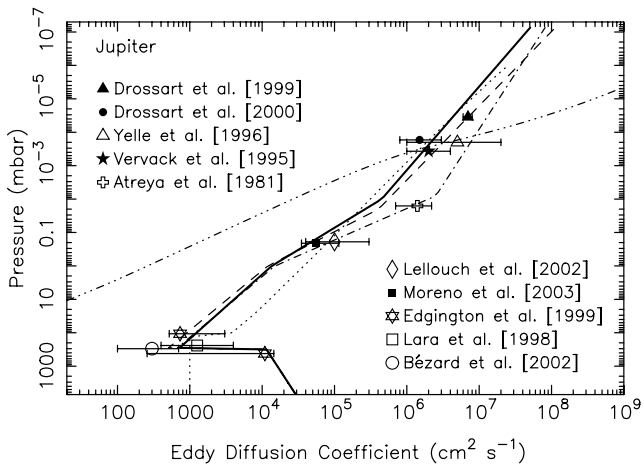

Figure 7. The eddy diffusion coefficients adopted for our models, as compared with observational constraints. The dot-dashed line represents Model A, the dashed line is Model B, the solid line is Model C, the dotted line is the preferred model of *Gladstone et al.* [1996], and the triple-dot-dashed line represents our adopted CH_4 molecular diffusion coefficient in Jupiter's stratosphere given the thermal structure shown in Figure 1. The individual data points represent constraints reported from various observations, as labeled. The error bars in the case of the *Lara et al.* [1998] and *Edgington et al.* [1999] points indicate the range of derived values at different latitudes rather than true error bars. The pressure levels for the reported values of K_h were estimated through information given in the published reports and/or through personal communications (e.g., P. Drossart, 1999, and G. R. Gladstone, 2002 to J. I. Moses) and are approximate. The model profiles were developed independently of the reported values for K and were designed to reproduce observations of species abundances.

observations of the H_2 *ortho-para* ratio along with estimates of the *para* hydrogen equilibration time scales to determine that $K \lesssim 3000$ cm^2 s^{-1} at ~300 mbar in Jupiter's upper troposphere. Observations of ammonia (NH_3) and phosphine (PH_3) at ultraviolet or infrared wavelengths can also help constrain K in the upper troposphere; high values of K allow these species to be carried to higher altitudes than they would otherwise be found. From ground-based thermal-infrared observations of NH_3, *Lara et al.* [1998] conclude that K ranges from $\lesssim$400 to ~4000 cm^2 s^{-1} at 240 mbar, with the exact value depending on latitude. By comparing ultraviolet Hubble Space Telescope (HST) Faint Object Spectrograph (FOS) observations with the PH_3 and NH_3 distributions from photochemical models, *Edgington et al.* [1998, 1999] also find that K varies with latitude, with derived values of K_{min} ranging from ~200 to 600 cm^2 s^{-1} at 80–1000 mbar. One advantage of these techniques is that observational inferences of the altitude distribution of NH_3 and PH_3 can provide information about the altitude variation of K. One drawback is that the results are sensitive to assumptions about photochemical production and loss mechanisms and scattering of radiation in the Jovian upper troposphere. *Bézard et al.* [2002a] demonstrate that K_{min} could also be determined through high-spectral-resolution observations of CO in the upper troposphere and lower stratosphere. From comparing observations of the 4.7 μm band of CO on Jupiter to current estimates of the influx rate due to impacts with Jupiter-family comets, *Bézard et al.* [2002a] favor low values (~100–700 cm^2 s^{-1}) for K_{min}, but the results are sensitive to the assumed cometary influx rate.

[23] Very few constraints on K exist for the middle stratosphere. From ISO observations of Jovian stratospheric H_2O that is presumably derived from the Shoemaker-Levy 9 (SL9) impacts, *Lellouch et al.* [2002] have inferred vertical eddy diffusion coefficients of $K = 4 \times 10^4$ to 3×10^5 cm^2 s^{-1} at ~0.2 mbar. Similarly, *Moreno et al.* [2003] use ground-based millimeter and submillimeter observations of SL9-derived CO, CS, and HCN to derive a value of $K = 5.5^{+6}_{-2} \times 10^4$ cm^2 s^{-1} at 0.2 mbar. We hope to place further constraints on K in the middle and lower stratosphere from ISO observations of the altitude distribution of C_2H_2 and C_2H_6 [see also *Fouchet et al.*, 2000b].

[24] Various observations have also been used to constrain K_h, the value of the eddy diffusion coefficient at the methane (or sometimes helium) homopause. The most direct way to determine K_h is to measure the altitude variation of the species of interest in the homopause region through such techniques as ultraviolet observations of the planet as it occults the Sun or another star. Ultraviolet occultation measurements were obtained during the Voyager and Cassini spacecraft flybys. The Cassini UVIS occultation results are not yet available. The 1979 Voyager 2 UVS observation of the occultation of the star α Leo at 51–169 nm [*Broadfoot et al.*, 1981] has provided determinations of the CH_4 mole fraction in the homopause region [*Atreya et al.*, 1981; *Festou et al.*, 1981; *Yelle et al.*, 1996]; however, the results are sensitive to assumptions about the temperature-density structure of the Jovian upper atmosphere, and the various analyses do not agree. Using very different assumptions about the temperature profile in the Jovian upper atmosphere, *Festou et al.* [1981] and *Atreya et al.* [1981] derive a CH_4 mole fraction of $2.5^{+3}_{-2} \times 10^{-5}$ at ~5 × 10^{-3} mbar, whereas *Yelle et al.* [1996] derive a mole fraction of (1.5 ± 0.5) × 10^{-4} at ~2 × 10^{-4} mbar. The resulting determinations of K_h are $1.4^{+0.8}_{-0.7} \times 10^6$ cm^2 s^{-1} [*Festou et al.*, 1981] and $5^{+1.5}_{-4} \times 10^6$ cm^2 s^{-1} [*Yelle et al.*, 1996]. Although the actual values of K_h derived from these separate analyses are consistent to within the quoted error bars, the results regarding the methane vertical distribution and the location of the homopause are quite different (see section 4.3). *Festou et al.* [1981] and *Atreya et al.* [1981] locate the methane homopause at a pressure more than an order of magnitude higher than that derived by *Yelle et al.* [1996].

[25] The *Yelle et al.* [1996] results regarding the falloff of methane with altitude are roughly consistent with the results from an analysis of fluorescence in the ν_3 band of methane (near 3.3 μm) as observed from ISO-SWS in 1996 [*Drossart et al.*, 1999]. These latter authors determine K_h to be (6–8) × 10^6 cm^2 s^{-1}, with a CH_4 mole fraction profile in the 10^{-3} to 10^{-4} mbar region. On the other hand, ground-based infrared observations of methane absorption in the 2.3 μm band during the occultation of star HIP9369 by Jupiter in 1999 [*Drossart et al.*, 2000] place the methane homopause at a higher pressure (lower altitude), with an inferred K_h of $1.5^{+1.5}_{-0.8} \times 10^6$ cm^{-2} s^{-1}. It is not clear whether the differences here reflect differences in model assumptions, real variations in K_h with time, and/or variations in K_h with spatial location. We note, however, that recent spatially resolved observations of fluorescence emission in the hot band $\nu_3 + \nu_4 - \nu_4$ of CH_4 obtained with the VLT/ISAAC instrument [*Drossart et al.*, 2001] demonstrate that the CH_4 mole fraction at the homopause is constant to within ±20% across the Jovian disk (P. Drossart, personal communication, 2002).

[26] Eddy diffusion coefficients in the homopause region can also be determined through ultraviolet airglow observations of the 1216 Å Lyman α line of atomic hydrogen and the 584 Å line of atomic helium [e.g., *Hunten*, 1969; *Wallace and Hunten*, 1973; *Broadfoot et al.*, 1981; *Ben Jaffel et al.*, 1988; *McConnell et al.*, 1981; *Vervack et al.*, 1995; *Gladstone et al.*, 1995, 1996; C. D. Parkinson et al., Enhanced transport in the polar mesosphere of Jupiter: Evidence from Cassini UVIS helium 584 Å airglow, unpublished manuscript, 2005]. At non-auroral latitudes, Ly α emission results predominantly from resonant scattering of solar photons. Methane is the primary absorber at Ly α; the larger the value of K_h, the more CH_4 that is mixed to high altitudes, and the weaker the resulting H emission. Conversely, 584 Å photons are absorbed predominantly by molecular hydrogen. The higher the eddy diffusion coefficient, the more He that is mixed to high altitudes, and the stronger the He 584 Å emission. Inferences from the Ly α airglow are complicated by the observed spatial inhomogeneities across the planet (e.g., the Ly α bulge) and by uncertainties in the contribution from "hot" hydrogen and auroral-produced hydrogen. Therefore the helium observations are preferred for inferences about K_h. From an analysis of the Voyager UVS He

584 Å emission data, *Vervack et al.* [1995] conclude that K_h is $2^{+2}_{-1} \times 10^6$ cm^2 s^{-1}.

[27] The various observational constraints are shown in Figure 7. Note that quotes of K_h in the literature are not helpful without (1) information about the assumed density-temperature structure of the atmosphere, (2) information about the assumed slope or shape of the K profile, and (3) information about the adopted expression(s) for the molecular diffusion coefficient(s). This information is seldom provided in the published reports. Specific information about the inferred distribution of CH_4 with pressure or the inferred He brightness is more useful to photochemical modelers than quotes of K_h because quotes that are quite different may actually be consistent with each other (and the converse is true) depending on the adopted assumptions [see *Moses et al.*, 2000a]. Differences in the assumed atmospheric temperature structure have had the most critical effect on inferences about the location of the methane homopause on Jupiter. For instance, all the values for K_h in Figure 7 except the helium results of *Vervack et al.* [1995] should line up along the dot-dashed curve that represents the CH_4 molecular diffusion coefficient. The wide scatter in pressure for the various observational constraints is caused by widely different assumptions about the temperature-pressure profile. Because of uncertainties in Jupiter's "average" thermal structure, both K_h and the pressure level of the methane homopause remain uncertain.

[28] We have developed three standard models that have different K profiles. All three models predict lower-stratospheric C_2H_2 and C_2H_6 abundances that are consistent with observations of the ν_5 band and ν_9 band emission, respectively. The main differences between the three are the magnitude of the eddy diffusion coefficient in the upper stratosphere and the rate coefficients of a few key reactions. "Model A" was designed to have a CH_4 profile consistent with the UVS analysis of *Yelle et al.* [1996] and with the ISO-SWS CH_4 ν_3 fluorescence data of *Drossart et al.* [1999]. However, Model A results in a predicted He 584 Å brightness that is ~2–3 times greater than was observed with either the Voyager UVS instrument or the EUVE satellite (see section 5.3), so we have also created a "Model B" that has the same chemistry as Model A but that has a different K profile. Model B is more consistent with the observed He 584 Å brightness and is still marginally consistent with the ISO ν_3 fluorescence results. However, the Model B CH_4 profile appears to be inconsistent with the *Yelle et al.* [1996] analysis of the UVS occultation results. We were unable to come up with a model that fits both the He 584 Å emission data and the Voyager UVS occultation results of *Yelle et al.* [1996]. Because the rate coefficients used in Models A and B (see Tables S2 and S3) lead to an underprediction of the C_2H_2 abundance at high altitudes, as indicated by the ISO data, we have also developed a "Model C" that has different chemistry from that of Models A and B. Certain rate coefficients in Model C have been altered to maximize the net production of C_2H_2 in the upper stratosphere (see Table 1), and Model C has a homopause level consistent with the He 584 Å emission data. These three K profiles are shown in Figure 7, along with the preferred K profile from *Gladstone et al.* [1996].

[29] For Model A, we use

$$K = 8.0 \times 10^6 (1.7 \times 10^{-4}/p)^{0.3} \quad \text{for } p < 8.0 \times 10^{-3} \text{ mbar}$$

$$K = 1.5 \times 10^6 (1/p)^{1.061184} \quad \text{for } 8.0 \times 10^{-2} \le p < 1 \text{ mbar}$$

$$K = 1.5 \times 10^4 (1/p)^{0.55} \quad \text{for } 1 \le p < 316 \text{ mbar}$$

for K in cm^2 s^{-1} and p in mbar. For Model B, we use

$$K = 4.05746 \times 10^5 (2 \times 10^{-2}/p)^{0.45} \quad \text{for } p < 2.0 \times 10^{-2} \text{ mbar}$$

$$K = 1.2 \times 10^4 (1/p)^{0.9} \quad \text{for } 2.0 \times 10^{-2} \le p < 1 \text{ mbar}$$

$$K = 1.2 \times 10^4 (1/p)^{0.56} \quad \text{for } 1 \le p < 316 \text{ mbar}$$

for K in cm^2 s^{-1} and p in mbar. For Model C, we use

$$K = 4.5 \times 10^5 (1 \times 10^{-2}/p)^{0.4} \quad \text{for } p < 1.0 \times 10^{-2} \text{ mbar}$$

$$K = 4.5 \times 10^5 (1 \times 10^{-2}/p)^{0.76} \quad \text{for } 1.0 \times 10^{-2} \le p < 1 \text{ mbar}$$

$$K = 1.358978 \times 10^4 (1/p)^{0.52} \quad \text{for } 1 \le p < 316 \text{ mbar}$$

for K in cm^2 s^{-1} and p in mbar. At $p \ge 316$ mbar, the model results are not sensitive to K, and all models use a profile that is consistent with that derived by *Edgington et al.* [1998].

4. Photochemical Model Results

[30] The photolysis rates for many of the observed molecules in our model Jovian stratosphere are given in auxiliary material Table S2, and the depth of penetration of solar radiation as a function of wavelength is shown in Figure 8. Hydrocarbon photochemistry is initiated by the photolysis of methane in the 10^{-4} to 10^{-2} mbar region. Because the methane column abundance is large in the Jovian stratosphere, hydrocarbon photochemistry is limited by the availability of photons rather than by the abundance of methane, and Ly α and other short-wavelength radiation is efficiently absorbed in the upper stratosphere (see Figure 8 and Table S2). In the middle and lower stratosphere, the photolysis of C_2H_2 at ~1400–1900 Å

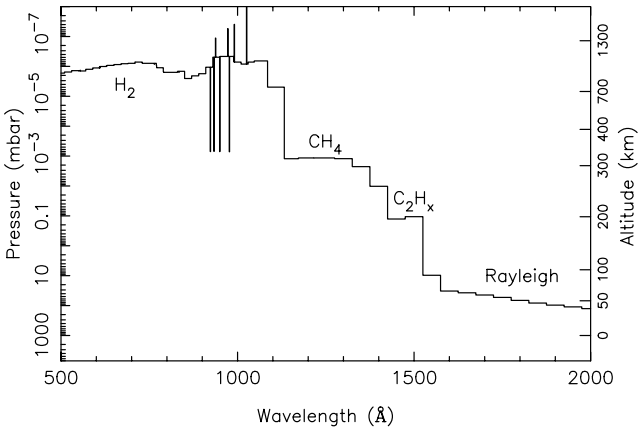

Figure 8. The depth of penetration of solar radiation as a function of wavelength in Jupiter's stratosphere. The solid curve represents the pressure level at which the total optical depth (scattering plus absorption) is unity in our Model A (30° latitude at equinox). Molecular hydrogen dominates the absorption at wavelengths less than ~1110 Å (except in a few microwindows that are coincident with solar emission lines), CH_4 absorption dominates in the 1110–1450 Å wavelength region, and ethane and acetylene dominate in the 1450–1550 Å wavelength region. Rayleigh scattering dominates the extinction at wavelengths greater than 1550 Å. Molecules like C_2H_4, CH_3C_2H, and CO also contribute to the opacity at wavelengths greater than 1500 Å.

leads to photosensitized dissociation of CH_4 [e.g., *Allen et al.*, 1980] and to additional hydrocarbon production and loss mechanisms.

4.1. Hydrocarbon Photochemistry

[31] Figure 9 displays the important reaction pathways for synthesizing and destroying hydrocarbons in our model. The major pathways for producing C_2 and higher-order hydrocarbons in Jupiter's stratosphere are similar to those in Saturn's, and the reader is referred to *Moses et al.* [2000a] for a more thorough discussion of the relevant photochemical schemes. Differences in stratospheric composition between Jupiter and Saturn are caused by Jupiter's smaller heliocentric distance (which leads to greater photolysis rates and greater H-atom production rates), Jupiter's greater stratospheric temperatures (which can allow some temperature-sensitive reactions such as R328 to become effective), and Jupiter's less vigorous upper stratospheric eddy mixing (which can affect the efficiency of CH_4 recycling schemes). Differences in auroral energy input probably also play a role, provided that transport of species produced by auroral chemistry can influence atmospheric composition on a global basis. The effect of auroral chemistry (not included in our models) on the global composition of Jupiter is currently poorly understood [see *Wong et al.*, 2000, 2003; *Friedson et al.*, 2002]; if auroral chemistry is found to influence abundances at latitudes other than the auroral regions, multidimensional models will be needed to track these compositional changes.

[32] Methane photolysis results in the production of the short-lived radicals CH, $^3CH_2$, $^1CH_2$, and CH_3, with pathways producing the latter two radicals being the most important at Ly α [e.g., *J. H. Wang et al.*, 2000]. Complex hydrocarbons are then formed largely through CH insertion reactions (e.g., R245, R251, R247, R249, R244, R254) and through radical-radical combination reactions (e.g., R287, R291, R299, R293, R295, R333, R296, R351), with C_2H and other radical insertion reactions (e.g., R316, R319, R290, R271, R266) also being important. Photodissociation (e.g., R20, R21, R37, R27, R32, R41, R68, R50, R64), cracking by atomic hydrogen (e.g., R195, R212, R209, R215, R203, R220), and disproportionation reactions (e.g., R294, R337) are the main mechanisms for destroying carbon-carbon bonds. Exchange and recycling reactions are prevalent and control the steady-state abundances of the major C, C_2, C_3, C_4 hydrocarbons in the model. Of all the methane destroyed by photolysis and other reactions in our Model A, ~49% is recycled, ~51% is permanently converted to C_2 hydrocarbons, and $\ll$1% is converted to higher-order hydrocarbons C_n, with $n \geq 3$. The corresponding values for Model B are ~59% of the methane is recycled, ~41% is converted to C_2 hydrocarbons, and $\ll$1% is converted to C_n hydrocarbons. The values for Model C are ~47% of the methane is recycled, ~53% is converted to C_2 hydrocarbons, and $\ll$1% is converted to C_n hydrocarbons. Note that the efficiency of CH_4 recycling versus the production of higher-order hydrocarbons depends on the pressure level at which the methane homopause is located. For a fixed reaction list, a methane homopause level at greater pressures leads to more efficient recycling of methane and less efficient production of C_2, C_3, C_4, and C_n hydrocarbons. The altitude profiles for the rates of the most important stratospheric reactions producing, destroying, and exchanging C, C_2, C_3, and C_4 hydrocarbons in Model A are shown in Figures 10, 11, 12, and 13.

[33] The volume mixing ratios of the major atmospheric constituents in our models are shown in Figure 14. The mixing ratios of all the model constituents are given in auxiliary material Table S4. Ethane, the most abundant product of methane photolysis on Jupiter, is produced predominantly from methyl-methyl recombination (R287: $2\ CH_3 + M \rightarrow C_2H_6 + M$). This reaction occurs throughout the stratosphere, with methane photolysis being responsible for the CH_3 production in the upper stratosphere and photosensitized CH_4 destruction via C_2H_2 photolysis contributing in the middle and lower stratosphere [see *Allen et al.*, 1980; *Gladstone et al.*, 1996; *Moses et al.*, 2000a]. Sequential addition of H atoms to unsaturated hydrocarbons, terminating with reactions R195 ($H + C_2H_5 \rightarrow 2\ CH_3$) and R287, helps produce and maintain C_2H_6 in the middle and lower stratosphere. Ethane is destroyed largely by photolysis, with a smaller contribution from CH insertion to form C_3H_6 (reaction R251) and reaction with C_2H to form C_2H_2 and C_2H_5 (reaction R323). Because the ultraviolet absorption cross sections for ethane drop sharply at wavelengths greater than 1600 Å, C_2H_6 is shielded from photolysis to a large extent by the more abundant CH_4 molecules. In fact, C_2H_6 loss processes are relatively inefficient in the Jovian stratosphere; ethane therefore has a long photochemical lifetime, and transport effects are important. The C_2H_6 molecules flow to the stagnant lower stratosphere and are removed mainly by diffusion through the lower boundary of our model.

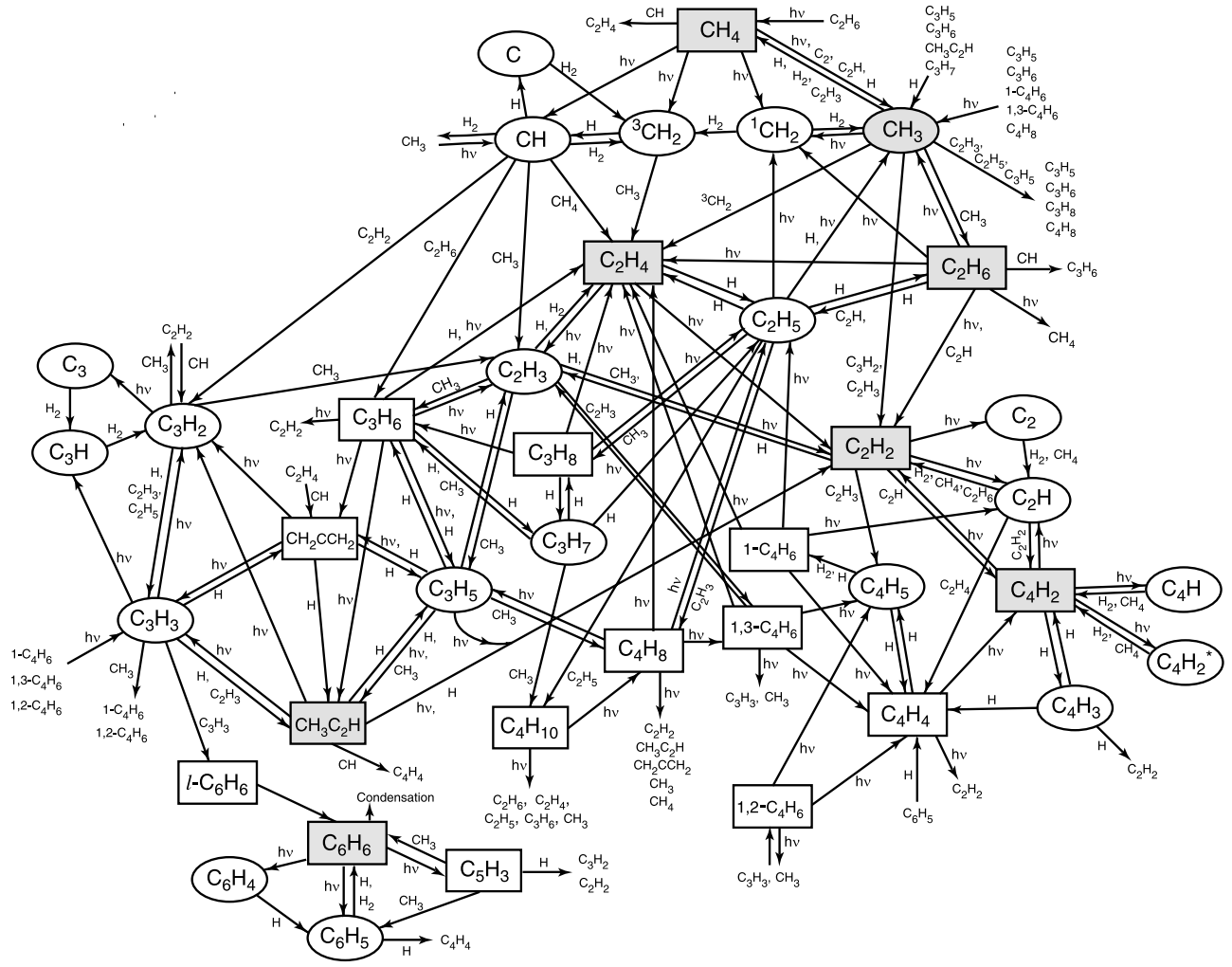

Figure 9. A schematic diagram illustrating the important reaction pathways for forming complex hydrocarbons in our "Model A" Jovian stratosphere (modified from *Moses et al.* [2004] (reprinted with permission) and *Moses et al.* [2000a]). The symbol hν corresponds to an ultraviolet photon, rectangles indicate stable molecules, and ovals indicate radicals. Shaded rectangles or ovals represent species that have been definitively identified in Jupiter's upper atmosphere.

[34] Ethylene is produced in the upper stratosphere through CH insertion into methane (reaction R245: CH + $CH_4 \rightarrow C_2H_4 + H$). In the middle and lower stratosphere for Models A and B and the lower stratosphere for Model C, C_2H_4 forms predominantly from the addition of H atoms with vinyl radicals (R192: $H + C_2H_3 + M \rightarrow C_2H_4 + M$), with an additional contribution from ethane photolysis. In Model C, reaction R328 ($C_2H_3 + H_2 \rightarrow C_2H_4 + H$) dominates C_2H_4 production in the 0.2–30 mbar region and is responsible for 37% of the total stratospheric production rate of C_2H_4. That contrasts with the situation in Models A and B, in which R328 accounts for only ~2% of the total column production of C_2H_4 in the stratosphere. Three-body addition of C_2H_4 with atomic H (R194) and C_2H_4 photolysis are responsible for most of the ethylene loss in the stratosphere. The C_2H_4 mixing ratio peaks in the upper stratosphere near $\sim 10^{-3}$ mbar because the dominant primary (i.e., non-recycling) production mechanism, R245, occurs preferentially in the methane photolysis region, because non-recycling production mechanisms are not very effective in the middle and lower stratosphere, and because permanent removal from the conversion of C_2H_4 to C_2H_6 and CH_4 occurs more effectively at the higher pressures found in the lower stratosphere.

[35] Acetylene is produced from the photolysis of C_2H_4 and C_2H_6 throughout the Jovian stratosphere and is lost through photolysis and three-body addition with H atoms. Unlike the situation for C_2H_4, however, C_2H_2 is recycled relatively efficiently in the middle and lower stratosphere due to reactions of the C_2H_2 photolysis products with H_2 and CH_4 (e.g., R313, R314) and due to reaction R191 ($H + C_2H_3 \rightarrow C_2H_2 + H_2$).

[36] The photochemistry of C_3 hydrocarbons at relevant Jovian stratospheric temperatures and pressures is less well understood than that of C_2 hydrocarbons. Laboratory data and theoretical investigations are relatively sparse in the published literature. Propane (C_3H_8) is predicted to be the most abundant C_3 hydrocarbon because it, like the other alkanes, is relatively stable in the hydrogen-dominated atmosphere and because it is better shielded from photolysis

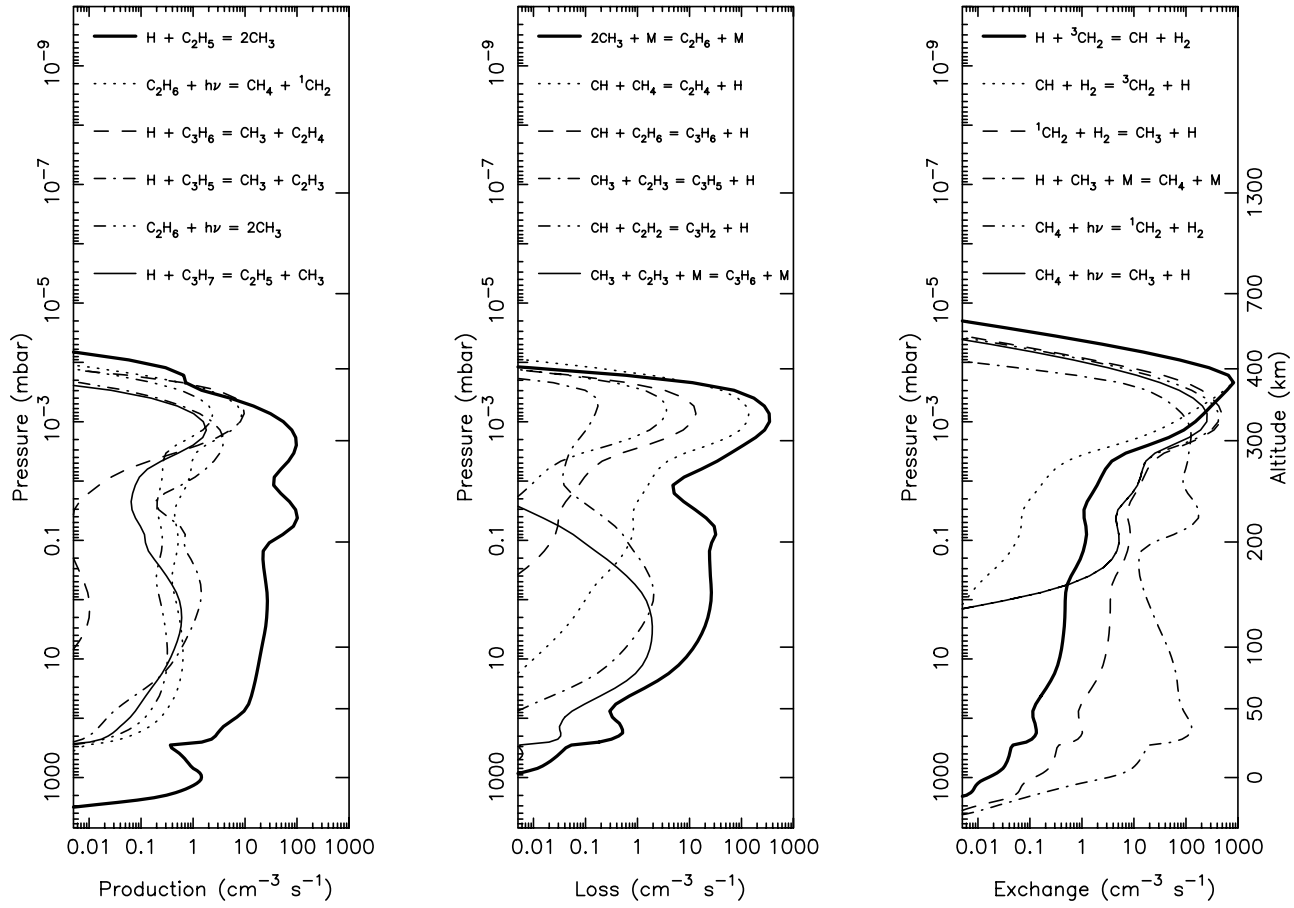

Figure 10. The reaction-rate profiles for the six most important reactions leading to the (left) production, (middle) loss, and (right) exchange of C_1 compounds in Model A. The reactions are listed in order of decreasing column rate in the stratosphere.

than are some of the unsaturated C_3 compounds. In our photochemical model, C_3H_8 is produced from the sequential addition of H atoms with unsaturated hydrocarbons (e.g., R213: $H + C_3H_6 + M \rightarrow C_3H_7 + M$, followed by R216: $H + C_3H_7 + M \rightarrow C_3H_8 + M$) and from methyl-ethyl combination (R293: $CH_3 + C_2H_5 + M \rightarrow C_3H_8 + M$). Propane is lost predominantly by photolysis. In our model, methylacetylene (CH_3C_2H) is produced mainly from the interconversion of other C_3 species rather than from direct production by C and C_2 hydrocarbons (see Figures 9 and 12, and the discussion of *Moses et al.* [2000a]). The three main reactions producing CH_3C_2H in our model stratospheres are R207 ($H + C_3H_5 \rightarrow CH_3C_2H + H_2$), R205 ($H + CH_2CCH_2 \rightarrow CH_3C_2H + H$), and R200 ($H + C_3H_3 \rightarrow CH_3C_2H + M$). Methylacetylene is lost through addition with atomic H (R204) and through photolysis. As with other unsaturated molecules in the model, the CH_3C_2H abundance is critically dependent on the atomic hydrogen abundance, and recycling reactions allow CH_3C_2H to survive longer than its photolysis rate would indicate.

[37] Diacetylene (C_4H_2) has been detected in the Jovian auroral regions by Cassini CIRS [*Kunde et al.*, 2004] but was not seen in ISO spectra from middle and lower latitudes [e.g., *Fouchet et al.*, 2000b]. Reaction of H with C_4H_3 (R221) is the dominant production mechanism; however, because the C_4H_3 derives mostly from C_4H_2 in the first place, this reaction is not considered a primary production mechanism. Photolysis of acetylene and the subsequent reaction of C_2H with C_2H_2 (R316) is the dominant primary (non-recycling) formation mechanism for diacetylene. Loss occurs through H-atom addition to form C_4H_3 and through photolysis. Recycling of C_4H_2 occurs in the middle and lower stratosphere through reactions R221, R47, and R356. Butane, the most abundant C_4 hydrocarbon in our model, is produced through reaction R303 ($CH_3 + C_3H_7 + M \rightarrow C_4H_{10} + M$) and reaction R345 ($2\ C_2H_5 + M \rightarrow C_4H_{10} + M$) and is lost via photolysis.

[38] The production and loss mechanisms for benzene (C_6H_6) are uncertain for conditions relevant to outer-planetary atmospheres (see the full discussion by *Wilson et al.* [2003] and *Lebonnois* [2005]). Reaction of acetylene with C_4H_5 to form benzene and hydrogen atoms (R383) will be ineffective at typical Jovian stratospheric temperatures [see *Westmoreland et al.*, 1989; *Wilson et al.*, 2003]. The addition of acetylene with C_4H_3 to form phenyl radicals (R381), a potential first step in benzene formation, is also likely to have a large energy barrier [e.g., *Westmoreland et al.*, 1989] that makes the reaction unimportant at Jovian temperatures. Propargyl-radical recombination (R351: $C_3H_3 + C_3H_3 + M \rightarrow l\text{-}C_6H_6 + M$) is relatively fast [e.g., *Fahr and Nayak*, 2000; *Atkinson and Hudgens*, 1999; *Morter et al.*, 1994; *Alkemade and Homann*, 1989], but

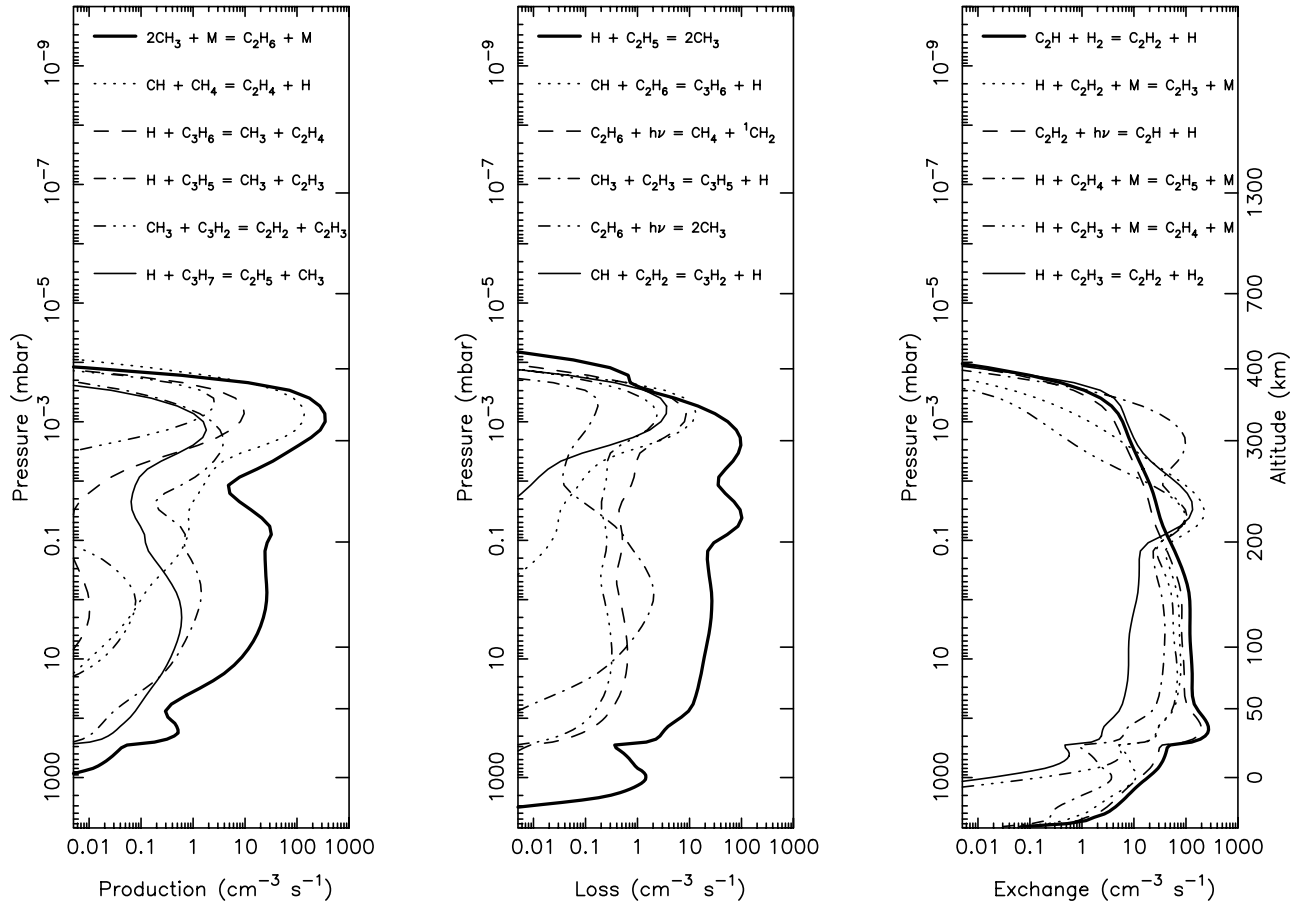

Figure 11. The reaction-rate profiles for the six most important reactions leading to the (left) production, (middle) loss, and (right) exchange of C_2 compounds in Model A. The reactions are listed in order of decreasing column rate in the stratosphere.

the reaction preferentially forms linear C_6H_6 isomers at laboratory pressures and temperatures of 67 mbar and 295 K [*Fahr and Nayak*, 2000]. However, a recent experimental study by *Howe and Fahr* [2003] demonstrates that the relative yields of different C_6H_6 isomers exhibit significant pressure and temperature dependencies. Benzene was observed to form preferentially at low pressures. For our model, we assume that R351 produces an unidentified linear C_6H_6 molecule, but that the *l*-C_6H_6 molecules then quickly isomerize to form benzene (R395: *l*-$C_6H_6 \rightarrow C_6H_6$), with a unimolecular rate constant of 10^3 s^{-1}. Therefore C_3H_3 recombination (R351) followed by isomerization of *l*-C_6H_6 to benzene (R395) is the dominant mechanism for producing benzene in our simulated Jovian stratosphere.

[39] Photolysis to form phenyl + H (R89) or $C_6H_4 + H_2$ (R90) are the dominant mechanisms that destroy benzene, but the photolysis products can react with H_2 and H to reform benzene. Recycling is not perfectly efficient, however, and some of the subsequent C_6H_4 and C_6H_5 reactions act to produce C_2 and C_4 hydrocarbons. As is discussed in section 2, we assume that benzene photolysis has a pressure dependence such that photoexcited "hot" benzene can be collisionally stabilized before being dissociated at the higher pressures found in the Jovian middle and lower stratosphere. In addition, benzene recycling is less efficient in the upper stratosphere. Benzene therefore has a peak concentration (at non-auroral latitudes) that is found lower in the stratosphere than is the case for most of the other hydrocarbons. At auroral latitudes, however, benzene is likely formed through ion chemistry initiated by the precipitation of auroral electrons [e.g., *Wong et al.*, 2000, 2003; *Friedson et al.*, 2002], and its peak concentration may be located in the upper stratosphere, where the precipitating electrons deposit the bulk of their energy.

4.2. Oxygen Photochemistry

[40] We add oxygen photochemistry to the model because it has a slight influence on the abundance of unsaturated hydrocarbons; the relevant reactions are taken from *Moses et al.* [2000b]. The external oxygen is assumed to derive from ablated micrometeoroids and is assumed to be released in the upper atmosphere in the form of CO, H_2O, and CO_2 (see section 2 and *Moses et al.* [2000b]). Unlike the situation for Saturn, the influx of water itself seems to be a minor component of the total oxygen influx on Jupiter [cf. *Lellouch et al.*, 2002; *Bézard et al.*, 2002a; *Moses et al.*, 2000b], and we assume the H_2O influx rate is much smaller than the CO influx rate. Although we cannot rule out a chemical difference that takes place during ablation, it seems likely that cometary impacts (including SL9) domi-

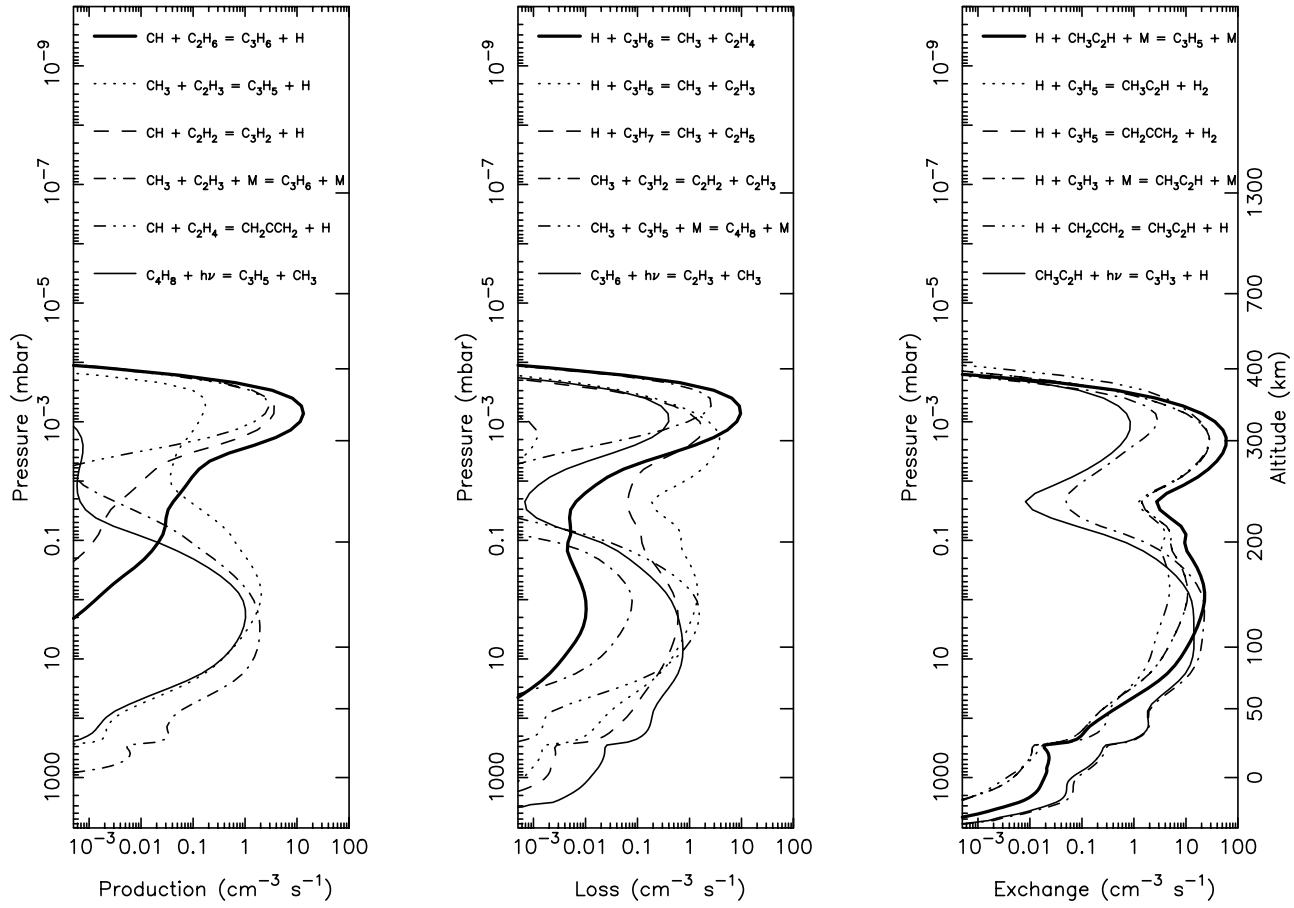

Figure 12. The reaction-rate profiles for the six most important reactions leading to the (left) production, (middle) loss, and (right) exchange of C_3 compounds in Model A. The reactions are listed in order of decreasing column rate in the stratosphere.

nate the delivery of oxygen compounds to Jupiter, whereas ring-derived material may play an important role on Saturn [*Bézard et al.*, 2002a; *Lellouch et al.*, 2002].

[41] Water vapor is lost by photolysis above and by condensation below ~10 mbar. The photolysis lifetime for H_2O is ~2 months at the top of the atmosphere but increases to ~5 months at 1 mbar due to shielding by CH_4 and other hydrocarbons. The primary photolysis products are OH + H (R104). The OH reacts with H_2, C_2H_6, and CH_4 to efficiently recycle the water, and the effective lifetime of H_2O is therefore much greater than its photolysis rate would indicate. Less than 1% of the total column loss of OH in the stratosphere goes to permanently converting the H_2O to CO through three-body addition reactions of OH with C_2H_2 or C_2H_4, followed by reactions that eventually produce CO [see *Moses et al.*, 2000b].

[42] Meteoritic carbon dioxide is assumed to be introduced directly into the upper atmosphere in our model. About 12% (Model C) to 15% (Model A) of the total column production rate of CO_2 in the stratosphere is due to the reaction of OH with CO (R463). Note that we are not specifically modeling the Shoemaker-Levy 9 impact debris here. Most of the CO_2 produced from photochemistry of the impact debris is expected to derive from reaction R463, with the OH produced from photolysis of comet-derived H_2O reacting with the abundant CO produced during the plume splashback phase of the impacts [*Lellouch et al.*, 2002; *Moses*, 1996]. CO_2 is lost primarily by photolysis.

[43] Through high-resolution observations of a CO band near 4.7 μm, *Bézard et al.* [2002a] have determined that external sources aside from SL9 have provided a CO column of $4^{+3}_{-2} \times 10^{16}$ molecules cm^{-2} on Jupiter. An internal CO source is also required to account for the ~1 ppb mixing ratio in the troposphere; however, the mixing ratio is observed to increase from the troposphere to the stratosphere due to the external source. CO is extremely stable on the giant planets. Photolysis is ineffective due to shielding by H_2 and CH_4. Chemical loss processes are also inefficient due to the strong carbon-oxygen bond. Three-body addition of CO with H to form HCO and reaction of CO with OH to form CO_2 + H both occur in our model, but in both cases, CO is efficiently recycled by subsequent reactions. Diffusion is primarily responsible for removing CO from the stratosphere. With our eddy diffusion coefficient profiles, the models generate a CO column of 4×10^{16} cm^{-2} above the 100 mbar level for external CO influx rates of 4×10^6 molecules cm^{-2} s^{-1}.

[44] Small amounts of other oxygen species are produced through the photolysis and subsequent reaction of meteoritic CO, H_2O, and CO_2. Moderate, but currently unobservable, amounts of HCO, H_2CO, CH_3OH, H_2CCO, and CH_3CHO are produced in the Jovian stratosphere (see *Moses et al.*

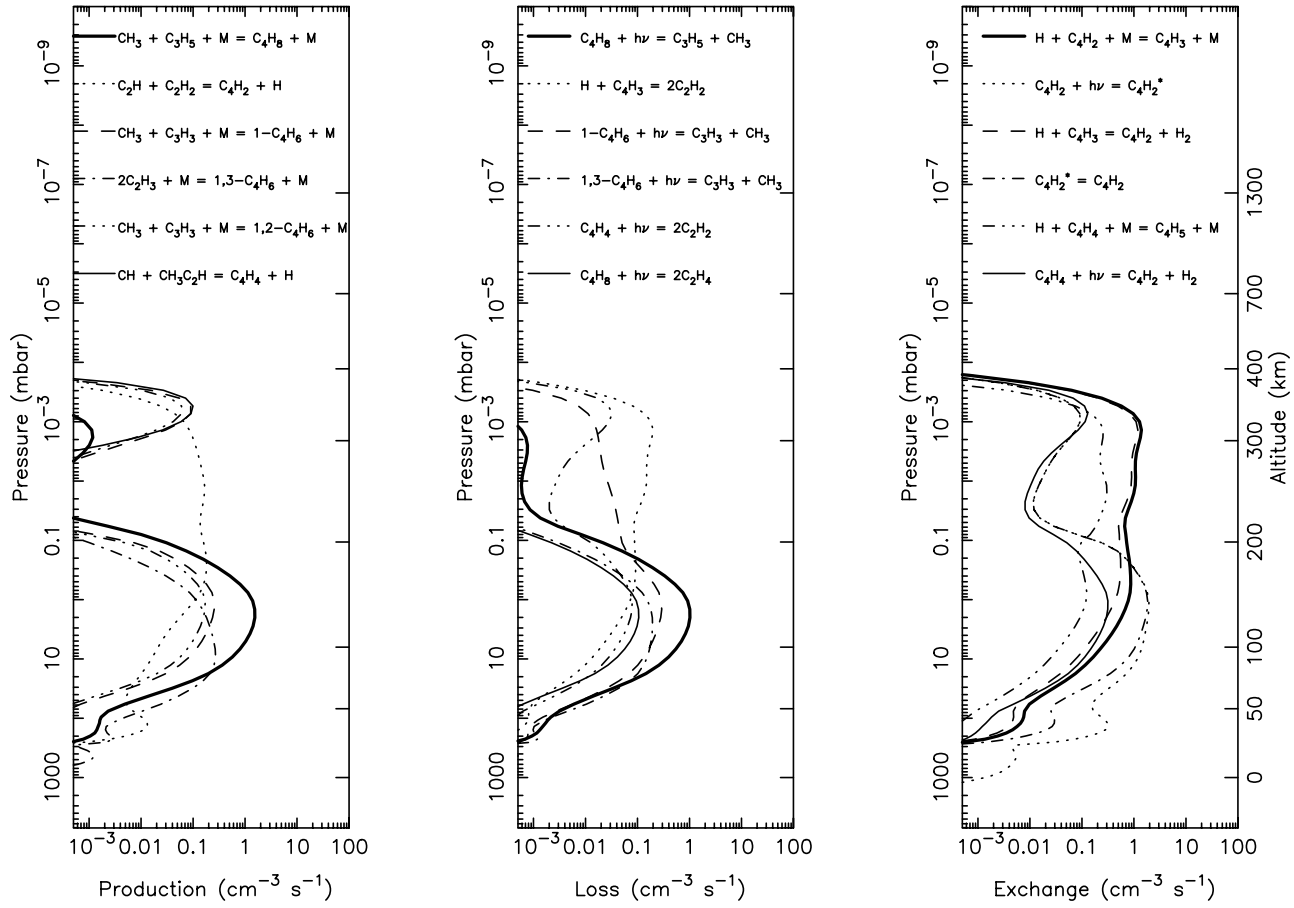

Figure 13. The reaction-rate profiles for the six most important reactions leading to the (left) production, (middle) loss, and (right) exchange of C_4 compounds in Model A. The reactions are listed in order of decreasing column rate in the stratosphere.

[2000b] for details on the production and loss of these species).

[45] Our models are designed to represent rough global averages, whereas observations of H_2O and/or CO_2 by the Submillimeter Wave Astronomy Satellite (SWAS), by ISO, and by Cassini/CIRS demonstrate that the distribution of these species is complicated; CO_2 is very inhomogeneous across Jupiter (more prevalent in the southern hemisphere), and H_2O is likely confined to pressures less than a few tenths of a mbar and may be globally inhomogeneous as well [e.g., *Bergin et al.*, 2000; *Lellouch et al.*, 2002; *Kunde et al.*, 2004]. Therefore global-average and 1-D models of oxygen compounds are not very meaningful for Jupiter in the post-SL9 era. *Lellouch et al.* [2002] provide model-data comparisons that suggest that H_2O and CO_2 originate from the deposition of oxygen compounds during the plume splashback phase of the 1994 Comet Shoemaker-Levy 9 impacts and that the current distribution of both these species is controlled by a combination of atmospheric transport and photochemistry. However, the CO_2 distribution predicted by Lellouch et al. does not resemble in detail the distribution determined by the high-spatial-resolution CO_2 spectra acquired by CIRS during the Cassini flyby [*Kunde et al.*, 2004]; the CIRS observations show that CO_2 is confined to very high southern latitudes. *Kunde et al.* [2004] suggest that either some kind of auroral oxygen input interacting with SL9 debris is responsible for the unusual distribution, or that stratospheric transport processes are controlling the distribution. *Lellouch et al.* [2005] favor the latter scenario.

4.3. Sensitivity to *K* Profile

[46] As is discussed in section 3, the eddy diffusion coefficient profile in Jupiter's stratosphere is not well constrained. K_h, the value of the eddy diffusion coefficient at the methane homopause, is particularly uncertain, with the results from the Voyager and EUVE He 584 Å emission data and those from the UVS occultation data appearing mutually inconsistent. Additional observations or a reanalysis of existing observations (e.g., the Voyager UVS occultation data with Galileo probe temperature constraints in mind) are required before this discrepancy can be resolved. Alternatively, the methane homopause level may be highly variable with location across the planet; the UVS occultation data sample a discrete region of the planet at a single time, whereas the He 584 Å emission data span a wide range of years and have varying spatial resolution.

[47] *Gladstone et al.* [1996] [see also *Moses et al.*, 2000a; *Summers and Strobel*, 1989; *Romani and Atreya*, 1988] have performed general sensitivity studies to illustrate how hydrocarbon mixing ratios change with such factors as the overall magnitude of K_h, the slope of the eddy diffusion coefficient, and the tropospheric eddy diffusion coefficient. We will not repeat those sensitivity studies here. Instead, we

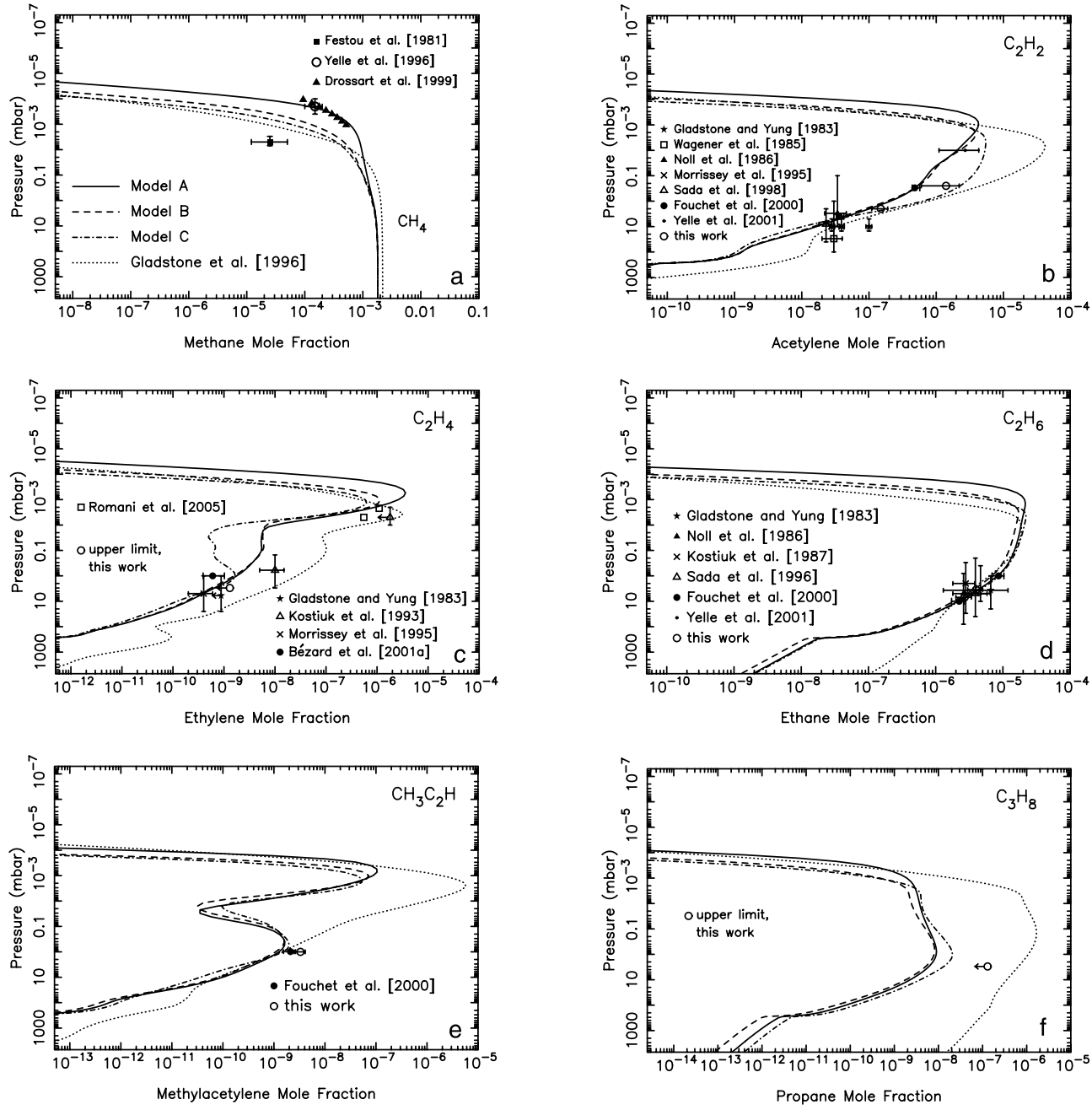

Figure 14. The volume mixing ratios of (a) CH_4, (b) C_2H_2, (c) C_2H_4, (d) C_2H_6, (e) CH_3C_2H, (f) C_3H_8, (g) C_4H_2, (h) C_4H_{10}, (i) C_6H_6, (j) CH_3, (k) H_2O, (l) CO, (m) CO_2, and (n) H and He in our models are shown as a function of pressure and are compared with various observations. The results from Model A (solid line), Model B (dashed line), and Model C (dot-dashed line) are plotted along with the results from *Gladstone et al.* [1996] (dotted line). The data points with associated error bars represent observational measurements, as labeled.

show in Figure 15 how the mixing ratio profile of the long-lived C_2H_6 molecule changes for a few specific assumptions about the K profile. For these tests, we use the same chemical reaction list and the same altitude-pressure-temperature grid; only the K profile is changed. Figure 15 shows how our Models A and B compare with models developed using the K profile expressions of *Gladstone et al.* [1996] and *Young et al.* [2005]; note that the high-altitude discrepancy between the exact Gladstone et al. K profile shown in Figure 7 and the profile shown in Figure 15 is due to our adoption of different thermospheric temperature profiles.

[48] One apparent result from Figures 14 and 15 is that the adoption of a lower value of K_h restricts CH_4 and its photochemical products to high pressures (lower altitudes). The main consequence of methane being photolyzed at higher pressures is more efficient recycling of CH_4 via reaction R186 and a corresponding reduction in the produc-

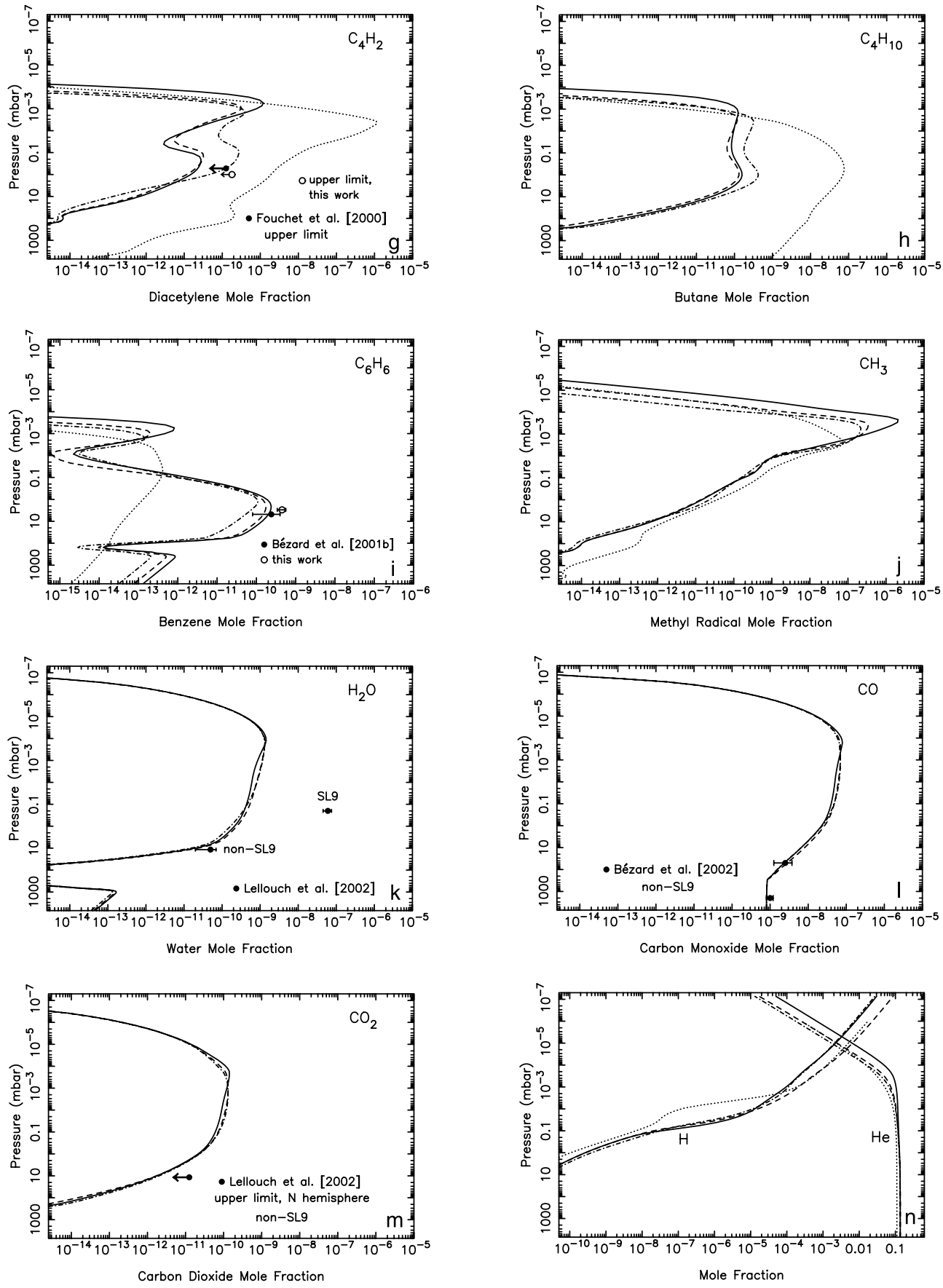

Figure 14. (continued)

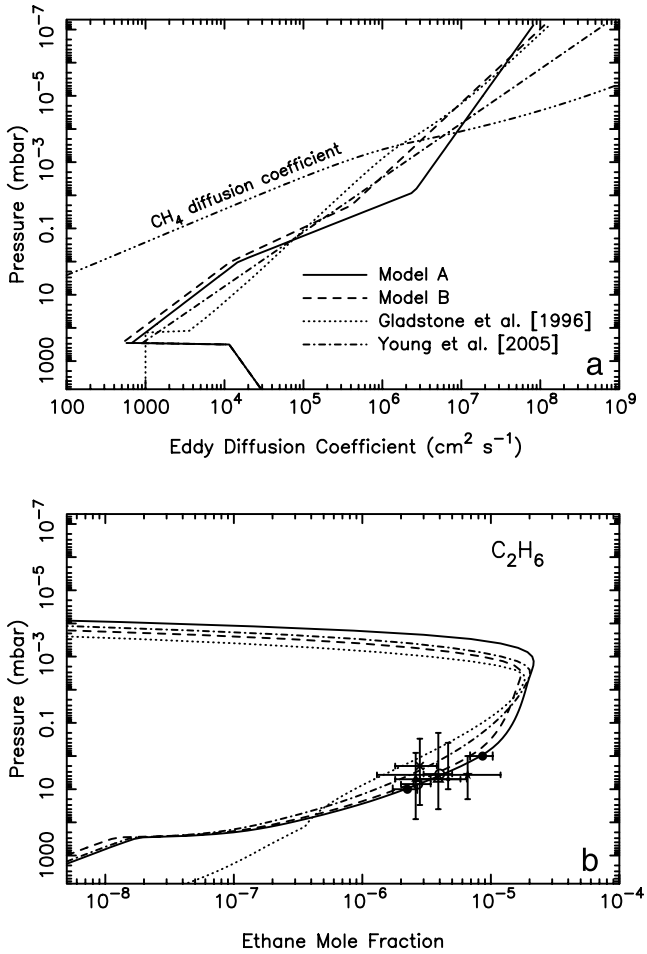

Figure 15. The sensitivity of the C_2H_6 ratio to the eddy diffusion coefficient profile for four different models that have the same chemical reaction list as Models A and B but that have different K profiles. Figure 15a shows the diffusion coefficients used in the four different models, along with the methane molecular diffusion coefficient (triple-dot-dashed line). Figure 15b shows the C_2H_6 mixing ratio profiles for these four different models. In both panels, the solid line represents Model A, the dashed line represents Model B, the dotted line represents a model that uses the favored K profile from *Gladstone et al.* [1996], and the dot-dashed line represents a model that uses the K profile from *Young et al.* [2005]. Note that smaller eddy diffusion coefficients in the lower stratosphere lead to larger ethane abundances; however, the location of the methane homopause also has an effect on the ethane abundance in the lower stratosphere (compare Models A and B).

tion rate of higher-order hydrocarbons. The eddy diffusion coefficients for Model B (with its lower value of K_h) then needed to be smaller than those for Model A in the middle and lower stratosphere in order to provide enough C_2H_6 to remain consistent with the ISO observations. The *Gladstone et al.* [1996] favored expression for $K(z)$ has a low K_h and a relatively large value of K in the lower stratosphere; this model greatly underpredicts the C_2H_6 abundance in Jupiter's stratosphere using our reaction scheme. Other reaction schemes [e.g., *Gladstone et al.*, 1996; *Lebonnois*, 2005] are able to deliver a decent fit to C_2H_6 observations using the *Gladstone et al.* [1996] eddy diffusion coefficient profile; however, C_2H_2 is then overpredicted compared with observations. The model using the *Young et al.* [2005] profile, which was developed to investigate gravity waves in Jupiter's stratosphere (and to determine whether diffusive filtering theory could be used to predict eddy diffusion coefficients), has a higher value of K_h, yet the value of K in the lower stratosphere is insufficient (assuming the Model A and B chemistry is correct) to account for the amount of C_2H_6 observed by ISO. We can use this result, along with comparisons with Model C, to place rough limits on the value of K in Jupiter's lower stratosphere. If our updated chemistry is correct, then K_{min} must be less than 1000 cm^2 s^{-1} and K must be less than $\sim 3 \times 10^4$ cm^2 s^{-1} at pressures greater than 1 mbar to remain consistent with the observed C_2H_6 abundance. In addition, the lower the assumed value of K_h, the smaller that K must be in the lower stratosphere to remain consistent with observations.

4.4. Sensitivity to Reaction Rates

[49] Although many of the reactions in our model have been studied at room temperature or higher, information at the low temperatures relevant to the Jovian stratosphere is frequently not available. In addition, measurements are often presented only at the high-pressure limit, whereas elucidating the rate behavior at low pressures is particularly important for our stratospheric study. We now examine the sensitivity of the model results to some key reaction rate coefficients that have not been well defined at low temperatures and/or pressures.

[50] Reaction R190 ($H + C_2H_2 + M \rightarrow C_2H_3 + M$) strongly affects the abundance of H atoms and consequently some of the unsaturated hydrocarbons in our model Jovian stratosphere. Many experimental data for this reaction are available in the literature for the temperature range ~200–1000 K. However, the rate coefficients, and especially the pressure-dependent behavior, are uncertain at temperatures below 200 K. Figure 3 illustrates how our adopted rate-coefficient expressions for R190 compare with the pressure- and temperature-dependent laboratory measurements of *Payne and Stief* [1976]. For Models A and B, we have adopted the standard expression of *Baulch et al.* [1994], which provides a reasonable but slightly low fit to the *Payne and Stief* [1976] data at high pressures and all temperatures in the 193–400 K range. For Model C, we have adopted an expression that provides a better fit to the data (see Figure 3). Recent theoretical calculations by *Miller and Klippenstein* [2004] suggest that our expression for Model C may also underestimate the rate coefficient for R190, especially at high temperatures and pressures. Although the two-dimensional master-equation calculations of *Miller and Klippenstein* [2004] are very useful in describing the nature of this reaction, the pressure dependence of the reaction is complicated, and their results have been cast in a form similar to our equations (1) and (2) only for pressures greater than 1 torr (1.333 mbar) and for temperatures greater than 300 K. In addition, no results relevant to Jovian stratospheric temperatures are presented at all. Their results are therefore difficult to incorporate into our model. The expressions for k_0, k_∞, and F_c that they provide (on their p. 1200) were not designed to be valid at low pressures and

temperatures; however, their expressions lead to rates coefficients that compare reasonably well with the *Payne and Stief* [1976] data in the pressure falloff regime at temperatures of 193–298 K.

[51] Miller and Klippenstein have recently extended the calculations of *Miller and Klippenstein* [2004] to temperatures as low as 100 K (G. P. Smith, personal communication, 2004). They find that k_0 for R190 continues to increase with decreasing temperature, and their results at 165 K, a typical Jovian stratospheric temperature, provide a rate coefficient that is higher at low pressures than any of the expressions we are currently adopting in our models. We use these results (G. P. Smith, personal communication, 2004), along with the data presented by *Miller and Klippenstein* [2004] and *Payne and Stief* [1976] to derive a new "theoretical" expression for R190 that has a much higher k_0 at low temperatures. The new expression is $k_{\infty,190} = 4.216 \times 10^{-17}\ T^{2.158}\ e^{(-986/T)}$ cm^3 s^{-1}; $k_{0,190} = 5.418 \times 10^{-20}\ T^{-4.579}\ e^{(-311/T)}$ cm^6 s^{-1} for $T \leq 228$ K; $k_{0,190} = 1.542 \times 10^{-43}\ T^{4.199}\ e^{(1184/T)}$ cm^6 s^{-1} for $T > 228$ K; $F_c = 0.21e^{(0.0025T)}$.

[52] Figure 16 shows how the model results are affected by changes in the rate coefficients for R190. Note that R190 does not have much effect on C_2H_6 abundances or even on C_2H_2 abundances, but it does have a substantial effect on H atom abundances and on those species (mostly unsaturated hydrocarbons) that are strongly affected by H atom abundances. The big uncertainty in the rate coefficient for R190 is k_0 and the pressure dependence of the reaction in the falloff regime. The values for k_∞ are better constrained. Experimental measurements of $k_{0,190}$ at temperatures of 100–200 K are greatly needed to help constrain models of outer-planet photochemistry.

[53] Reactions R191 ($H + C_2H_3 \rightarrow C_2H_2 + H_2$) and R192 ($H + C_2H_3 + M \rightarrow C_2H_4 + M$) that deal with the reaction of H with vinyl radicals are of particular importance to Jovian photochemical models because their relative efficiency helps control whether unsaturated hydrocarbons like C_2H_2 or C_2H_4 can be readily converted to C_2H_6 or whether the C_2H_6/C_2H_2 ratio will remain low. Theoretical calculations by *Klippenstein and Harding* [1999b] suggest that the abstraction branch (R191) dominates the total reaction such that the addition reaction (R192) accounts for $\lesssim$1% of the total reaction at temperatures of 100–300 K and 1 torr total pressure. If true, then an effective pathway for the conversion of ethylene and acetylene to ethane is eliminated in outer-planetary stratospheres. However, from discharge-flow kinetic experiments, *Monks et al.* [1995] derive branching ratios for the addition of H with deuterated vinyl radicals at 213 and 298 K and 1 torr that are more than an order of magnitude higher than those estimated by *Klippenstein and Harding* [1999b]. Even these higher branching ratios for R192 might not be large enough to make the above mentioned conversion scheme viable. To produce a model that has a C_2H_6/C_2H_2 ratio consistent with observations, we have assumed in Models A and B that R192 can compete with R191 at low temperatures. Our adopted expressions for R191 and R192 in Models A and B are $k_{191} = 1.5 \times 10^{-12}\ T^{0.5}$ cm^3 s^{-1}, $k_{0,192} = 2.3 \times 10^{-24}\ T^{-1}$ cm^6 s^{-1}, $k_{\infty,192} = 1.8 \times 10^{-10}$ cm^3 s^{-1}. These expressions fit the total rate for the $H + C_2H_3$ reaction as determined by *Monks et al.* [1995] and *Fahr* [1995]; however, the R192 branching ratio of 0.8 at 213 K, 1 torr is a factor of $\sim$3 larger than that determined by *Monks et al.* [1995] for $H + C_2D_3$. Our chemistry adopted for Model C is quite different from Models A and B, and R192 is not as important for keeping the C_2H_2/C_2H_6 ratio within observational constraints. Our adopted expressions for R191 and R192 in Model C have branching ratios and a total rate for R191 + R192 that are much more consistent with *Klippenstein and Harding* [1999b]. However, our expressions in Model C show no pressure dependence at 213 and 298 K for pressures ranging from 1–100 torr, a conclusion that is at odds with the combined data of *Fahr* [1995] and *Monks et al.* [1995] but that is consistent with the theoretical conclusions of *Klippenstein and Harding* [1999b].

[54] Figure 17 shows how different assumptions about the rate coefficients for R191 and R192 affect species abundances. The solid line represents Model A. The dot-dashed line represents a model that has the same chemistry as Model A, but the rate coefficients are compiled from recommendations from *Monks et al.* [1995], *Fahr* [1995], and *Durán et al.* [1988]: $k_{191} = 7.6 \times 10^{-11}$ cm^3 s^{-1}, $k_{0,192} = 5.76 \times 10^{-24}\ T^{-1.3}$ cm^6 s^{-1}, and $k_{\infty,192} = 8.9 \times 10^{-10}\ e^{(-494/T)}$ cm^3 s^{-1}. The resulting R192 branching ratio for this model is 0.36 at 298 K, 1 torr and 0.35 at 213 K, 1 torr, compared with the corresponding values determined by *Monks et al.* [1995] of 0.33 and 0.24 for the addition of $H + C_2D_3$. The dashed line represents a model that has the same chemistry as Model A, but the relative efficiency of R191 and R192 is more consistent with the predictions of *Klippenstein and Harding* [1999b]. In this model, $k_{0,192} = 1.49 \times 10^{-26}\ T^{-1}$ cm^6 s^{-1}, $k_{\infty,192} = 7.0 \times 10^{-11}\ T^{0.18}$ cm^3 s^{-1}, and $k_{191} = k_{\infty,192} - k_{192}[M]$, and the R192 branching ratio is 0.015 at 213 K, 1 torr and 0.11 at 213 K, 10 torr, compared with the corresponding calculated values from *Klippenstein and Harding* [1999b] of 0.003 and 0.11. Throughout the stratospheric region of interest, R191 dominates over R192 with this model. The dotted line represents a model that has the same chemistry as Model A, except the rate coefficients for R191 and R192 are taken from *Moses et al.* [2000a]: $k_{191} = 2.0 \times 10^{-11}$ cm^3 s^{-1}, $k_{0,192} = 5.5 \times 10^{-27}$ cm^6 s^{-1}, and $k_{\infty,192} = 1.82 \times 10^{-10}$ cm^3 s^{-1}. The R192 branching ratio at 213 K, 1 torr in this model is 0.76.

[55] Figure 17 demonstrates that the more efficient that reaction R191 is compared with R192, the greater the stratospheric abundance of C_2H_2 and other heavier hydrocarbons. The effect on C_2H_4 is complicated and depends on both the absolute rate of R191 + R192 as well as the R191/R192 ratio. In general, the more efficient that reaction R191 is compared with R192, the smaller the abundance of C_2H_4 in the middle stratosphere, the region probed by the infrared observations.

[56] Reaction R194 ($H + C_2H_4 + M \rightarrow C_2H_5 + M$) is another reaction that can affect the C_2H_2/C_2H_6 ratio on the outer planets because it is one of the intermediate reactions in the sequential addition of hydrogen to unsaturated hydrocarbons. As with many of the reactions in our list, reaction R194 has been well studied at 200 K and higher, but information at low temperatures is sparse. Figure 18 illustrates how changes in the rate coefficient for R194 affect species abundances. The solid lines represent Model A, in which the rate coefficients are taken from the data compilations of *Baulch et al.* [1994], except a limit of $k_0 = 3.7 \times 10^{-30}$ cm^6 s^{-1} is placed on the low-pressure limiting rate

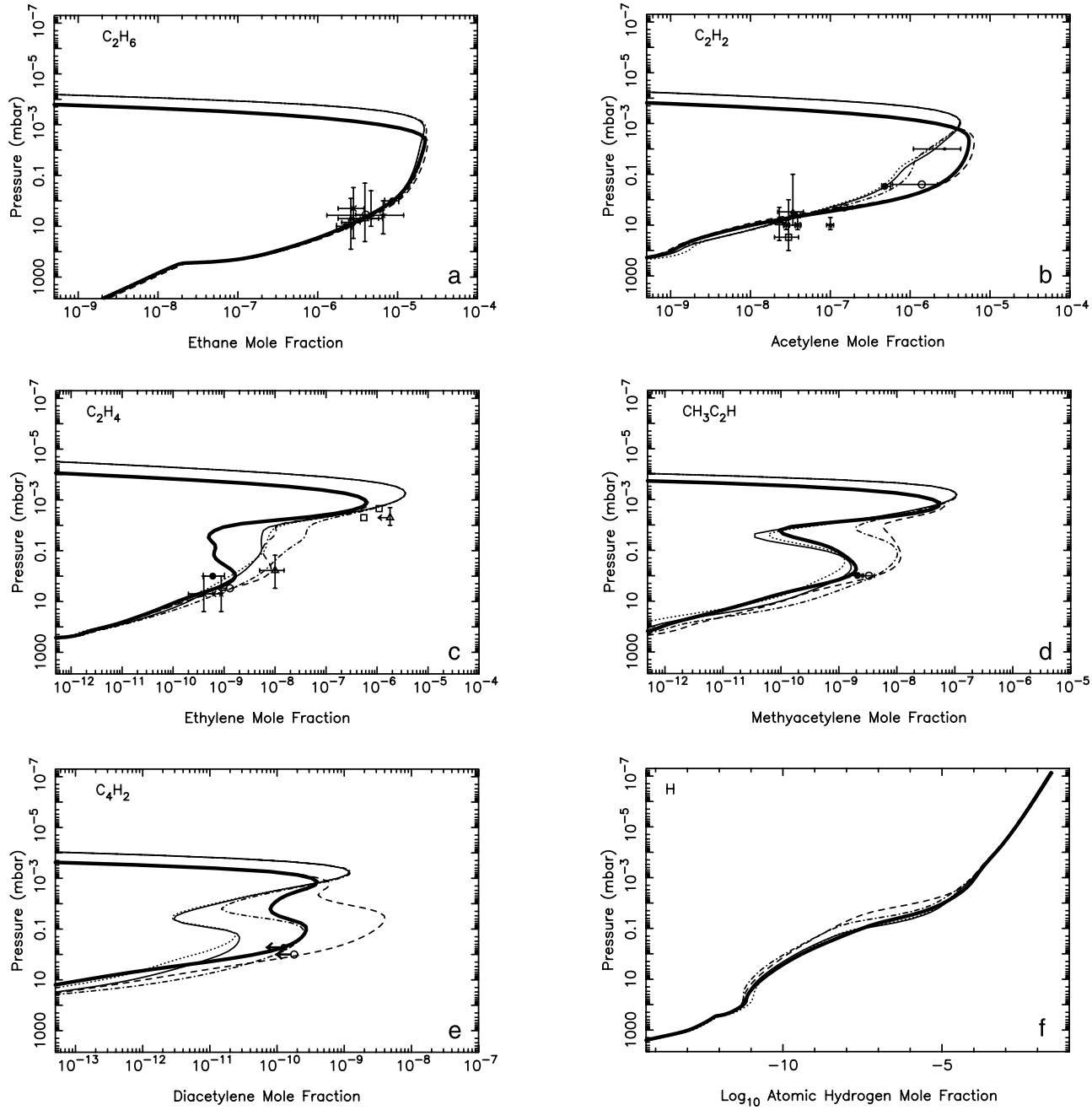

Figure 16. The sensitivity of the mixing ratio profiles of (a) C_2H_6, (b) C_2H_2, (c) C_2H_4, (d) CH_3C_2H, (e) C_4H_2, and (f) H to the rate coefficient for reaction R190 ($H + C_2H_2 + M \rightarrow C_2H_3 + M$). The thick solid line represents Model C; the dashed line represents a model with the same chemistry as Model C, except our new theoretical expression for k_{190} is used (see text); the thin solid line represents Model A; the dot-dashed line represents a model with the same chemistry as Model A, except our new theoretical expression for R190 is used; and the dotted line represents Model A, except the expression of *Miller and Klippenstein* [2004, p. 1200] is used.

coefficient below 302.4 K. The dot-dashed lines represent a model that has the same chemistry as Model A, except F_c = 0.6 and rate coefficient expressions from *Lightfoot and Pilling* [1987] are adopted: $k_{194,0} = 1.39 \times 10^{-29}\ e^{(-569/T)}$ cm^6 s^{-1}, and $k_{194,\infty} = 4.56 \times 10^{-11}\ e^{(-1134/T)}$ cm^3 s^{-1}. These expressions, in combination with equations (1) and (2), provide a rate coefficient in the falloff pressure regime that is generally lower than available data. The dashed lines represent a model that has the same chemistry as Model A, except the Model C rate coefficient expressions are used: $k_{0,194} = 1.68 \times 10^{-38}\ T^{2.87}\ e^{(923/T)}$ cm^6 s^{-1} (fit to data), $k_{\infty,194} = 6.6 \times 10^{-15}\ T^{1.28}\ e^{(-650/T)}$ cm^3 s^{-1} [*Baulch et al.*, 1994], and $F_c = 0.24e^{(-T/40)} + 0.76e^{(-T/1025)}$ [*Baulch et al.*, 1994]. The rate coefficients derived from this expression are consistent with the He-bath-gas data of *Lightfoot and Pilling* [1987] in the 285–604 K range. The recent theoretical

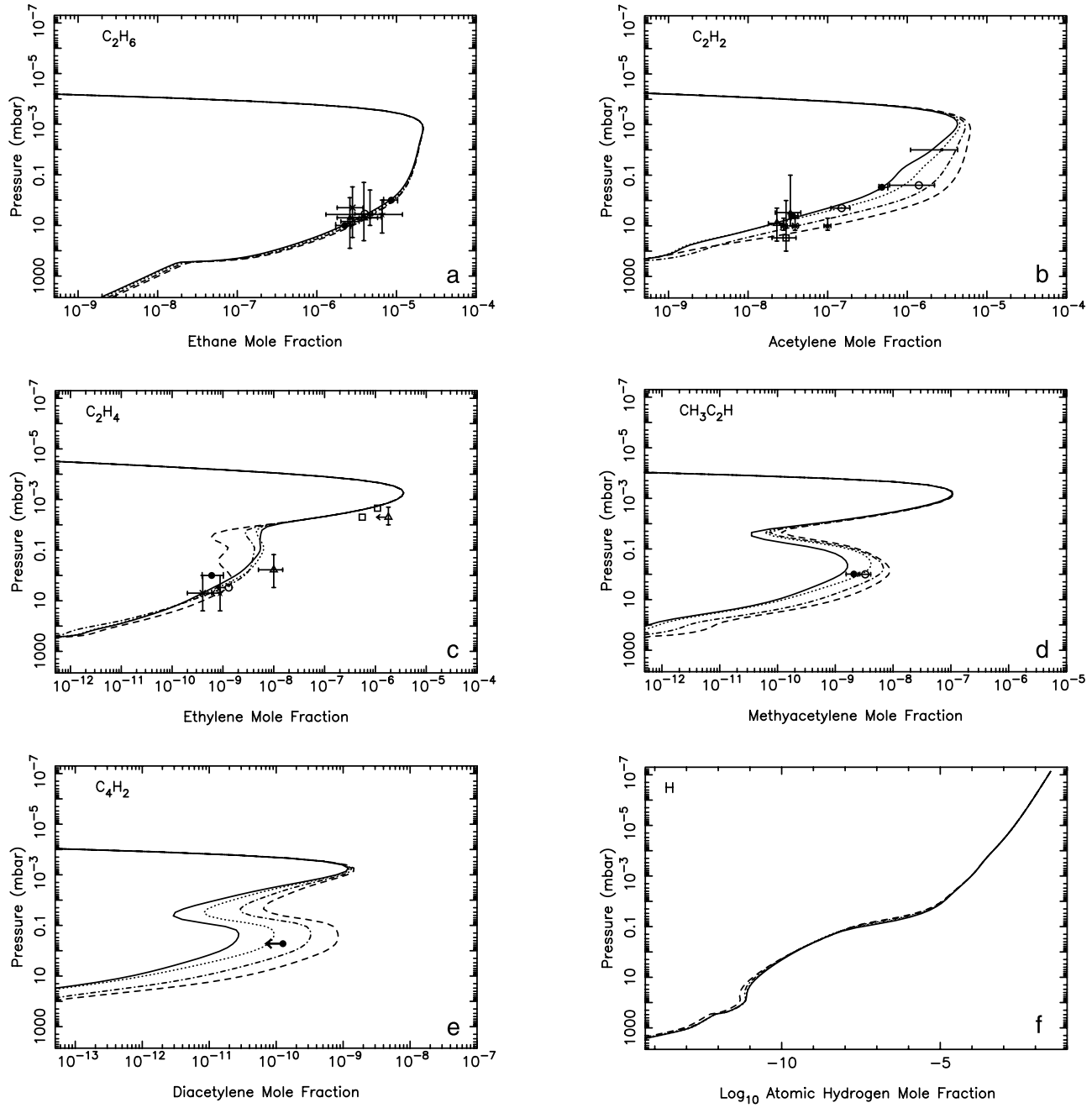

Figure 17. The sensitivity of the mixing ratio profiles of (a) C_2H_6, (b) C_2H_2, (c) C_2H_4, (d) CH_3C_2H, (e) C_4H_2, and (f) H to the rate coefficient for reactions R191 ($H + C_2H_3 \rightarrow C_2H_2 + H_2$ and R192 ($H + C_2H_3 + M \rightarrow C_2H_4 + M$). The solid line represents Model A. The dot-dashed line represents a model that has the same chemistry as Model A, except for the rate coefficients $k_{191} = 7.6 \times 10^{-11}$ cm^3 s^{-1}, $k_{0,192} = 5.76 \times 10^{-24}\ T^{-1.3}$ cm^6 s^{-1}, and $k_{\infty,192} = 8.9 \times 10^{-10}\ e^{(-494/T)}$ cm^3 s^{-1}. The dashed line represents a model that has the same chemistry as Model A, except the rate coefficients $k_{0,192} = 1.49 \times 10^{-26}\ T^{-1}$ cm^6 s^{-1}, $k_{\infty,192} = 7.0 \times 10^{-11}\ T^{0.18}$ cm^3 s^{-1}, and $k_{191} = k_{\infty,192} - k_{192}[M]$. The dotted line represents a model that has the same chemistry as Model A, except $k_{191} = 2.0 \times 10^{-11}$ cm^3 s^{-1}, $k_{0,192} = 5.5 \times 10^{-27}$ cm^6 s^{-1}, and $k_{\infty,192} = 1.82 \times 10^{-10}$ cm^3 s^{-1}.

calculations for this reaction by *Miller and Klippenstein* [2004] have been extended to low temperatures (G. P. Smith, personal communication, 2004); the low-temperature calculations suggest that our Model C expression may underestimate k_0 slightly and that the reaction rate coefficient is difficult to fit over a large temperature range using equations like (1) and (2). The dotted line represents a model that has the same chemistry as that for the dashed line, except k_0 has been increased by a factor of three.

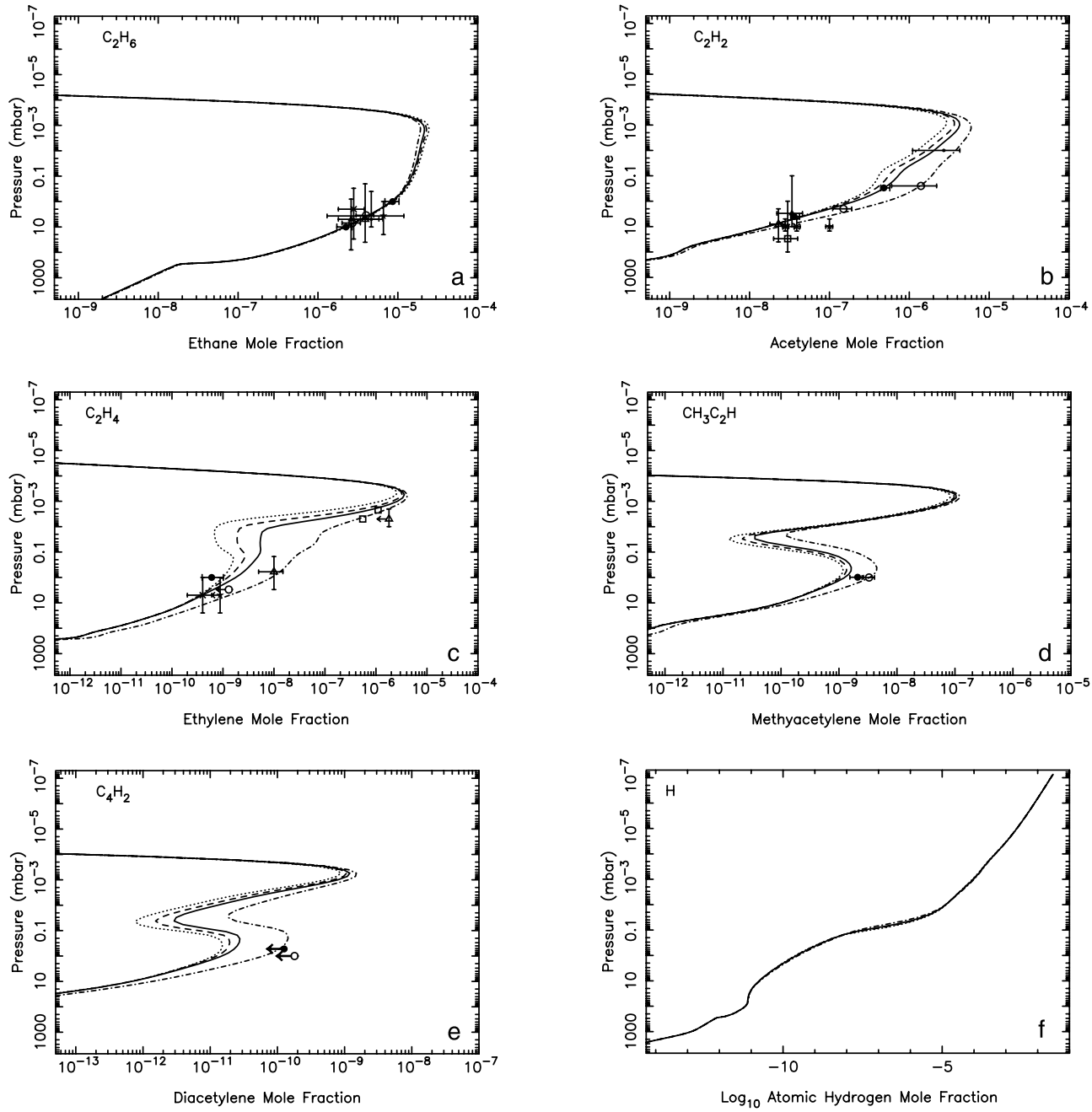

Figure 18. The sensitivity of the mixing ratio profiles of (a) C_2H_6, (b) C_2H_2, (c) C_2H_4, (d) CH_3C_2H, (e) C_4H_2, and (f) H to the rate coefficient for reaction R194 ($H + C_2H_4 + M \rightarrow C_2H_5 + M$). See text for a description of the different models and their corresponding line styles in the figure.

[57] Figure 18 demonstrates that the larger the value of k_{194}, the smaller the abundance of C_2H_2, C_2H_4, CH_3C_2H, and C_4H_2 in our model atmosphere. The effect on atomic hydrogen, however, is much smaller than that of R190 ($H + C_2H_2$).

[58] The reaction of atomic H with C_3H_5 radicals is very important in our models, not only for C_3H_x chemistry and abundances, but also for C_2H_x abundances. The main production mechanism for C_3H_5 radicals in our model is reaction R204 ($H + CH_3C_2H + M \rightarrow C_3H_5 + M$). The C_3H_5 isomer produced in this reaction is CH_3CCH_2 rather than the more thermodynamically stable allyl radical [*Wagner and Zellner*, 1972; *B. Wang et al.*, 2000]. Although there are several reports of H + allyl kinetics in the literature because of that reaction's importance in combustion studies [e.g., *Harding and Klippenstein*, 2000; *Baulch et al.*, 1994; *Hanning-Lee and Pilling*, 1992; *Tsang*, 1991; *Allara and Shaw*, 1980], we could find no laboratory or theoretical studies of the reaction of H with CH_3CCH_2 other than some discussion by *Wagner and Zellner* [1972]. The possible pathways of the reaction of H with CH_3CCH_2 include $CH_3C_2H + H_2$ (R207), $CH_2CCH_2 + H_2$ (R208), $CH_3 + C_2H_3$ (R209), and three-body addition to form C_3H_6 (R210). Note that R209 would be endothermic with allyl

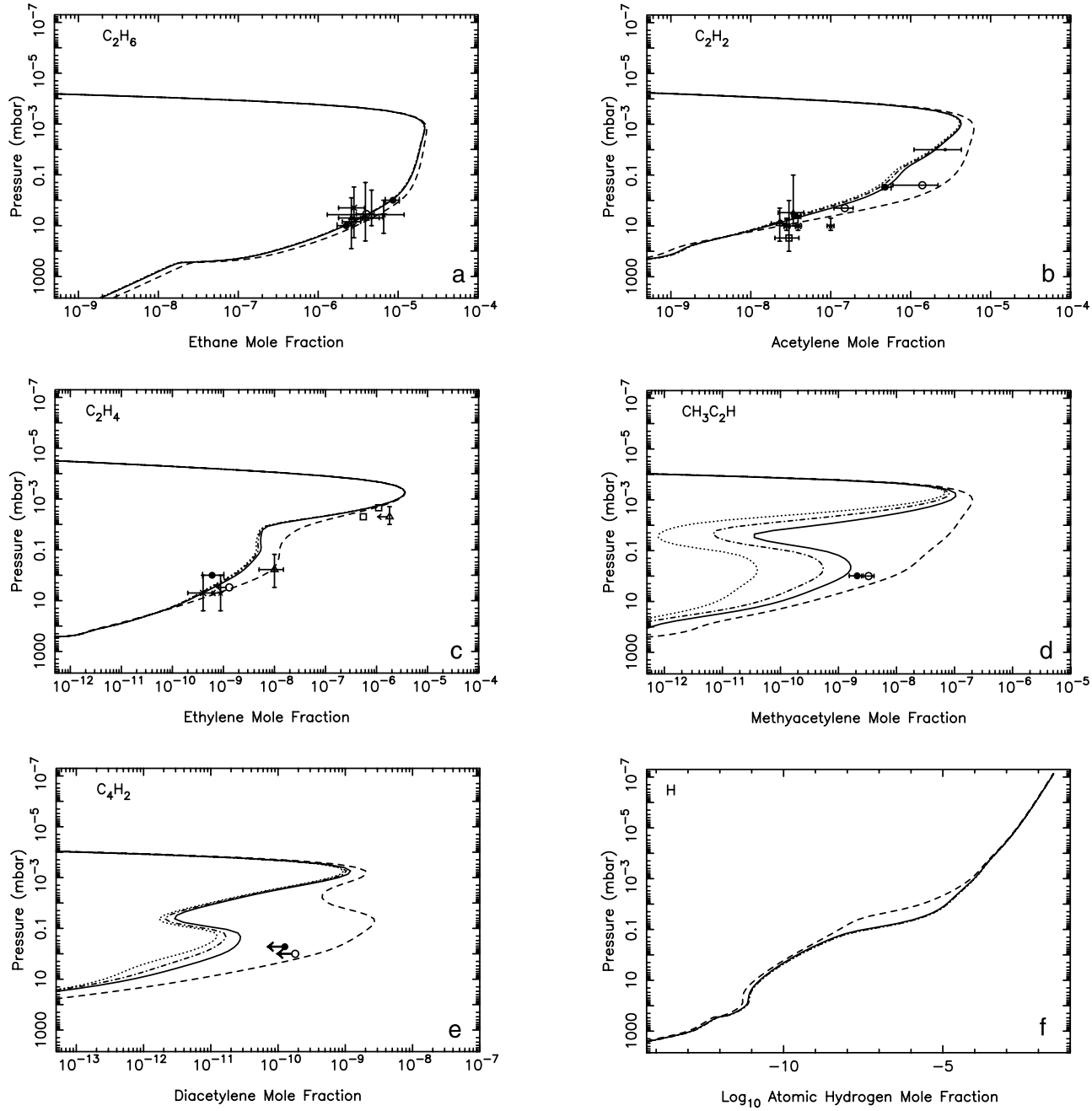

Figure 19. The sensitivity of the mixing ratio profiles of (a) C_2H_6, (b) C_2H_2, (c) C_2H_4, (d) CH_3C_2H, (e) C_4H_2, and (f) H to the rate coefficient for reactions R207–R210 that deal with the reaction of H + C_3H_5. The solid lines in Figure 19 represent Model A, with rate coefficients of $k_{207} = k_{208} = 3.0 \times 10^{-11}$ cm^3 s^{-1}, $k_{209} = 4.0 \times 10^{-12}$ cm^3 s^{-1}, $k_{0,210} = 1.5 \times 10^{-29}$ cm^6 s^{-1}, and $k_{\infty,210} = 2.4 \times 10^{-10}$ cm^3 s^{-1}. The dashed lines represent a model that is identical to Model A, except $k_{209} = 0$. The dot-dashed line represents a model that is identical to Model A, except $k_{207} = k_{208} = 1.0 \times 10^{-11}$ cm^3 s^{-1}. The dotted line represents a model that is identical to Model A, except $k_{0,210} = 1.0 \times 10^{-24}$ cm^6 s^{-1} and $k_{\infty,210} = 2.8 \times 10^{-10}$ cm^3 s^{-1}.

as the C_3H_5 radical but is energetically possible with CH_3CCH_2. R209 is important in removing atomic hydrogen in our model because both products (CH_3 and C_2H_3) react readily with H, whereas the products of R207, R208, and R210 often lead to recycling of atomic H. The relative rates of R207, R208, R209, and R210 therefore affect the abundances of many hydrocarbons in our model. We have used the reported rate coefficients for H + allyl as a guide in estimating the rate coefficients for R207, R208, and R210; however, the rate coefficients for all four reactions (R207–R210) could be considered free parameters in the model due to a lack of relevant laboratory data.

[59] Figure 19 illustrates how the adopted rate coefficients for reactions R207–R210 affect species abundances.

Note the high sensitivity to R209. The results for the C_2H_x hydrocarbons are less sensitive to assumptions about k_{207}, k_{208}, and k_{210}. Studies of the reaction of atomic hydrogen with CH_3CCH_2 radicals are greatly needed to help constrain photochemical models of the outer planets.

[60] Excited singlet methylene ($^1CH_2$) is a major product of methane photolysis at Lyman α wavelengths. The dominant loss process for $^1CH_2$ is interaction with molecular hydrogen, leading to either a reaction to form CH_3 + H (R259) or collision-induced intersystem crossing to form $^3CH_2$ (R258). Both the absolute and relative rates of R258 and R259 are important. It is now well established that R259 dominates over R258 at room temperature [e.g., *Blitz et al.*, 2001; *Langford et al.*, 1983; *Braun et al.*, 1970]. The temperature and pressure dependence of these reactions are uncertain, however. Figure 20 illustrates how the rate coefficients for R258 and R259 can affect species abundances. The higher the k_{258}/k_{259} ratio, the less atomic hydrogen is produced in the upper atmosphere and the less efficient methane recycling becomes; in addition, an increased rate of production of $^3CH_2$ leads to an increased production of CH and, through CH insertion reactions, an increased production rate of unsaturated hydrocarbons.

[61] The reaction of vinyl (C_2H_3) radicals with H_2 to form C_2H_4 + H (R328) is highly temperature dependent, and the rate constant is unknown at the low temperatures typical of the Jovian stratosphere. Although the rate constant will be very small at low temperatures, the large H_2 abundance on Jupiter makes the reaction potentially important as a C_2H_3 loss mechanism. The reaction will be of less importance on the other giant planets (except for perhaps Neptune in certain altitude regions) due to the lower temperatures generally found in the stratospheres of those planets. As is discussed by *Allen et al.* [1992], *Fahr et al.* [1995], *Gladstone et al.* [1996], and *Romani* [1996], reaction R328 contributes to a potential mechanism for aiding the conversion of acetylene to ethane in Jupiter's atmosphere. However, the importance of this reaction in the overall C_2H_2-to-C_2H_6 conversion scheme is unclear because of uncertainties in the low-temperature rate constant. The room-temperature value is itself uncertain, as different theoretical extrapolations and/or experimentally measured rates differ by several orders of magnitude [e.g., *Knyazev et al.*, 1996; *Mebel et al.*, 1995; *Fahr et al.*, 1995; *Weissman and Benson*, 1988; *Callear and Smith*, 1986; *Tsang and Hampson*, 1986; *Laufer et al.*, 1983]. For Models A and B, we adopt an intermediate expression from the transition-state theory calculations of *Knyazev et al.* [1996]. For Model C, we have adjusted the rate constants of several reactions in an attempt increase in the net production rate of C_2H_2 in the upper portions of Jupiter's stratosphere to better match ISO data. Because these changes reduced the effectiveness of the mechanism of successive addition of H atoms to unsaturated hydrocarbons that helps convert C_2H_2 to C_2H_6, the changes caused the resulting C_2H_2 abundance in the lower stratosphere to be higher than is indicated by the observations. To keep the overall C_2H_2 abundance consistent with observations, some other competing process is needed to help convert C_2H_2 to C_2H_6. Reaction R328 can satisfy this criterion if its rate coefficient is high enough at low temperatures. Therefore, for Model C, we have adopted an expression that gives a high rate constant at low temperatures, as was derived from the transition-state theory calculations of *Weissman and Benson* [1988].

[62] Figure 21 illustrates the sensitivity of species abundances to the rate coefficient for reaction R328. Note that k_{328} has little effect on C_2H_6, C_2H_4, and H abundances, but it does affect C_2H_2 and other unsaturated hydrocarbons that are sensitive to C_2H_2 abundances (e.g., CH_3C_2H and C_4H_2).

5. Observations and Model-Data Comparisons

[63] The ISO satellite [*Kessler et al.*, 1996] performed routine operations from February 1996 to April 1998. Spectra of Jupiter were acquired by the SWS instrument [*de Graauw et al.*, 1996] on several dates within this time period; the spectra used in our analysis of the hydrocarbon abundances were all obtained in late May 1997. Table 2 provides some details about these observations. Previous descriptions of ISO-SWS spectra of Jupiter are given by *Encrenaz et al.* [1996, 1999], *Feuchtgruber et al.* [1997, 1999], *Brooke et al.* [1998], *Drossart et al.* [1999], *Fouchet et al.* [2000a, 2000b, 2003], *Lellouch et al.* [2001, 2002], *Bézard et al.* [2001b], and *Encrenaz* [2003]. Our spectra were acquired by the two SWS grating spectrometers that provide medium spectral resolution in the wavelength range 2.4–45 μm (with resolving power ~1000–3000, depending on wavelength). We use observations from two different "Astronomical Observation Template" (AOT) modes: the AOT 01 mode, in which the entire SWS spectral range was observed at relatively low resolution, and the AOT 06 mode, in which the focus was specific spectral regions (7.0–12.0 μm and 12.0–16.5 μm) at slightly higher spectral resolution. For the Jupiter observations, the instrument aperture (14″ × 20″ half maximum for wavelengths less than 12.5 μm and 14″ × 27″ half maximum for wavelengths greater than 12.5 μm) was centered on the planet (41″ equatorial diameter), with the long axis roughly parallel to the north-south polar axis. The auroral regions were not included in the field of view. More details about these observations and the data reduction are given by *Fouchet et al.* [2000b], *Lellouch et al.* [2001], and *Bézard et al.* [2001b].

[64] For most of the hydrocarbon analyses, we use spectra acquired with the high-resolution AOT 06 mode on 25 May 1997. However, these spectra were obtained using subdivided spectral bands that have a cutoff at 12.1 μm, right in the middle of the ν_9 ethane band. Because the two instrument spectral bands on either side of the 12.1 μm cutoff employ different apertures and because the intercalibration between the two bands is not precise enough for our purposes, we do not use the 25 May 1997 AOT 06 spectra for our ethane analysis. Instead, we use an AOT 01 spectrum taken on 23 May 1997. The AOT 01 mode applies a different scanning strategy, and the relevant band extends to 12.4 μm rather than 12.1 μm. However, we trade consistency and continuity for spectral resolution, as the AOT 01 spectra have lower resolution than the AOT 06 spectra by an average of 1.4. In our spectral region of interest, the AOT 01 mode has a resolving power of ~1500 at 11 μm and ~2000 at 13 μm, compared with the AOT 06 mode resolving power of ~2000 at 11 μm and ~3000 at

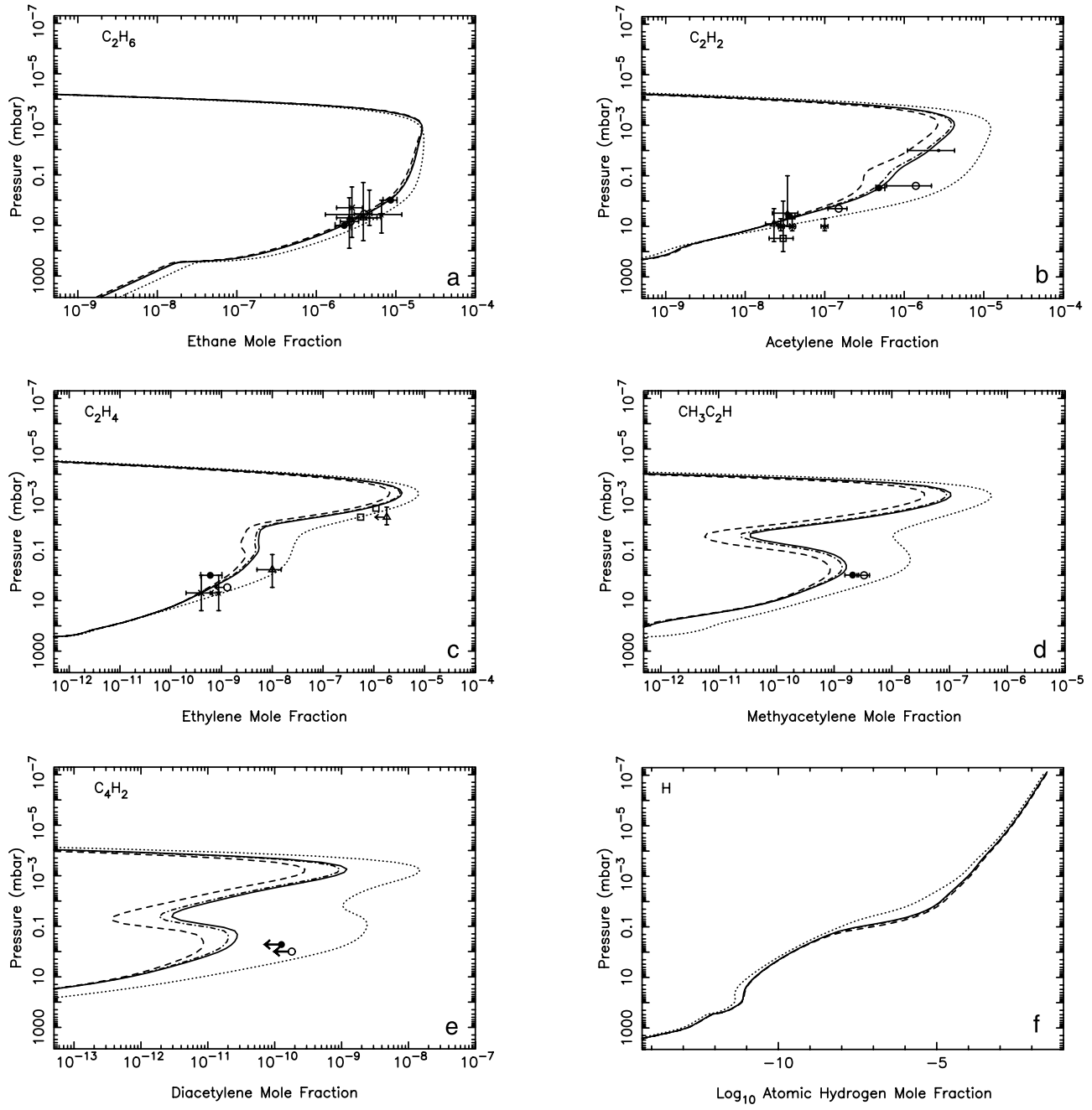

Figure 20. The sensitivity of the mixing ratio profiles of (a) C_2H_6, (b) C_2H_2, (c) C_2H_4, (d) CH_3C_2H, (e) C_4H_2, and (f) H to the rate coefficient for reactions R258 ($^1CH_2 + H_2 \rightarrow {}^3CH_2 + H$) and R259 ($^1CH_2 + H_2 \rightarrow CH_3 + H$). The solid line represents Model A, for which $k_{258} = 1.26 \times 10^{-11}$ cm^3 s^{-1} and $k_{259} = 9.24 \times 10^{-11}$ cm^3 s^{-1}. The dashed line represents a model that is identical to Model A, except $k_{258} = 0$ and $k_{259} = 1.16 \times 10^{-10}$ cm^3 s^{-1}. The dot-dashed line represents a model that is identical to Model A, except the rate coefficients for R258 and R259 are consistent with *Blitz et al.* [2001]: $k_{258} = 8.64 \times 10^{-12}$ cm^3 s^{-1} and $k_{259} = 8.14 \times 10^{-11}$ cm^3 s^{-1}. The dotted line represents a model that is identical to Model A, except $k_{258} = k_{259} = 5.8 \times 10^{-11}$ cm^3 s^{-1}. The latter model is unlikely to be realistic but illustrates the sensitivity of the model to the k_{258}/k_{259} ratio, which is unknown at temperatures relevant to the Jovian stratosphere.

13 μm. For benzene and methylacetylene, the 25 May 1997 spectrum in the 3A band (12.0–16.5 μm) suffers from severe fringing problems due to Fabry-Pérot effects occurring in both the detector and the order-sorting filter of the entrance aperture. The fringes can be removed by spectral filtering, but this method alters some real features in the spectrum, and benzene and methylacetylene are then not detected. An alternative is to use the so-called "off-band" spectra: light that has been filtered through the 3A band but that is detected with the longer wavelength detector 4,

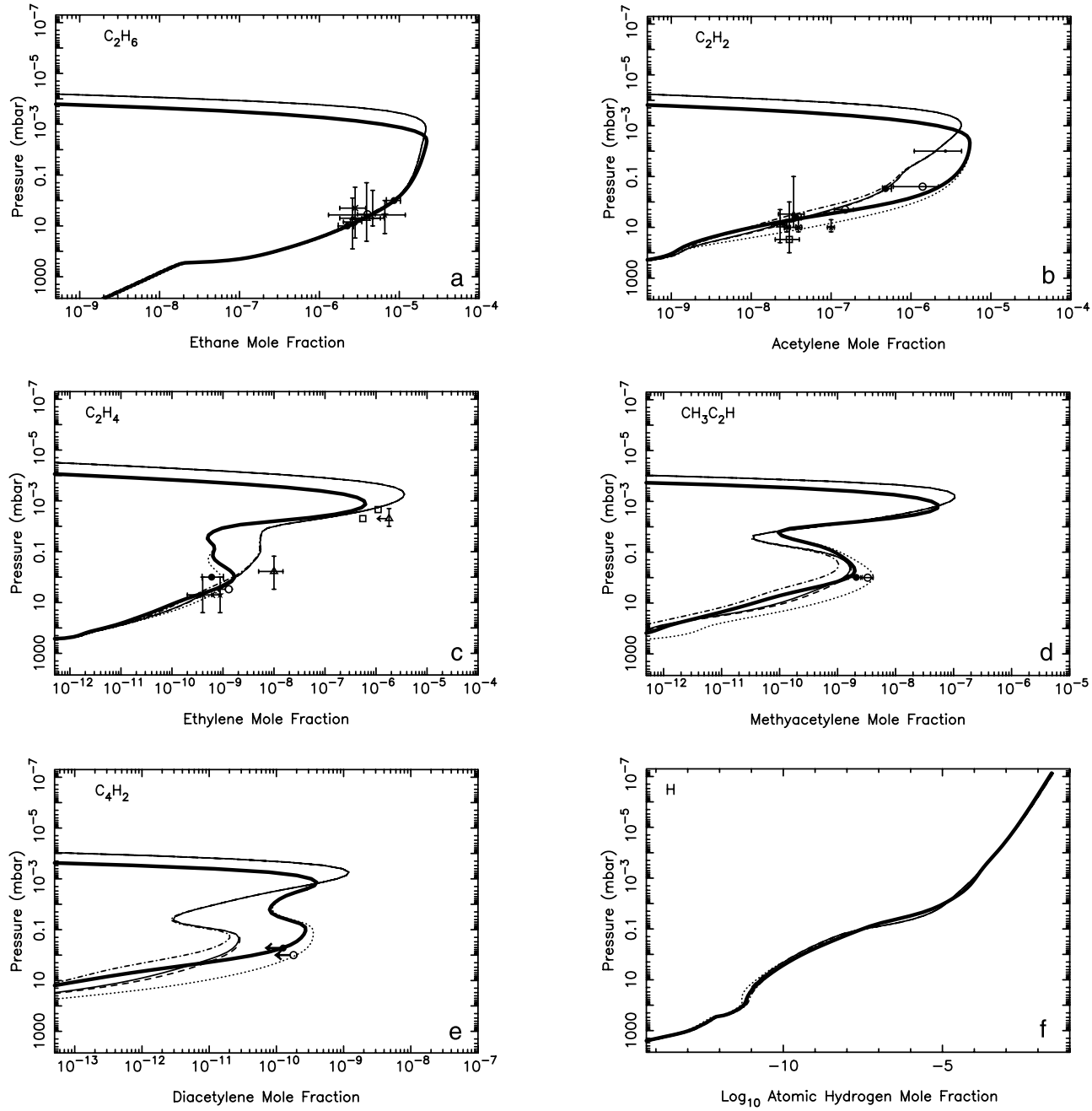

Figure 21. The sensitivity of the mixing ratio profiles of (a) C_2H_6, (b) C_2H_2, (c) C_2H_4, (d) CH_3C_2H, (e) C_4H_2, and (f) H to the rate coefficient for reaction R328 (C_2H_3+ $H_2 \rightarrow C_2H_4$+ H). The thin solid line represents Model A, in which the rate coefficient recommendation of *Knyazev et al.* [1996] is used: $k_{328} = 1.57 \times 10^{-20}\ T^{2.56}\ e^{(-2529/T)}$ cm^3 s^{-1}. The dashed line represents a model that is identical to Model A, except the adopted rate coefficient expression for R328 is the lowest value available in the literature for Jovian temperatures; i.e., that of *Tsang and Hampson* [1986]: $k_{328} = 5.0 \times 10^{-20}\ T^{2.63}\ e^{(-4298/T)}$ cm^3 s^{-1}. The dot-dashed line represents a model that is identical to Model A, except the adopted rate coefficient expression for R328 provides the highest value available in the literature for Jovian temperatures; i.e., that of *Weissman and Benson* [1988]: $k_{328} = 5.23 \times 10^{-15}\ T^{0.7}\ e^{(-2574/T)}$ cm^3 s^{-1}. The thick solid line represents Model C, in which the chemistry differs from Model A (see Table S3), and the high value of k_{328} from *Weissman and Benson* [1988] is used. The dotted line represents a model that is identical to Model C, except the intermediate value of k_{328} from *Knyazev et al.* [1996] is used.

which does not suffer from Fabry-Pérot effects. The fringing pattern is then only due to the filter and can be removed without damaging the spectrum. The drawbacks to this method are that the absolute flux cannot be trusted, and some spectral gaps exist. Therefore we only use the "off-band" data in the vicinity of the benzene and methylacetylene bands. To increase the signal-to-noise ratio for benzene, six observations made on the center of the planet on 26 May

Table 2. Observations

TDT Number	Date, UT	Integration Time, s	AOT Mode	Resolving Power ($\lambda/\Delta\lambda$)	Spectral Range, μm	Target Hydrocarbons
55400801	23 May 1997	2431	S01	2000	7.0–12.4	C_2H_6
55601319	25 May 1997	3440	S06	1200–2000	3.02–7.0	CH_4
55601720	25 May 1997	2796	S06	1400–2700	7.0–12.0	CH_4, C_2H_4
55602018	25 May 1997	1910	S06	1550–2000	2.4–3.02	CH_4
				1300–1700	12.0–16.5	C_2H_2, CH_3C_2H, C_3H_8, C_4H_2
55700103	26 May 1997	952	S06	1250	12.97–16.09	C_6H_6
55700206	26 May 1997	952	S06	1250	12.97–16.09	C_6H_6
55700309	26 May 1997	952	S06	1250	12.97–16.09	C_6H_6
55700412	26 May 1997	952	S06	1250	12.97–16.09	C_6H_6
55700515	26 May 1997	952	S06	1250	12.97–16.09	C_6H_6
55700618	26 May 1997	952	S06	1250	12.97–16.09	C_6H_6

1997 were co-added. The resulting spectrum is identical to that used by *Bézard et al.* [2001b].

5.1. Generation of Synthetic Spectra

[65] To constrain the hydrocarbon abundances in Jupiter's stratosphere, we compare the ISO-SWS observations with synthetic spectra generated from a line-by-line radiative transfer program. The program includes collision-induced absorption from H_2-He-CH_4, and molecular opacity from PH_3, NH_3, CH_4, CH_3D, C_2H_2, C_2H_6, CH_3C_2H, and C_6H_6. In test calculations, we also include opacity from compounds not detected in the ISO spectra (e.g., CH_3, C_2H_4, C_3H_8, C_4H_2) in order to put upper limits on the abundances of these species. Line parameters for all species except CH_3, C_4H_2, and C_6H_6 are obtained from the Geisa databank [*Jacquinet-Husson et al.*, 1999]. Line parameters for C_6H_6 are identical to those of *Bézard et al.* [2001b]; they were provided by M. Dang-Nhu (personal communication to B. Bézard, 1990) and are derived from molecular constants from *Lindemayer et al.* [1988] and integrated band intensities from *Dang-Nhu and Pliva* [1989]. Consistent with the laboratory measurements of C_6H_6 broadening by air and He [*Waschull et al.*, 1998], we adopt a Lorenz halfwidth of 0.11 cm^{-1} atm^{-1} at 296 K and assume this value varies with temperature to the power of −0.75. Line parameters for CH_3 are taken from *Bézard et al.* [1998], updated for the new band strengths measured by *Stancu et al.* [2005], and those for C_4H_2 and CH_2CCH_2 are taken from *Moses et al.* [2000a]. The H_2-H_2, H_2-He, and H_2-CH_4 absorption coefficients are calculated from subroutines provided by A. Borysow and are based on the models of *Borysow et al.* [1985, 1988] and *Borysow and Frommhold* [1986]. The NH_3 vertical distribution is taken from *Fouchet et al.* [2000a]. Disk-averaged spectral radiances are calculated and then converted to fluxes taking into account the fraction of Jupiter's disk included in the SWS aperture.

[66] The tropospheric temperature profile used in the radiative-transfer modeling is inverted from ISO data from the 14–16-μm spectral region, which sounds pressures between 100 and 300 mbar. The stratospheric temperature profile is retrieved from the CH_4 ν_4 emission. This band probes pressures between 1 and 30 mbar. At lower pressures, the profile is kept isothermal and is connected to the Galileo Probe ASI measurements for the upper stratosphere [*Seiff et al.*, 1998]. The derived stratospheric temperature has a local maximum at 4 mbar and a local minimum at 1 mbar. This oscillation of about 10 K was also observed ~3.5 years later by the CIRS instrument aboard the Cassini spacecraft [*Flasar and the Cassini CIRS Investigation Team*, 2004]. It is interpreted as a manifestation of the Quasi-Quadrennial Oscillation, which affects the stratospheric temperature and wind fields. Since this oscillation does not represent mean Jovian seasonal and spatial conditions, a smoothed version of the profile was adopted for the photochemical model, while the oscillating profile was used for generating the synthetic spectra.

5.2. Comparisons With ISO-SWS Spectra

[67] Figures 22–28 show a comparison of the ISO data with synthetic spectra generated from our photochemical models A, B, and C (and/or with model profiles multiplied by a constant factor in the case of a poor fit). Plots of the

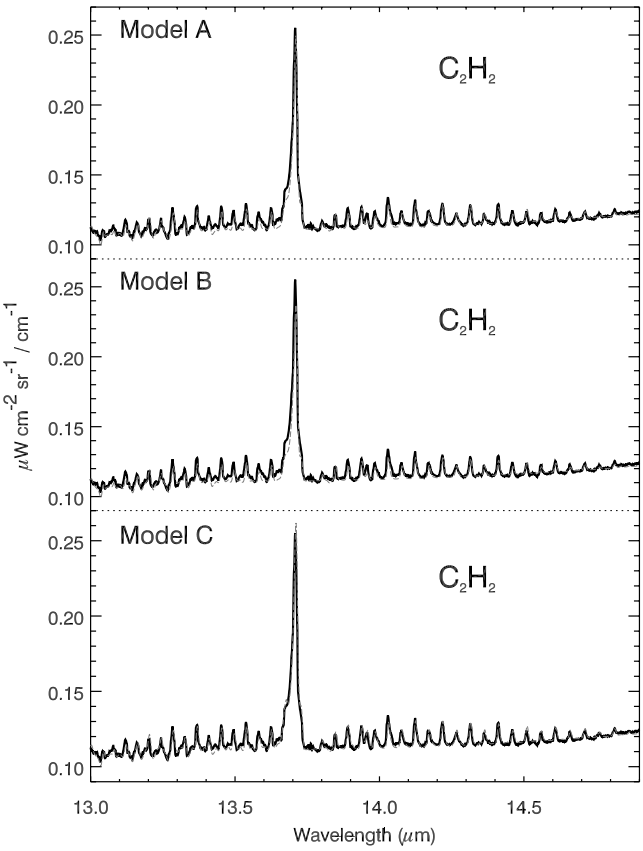

Figure 22. ISO spectra in the vicinity of the C_2H_2 ν_5 band compared with synthetic spectra generated from (top) Model A, (middle) Model B, and (bottom) Model C. The thick solid lines represent the data, whereas the thin dashed lines represent the models.

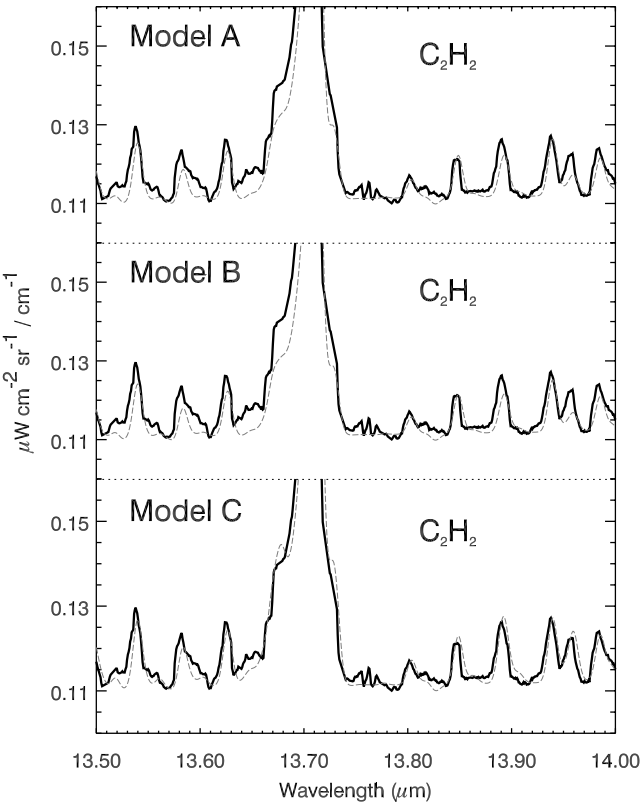

Figure 23. Comparison of the ISO data with synthetic spectra generated from (top) Model A, (middle) Model B, and (bottom) Model C in the spectral region containing C_2H_2 $\nu_5 + \nu_4 - \nu_4$ hot bands at 13.68 and 13.96 μm. The thick solid lines represent the data, whereas the thin dashed lines represent the models.

contribution functions associated with the C_2H_6 and C_2H_2 emission features are shown in Figure 29. The contribution function, as defined by *Moses et al.* [2000a], provides a measure of the relative contribution of a given pressure level to the observed emission.

[68] Figures 22 and 23 show that Models A, B, and C have mixed success in reproducing the various emission features associated with the C_2H_2 fundamental ν_5 band in the 13–15 μm region and the two Q branch components of the $\nu_5 + \nu_4 - \nu_4$ hot band on either side of the main ν_5 Q branch near 13.7 μm. Emission from the main ν_5 Q branch originates from the 2-mbar level, whereas emission from the hot bands originates from higher atmospheric levels near 0.25-mbar. Therefore the relative intensities of the features from the hot and fundamental bands are sensitive to the mixing-ratio gradient in the 0.1–4 mbar region. All three models do a good job of reproducing the emission due to the P, Q, and R branches of the ν_5 fundamental, with Model C slightly overestimating the Q branch emission. However, it is clear from an examination of the hot bands at 13.68 and 13.96 μm (see Figure 23) that Models A and B do not have enough C_2H_2 in the upper stratosphere to explain the observations. Model C provides a much better fit to the hot-band emission; Model C slightly overestimates the acetylene abundance around 0.25-mbar, but the discrepancy remains within the observational uncertainty. Note that the temperature in the upper stratosphere is not very well constrained by ISO observations due to the fact that the CH_4 ν_4 band only probes pressures in the 1–30 mbar region; therefore the error bars for the mixing ratio at the 0.25-mbar level are larger than those for the 2-mbar level. Information for this region of the stratosphere is not completely absent, however, as stellar occultation profiles and Galileo in situ measurements suggest that the temperature remains constant within a few kelvins between 1 mbar and a few microbars.

[69] All three models do a decent job of reproducing the emission from the ν_9 band of C_2H_6 in the 11.8–12.4 μm region (Figure 24). Model B, which has the smallest conversion rate from photolyzed methane to C_2 hydrocarbons, provides the best fit. The ${}^RQ_0$ multiplet at 12.16 μm probes the 3.5-mbar level, whereas the rest of the ν_9 band consists of weaker multiplets that probe deeper levels $\gtrsim$7 mbar. As explained by *Fouchet et al.* [2000b], the combination of strong and weak multiplets makes the band sensitive to the vertical profile of ethane. The success of the model-data comparisons here suggests that the modeled C_2H_6 abundances have the right magnitude and slope in the 3–10 mbar region.

[70] Emission from the other hydrocarbons detected by ISO (CH_3C_2H and C_6H_6) is optically thin, so the emission is proportional to the column density of the species. No information on the vertical profile can be obtained. The

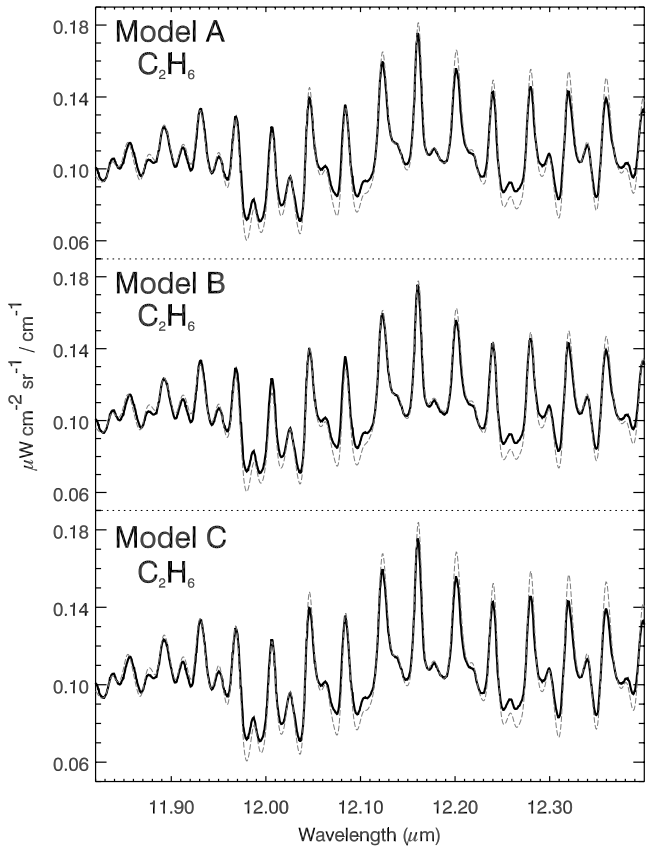

Figure 24. ISO spectra in the vicinity of the C_2H_6 ν_9 band compared with synthetic spectra generated from (top) Model A, (middle) Model B, and (bottom) Model C. The thick solid lines represent the data, whereas the thin dashed lines represent the models.

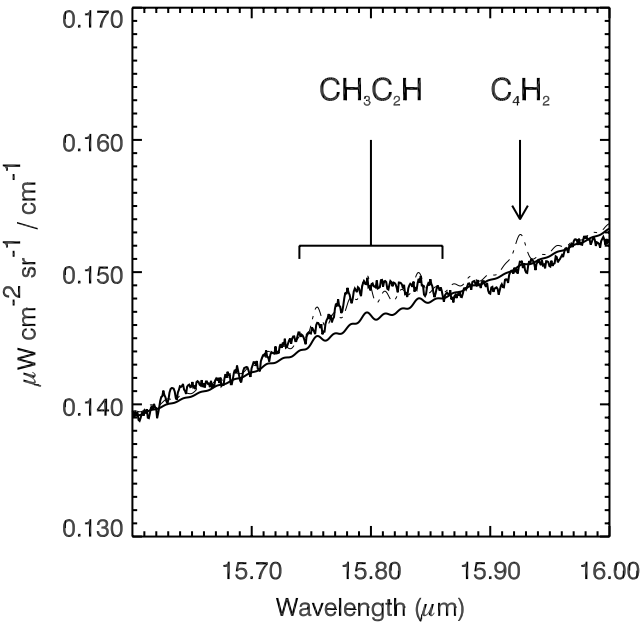

Figure 25. ISO spectra in the vicinity of the ν_9 band of CH_3C_2H and the ν_8 band of C_4H_2. The thick solid line represents the ISO data, the thin solid line represents the synthetic spectrum from Model A, and the dashed line represents a synthetic spectrum in which Model A CH_3C_2H and C_4H_2 abundances have been multiplied by a factor of 2.7.

peaks in the contribution functions are located roughly where the species concentration reaches a maximum, i.e., ~1–10 mbar for CH_3C_2H and ~3–30 mbar for C_6H_6. Figure 25 demonstrates that Models A, B, and C underestimate the emission in the ν_9 band of CH_3C_2H. The observed emission at 15.8 μm is best fit if the profiles in Models A, B, and C are multiplied by factors of 2.7, 3.1, and 3.4, respectively. From the ISO observations and the predicted vertical profiles of CH_3C_2H from our photochemical models, we determine that the methylacetylene column abundance is $(1.5 \pm 0.4) \times 10^{15}$ molecules cm^{-2} above 30 mbar. Similarly, Figure 26 demonstrates that Models A, B, and C underestimate the emission in the ν_4 band of C_6H_6. The observed emission at 14.82 μm is best fit when the predicted vertical distributions for benzene in Models A, B, and C are multiplied by a factor of 1.7, 2.3, and 7.1, respectively. From the ISO observations and the predicted vertical proles of C_6H_6, we determine that the benzene column abundance is $(8.0 \pm 2) \times 10^{14}$ molecules cm^{-2} above 30 mbar. However, as demonstrated by *Bézard et al.* [2001b], the results regarding the column abundance of C_6H_6 are sensitive to the vertical distribution, and the chemistry of benzene on the outer planets is not well enough known to make this conclusion firm.

[71] Other hydrocarbons that have rovibrational bands in the wavelength range covered by the spectrometer but that were not detected by ISO-SWS include CH_3 (the ν_2 band at 16.5 μm), C_2H_4 (the ν_7 band at 10.5 μm), C_3H_8 (the ν_{21} band at 13.4 μm), and C_4H_2 (the ν_8 band at 15.92 μm). Figures 25, 27, and 28 show the model-data comparisons in the region of these bands. Conservative estimates for ethylene, propane, and diacetylene abundance upper limits are 1.8, 10, and 4 times that predicted from photochemical Model C. Ethylene has been detected using IRTF/TEXES high-resolution spectra [*Bézard et al.*, 2002b]. The inferred column density, 6×10^{14} molecules cm^{-2} above 30 mbar is ~1.5 times lower than that in our Model C. The CH_3 ν_2 band lies at 16.5 μm, close to the edge of band 3A, where instrumental fringes are strong. For this reason, no useful CH_3 upper limit could be derived.

[72] The column densities and mixing ratios implied by our analysis of the ISO observations are shown in Table 3. The error bars include errors due to the spectroscopic data and radiative transfer model and to uncertainties from the ISO calibration. Errors in spectroscopic parameters are about 10% for the best studied molecules (C_2H_2 and C_2H_6) and 20% for CH_3C_2H and C_6H_6. As discussed previously, the C_2H_2 abundance at 0.25-mbar suffers from uncertainties on the temperature profile in this pressure region, where the ISO constraints are loose. An additional 25% uncertainty is thus assigned to the acetylene mixing ratio in the upper stratosphere. The absolute accuracy of the flux scale for the AOT06 measurements is estimated to be ~15% between 12–16 μm. For Jupiter, due to strong saturation effects, the absolute calibration was poor for the 7–12 μm band (~30%), but overlapping bands allowed us to recalibrate the 7–12 μm band within ~5%

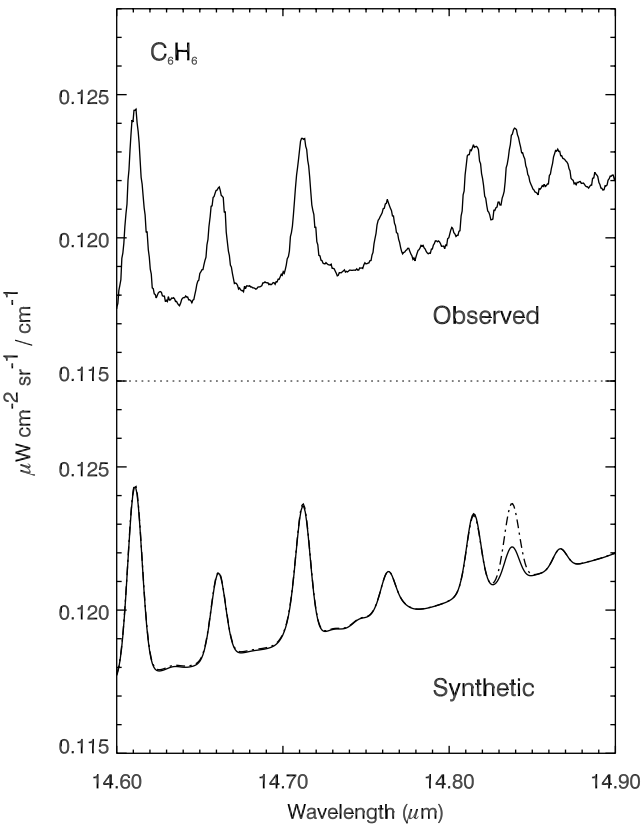

Figure 26. (top) ISO spectra in the vicinity of the ν_4 band of benzene compared with (bottom) synthetic spectra generated by the photochemical models. In the bottom panel the solid line represents the synthetic spectrum generated from Model A, whereas the dot-dashed line represents a model in which the Model A benzene abundance has been multiplied by a factor of 1.7.

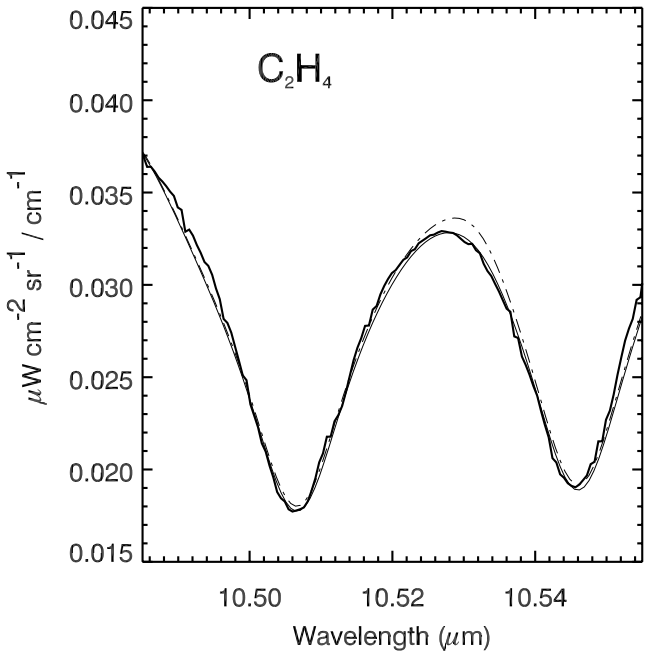

Figure 27. ISO spectra in the vicinity of the ν_7 band of ethylene (thick solid line) compared with models. The thin solid line represents Model A, whereas the dot-dashed line represents a model in which the Model A C_2H_4 abundance has been multiplied by a factor of 2.0.

to the 12–16 μm wavelength range. The error in relative calibration between the two bands propagate in the form of temperature error that leads to a ~5% uncertainty in the synthetic spectra. This results in a ±5% error in the column density of optically thin molecules (CH_3C_2H and C_6H_6), and a ±15% error in the mixing ratios of C_2H_2 and C_2H_6.

5.3. Comparisons With Ultraviolet H and He Emission

[73] Information on the structure and composition of the Jovian upper stratosphere can be obtained from ultraviolet observations of the H Ly α and He 584 Å dayglow [e.g., *Hunten*, 1969; *Carlson and Judge*, 1971; *Wallace and Hunten*, 1973; *Yung and Strobel*, 1980; *Broadfoot et al.*, 1981; *McConnell et al.*, 1981; *Ben Jaffel et al.*, 1988, 1993; *Skinner et al.*, 1988; *Clarke et al.*, 1991; *Emerich et al.*, 1993; *Vervack et al.*, 1995; *Gladstone et al.*, 1995, 1996]. It is now commonly accepted that Ly α emission results predominantly from resonant scattering of solar photons, with a smaller contribution from scattering from interplanetary Ly α [e.g., *Yelle and Miller*, 2004]. The observed emission is therefore dependent on solar cycle. As is discussed in section 3, an increase in K_h will result in an increase in the brightness of the He I 584 Å line and a decrease in the brightness of the Ly α 1216 Å line; therefore the relative brightness of the two lines can be used to derive the eddy diffusion coefficient in the homopause region. *Yelle and Miller* [2004] and *Gladstone et al.* [1996] review the various sounding-rocket, satellite, and spacecraft observations of Jovian emission at Ly α and He 584 Å over the last three decades.

[74] Previous photochemical models by *Gladstone et al.* [1996] and *Yung and Strobel* [1980] suggest that a column of $\sim 10^{17}$ H atoms cm^{-2} is expected above the level where the methane optical depth at Ly α is unity ($\sim 10^{-3}$ mbar) in Jupiter's stratosphere. Assuming this hydrogen is at ambient temperatures, the expected disk-averaged brightness of Jupiter would be ~5 kR for low-to-moderate solar consitions. Early rocket observations generally measured about 2–4 kR of Ly α emission from Jupiter's disk [e.g., *Rottman et al.*, 1973; *Giles et al.*, 1976], an emission brightness in accord with Copernicus results [*Atreya et al.*, 1977] but considerably larger than the 0.4 kR (later revised to 1 kR by *Shemansky and Judge* [1988]) seen by Pioneer 10 [*Carlson and Judge*, 1974]. Even larger than these early measurements are the ~14 kR observed by the Voyager ultraviolet spectrometers [e.g., *Broadfoot et al.*, 1981] and the 7–13 kR observed over many years by the International Ultraviolet Explorer (IUE) [e.g., *Skinner et al.*, 1988]. Such a strong variability with time has generally been taken as evidence for a large change in the structure of Jupiter's upper atmosphere, and the discovery of an evolving Ly α bulge [*Clarke et al.*, 1980; *Sandel et al.*, 1980; *McGrath*, 1991] added to this perception.

[75] The interpretation of Ly α brightnesses in terms of H column densities is complicated by several factors, including (1) an anomalously broad line shape [e.g., *Clarke et al.*, 1991] that suggests that a small component (~0.1–1%) of "hot" hydrogen has a large effect on both the line profile and the reflected brightness [e.g., *Ben Jaffel et al.*, 1993; *Gladstone et al.*, 2004], (2) evidence that atmospheric turbulence influences the line profile [*Emerich et al.*, 1996], and (3) the uncertain contribution of aurorally produced atomic hydrogen to the global hydrogen budget. These complications make it much more difficult to get useful information on such properties as long-term variations in the eddy diffusion coefficient at the homopause than was previously supposed. The much simpler He I 584 Å emission is preferred for such studies.

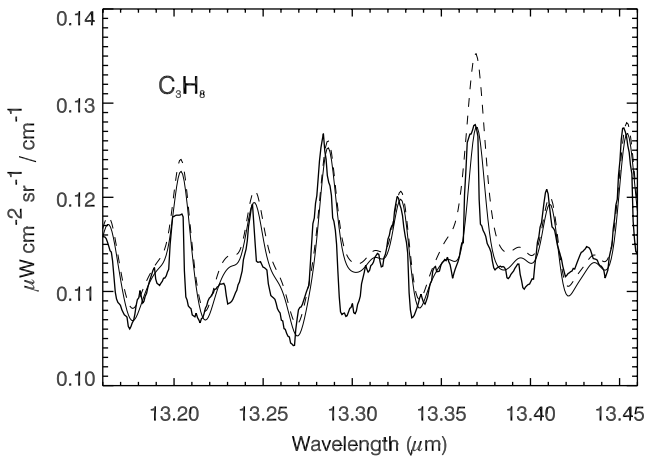

Figure 28. ISO spectra in the vicinity of the ν_{21} band of propane. The thick solid line represents the data, the thin solid line represents Model A, and the dashed line represents a model in which the Model A abundances have been multiplied by a factor of 20.

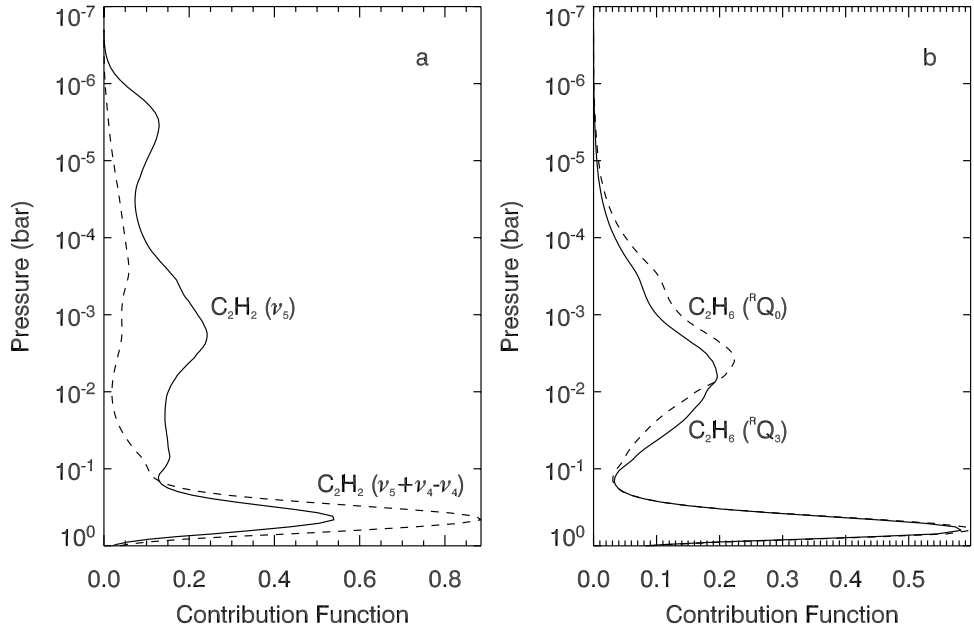

Figure 29. Contribution functions calculated at the peaks of the emission bands from the detected hydrocarbons. The functions exhibit a peak at 500 mbar in the troposphere due to H_2-He-CH_4 collision-induced opacity.

[76] Jovian He 584 Å emission measurements have been recorded by the Voyager UVS instrument, the EUVE satellite, and Cassini UVIS. The Voyager UVS data were analyzed by *McConnell et al.* [1981], *Shemansky* [1985], and *Vervack et al.* [1995]; the disk-center He 584 Å brightness was determined to be ~4 R. The Voyager observations were taken at solar maximum. The EUVE satellite, on the other hand, acquired data at solar minimum. As reported by *Gladstone et al.* [1995], no He 584 Å emission was detected in April 1993 (upper limit 1.8 R), but He 584 Å was detected in July 1994, with a disk-averaged brightness of 2.9 ± 0.9 R. A full description of the Cassini UVIS results from the Jupiter flyby (at solar maximum) is not yet available, but preliminary results are presented in an unpublished manuscript by C. D. Parkinson et al.

[77] Table 4 lists the disk-averaged and subsolar brightnesses calculated for resonantly scattered sunlight from Models A, B, and C for Jupiter, and Models A and C for Saturn. These brightnesses were calculated using the partial-frequency-redistribution resonance-line radiative transfer program of *Gladstone* [1988]. The solar full-disk line-integrated fluxes at 1 AU adopted for these models were 4.6×10^{11} photons cm^{-2} s^{-1} for Ly α and 3.0×10^9 photons cm^{-2} s^{-1} for He 584 Å. These values represent moderate solar conditions [cf. *Woods et al.*, 2000; *Torr et al.*, 1979]; typical ranges from solar minimum to maximum are $3.7–5.6 \times 10^{11}$ photons cm^{-2} s^{-1} for Ly α and $1.3–4.3 \times 10^9$ photons cm^{-2} s^{-1} for He 584 Å at 1 AU. Brightness estimates for other specific epochs may be obtained by multiplying the *I*/*F* values provided in Table 4 by the appropriate full-disk solar flux at the planet. A sum

Table 3. Constraints From ISO Spectra

		Observed	Model A	Model B	Model C
Species	Pressure, mbar	Column Density, cm^{-2}, or Mixing Ratio	Column Density, cm^{-2}, or Mixing Ratio	Column Density, cm^{-2}, or Mixing Ratio	Column Density, cm^{-2}, or Mixing Ratio
C_2H_2	0.25	$1.4 \pm 0.8 \times 10^{-6}$	5.2×10^{-7}	5.3×10^{-7}	2.2×10^{-6}
C_2H_2	2.0	$1.5 \pm 0.4 \times 10^{-7}$	1.1×10^{-7}	9.1×10^{-8}	2.1×10^{-7}
C_2H_6	3.5	$4.0 \pm 1.0 \times 10^{-6}$	4.2×10^{-6}	3.6×10^{-6}	4.5×10^{-6}
C_2H_6	7.0	$2.7 \pm 0.7 \times 10^{-6}$	2.8×10^{-6}	2.4×10^{-6}	3.0×10^{-6}
CH_3C_2H	1.0	$3.3 \pm 0.8 \times 10^{-9}$	1.2×10^{-9}	1.1×10^{-9}	1.5×10^{-9}
CH_3C_2H	above 30	$1.5 \pm 0.4 \times 10^{15}$	5.5×10^{14}	4.7×10^{14}	4.4×10^{14}
C_6H_6	3.0	$4.5 \pm 1.1 \times 10^{-10}$	2.3×10^{-10}	1.7×10^{-10}	7.6×10^{-11}
C_6H_6	above 30	$8.0 \pm 2 \times 10^{14}$	3.9×10^{14}	2.9×10^{14}	1.0×10^{14}
C_2H_4	3.0	$<1.3 \times 10^{-9}$	6.7×10^{-10}	5.8×10^{-10}	7.3×10^{-10}
C_2H_4	above 30	$<3.3 \times 10^{15}$	1.6×10^{15}	1.2×10^{15}	8.7×10^{14}
C_3H_8	3.0	$<1.3 \times 10^{-7}$	6.2×10^{-9}	5.2×10^{-9}	1.3×10^{-8}
C_3H_8	above 30	$<1.6 \times 10^{17}$	7.7×10^{15}	6.3×10^{15}	1.5×10^{16}
C_4H_2	1.0	$<1.8 \times 10^{-10}$	1.5×10^{-11}	1.1×10^{-11}	4.4×10^{-11}
C_4H_2	above 30	$<7.0 \times 10^{13}$	5.8×10^{12}	4.8×10^{12}	1.9×10^{13}

Table 4. Constraints From Ly α and He 584 Å Brightnesses

	Predicted $I_{Ly\ \alpha}$, kR		Predicted I_{584}, kR	
Model	Disk-Average	Subsolar	Disk-Average	Subsolar
		Jupiter		
A	8.73 (0.128)[a]	8.43 (0.124)	3.57 (0.0107)	6.12 (0.0138)
B	12.72 (0.187)	12.93 (0.190)	2.77 (0.0062)	3.62 (0.0081)
C	9.22 (0.136)	9.34 (0.137)	2.16 (0.0049)	2.85 (0.0064)
		Saturn		
A	0.94 (0.047)	1.07 (0.054)	1.50 (0.012)	1.93 (0.015)
C	0.94 (0.047)	1.07 (0.054)	1.52 (0.012)	1.94 (0.015)

[a]Values in parentheses are *I*/*F*.

of equal and offset Gaussians was used to represent the shape for both solar lines, i.e.,

$$\pi F(\lambda) = \frac{\pi F}{2\sqrt{\pi}\lambda_{dis}}\left[e^{-\left(\frac{\lambda-\lambda_{off}}{\lambda_{dis}}\right)^2} + e^{-\left(\frac{\lambda+\lambda_{off}}{\lambda_{dis}}\right)^2}\right], \qquad (3)$$

where λ_{dis} = 0.216 Å and λ_{off} = 0.220 Å for the solar Ly α line and λ_{dis} = 0.072 Å and λ_{off} = 0.0 Å for the solar He 584 Å line. The calculations assume that a hot H component is present, with a distribution and abundance (0.1% of the total ambient H column), equivalent to the best fit of *Gladstone et al.* [2004]. If the hot component is removed, the disk-averaged Ly α brightnesses drop to 5.31, 8.19, and 5.94 for Models A, B, and C, respectively. The subsolar brightnesses drop to 6.02, 9.18, and 7.25 kR, respectively.

[78] For Jupiter, the predictions from Models A and C are most consistent with the various Ly α observations taken over the years (see above). The Model B disk-averaged prediction for moderate solar conditions (12.72 kR) is at the upper range of that observed by the IUE. At solar maximum, the Model B disk-averaged estimated brightness at Ly α would be ∼16 kR, which exceeds all observed values, including the Voyager observed value of ∼14 kR at solar maximum. Therefore we favor Models A and C over Model B in this regard. However, this result is sensitive to the assumed H influx rate, and that rate is not well constrained from photochemical models due to the overall uncertainties in the reaction schemes. Model A overpredicts the disk-center He 584 Å brightness at solar maximum by a factor of ∼2–3 as compared with the Voyager solar-maximum observations, whereas the Model C predictions of He 584 Å brightness are much more in line with the observed Voyager and EUVE values. The eddy diffusion coefficient profile developed for Model C is thus our preferred profile from the standpoint of consistency with the Ly α and He 584 Å data.

[79] We also show in Table 4 what the predicted Ly α and He 584 Å brightnesses would be for Saturn based on the new models described in section 6. The similarity in the predictions for Models A and C for Saturn is due to the adoption of a similar upper-stratospheric eddy diffusion coefficient profile for the two models. The I_{584} and $I_{Ly\ \alpha}$ predictions are reasonably consistent with the Ly α and He 584 Å brightnesses observed at Saturn by Voyager, IUE, and EUVE [e.g., *Yelle et al.*, 1987a; *McGrath and Clarke*, 1992; *Parkinson et al.*, 1998]. See *Moses et al.* [2000a] for more details about the observations.

6. Comparisons With the Other Giant Planets

[80] Model C provides the best overall fit to all the available ISO, He 584 Å, and Ly α emission data for Jupiter. However, all three of our standard photochemical Models A, B, and C provide a reasonable fit to the lower stratospheric C_2H_2 and C_2H_6 abundances on Jupiter, as can be seen from the fit to the ν_5 acetylene emission and the ν_9 ethane emission in Figures 22 and 24. The number of free parameters in the modeling clearly limits our ability to judge the validity of our photochemical schemes. As discussed by *Lee et al.* [2000], a more stringent test of our understanding of hydrocarbon photochemical processes is furnished when a consistent set of reactions is applied to studies of photochemistry on the other giant planets. Jupiter, Saturn, Uranus, and Neptune all have cold, hydrogen-dominated atmospheres in which methane photolysis dominates the stratospheric photochemistry. Differences in stratospheric composition between the giant planets can be caused by (1) differences in heliocentric distance (through its effect on photolysis rates), (2) differences in stratospheric temperature (through its effect on condensation and reaction rates), (3) differences in the strength of atmospheric mixing (through its effect on the production rate and overall lifetime of complex hydrocarbons), (4) differences in auroral energy input (through its potential effect on global abundances), and (5) differences in the influx and nature of external material (through its effect on the abundances of minor species). All these differences can be accounted for in one-dimensional photochemical models. Global stratospheric circulation may also play a role in affecting the observed composition of the giant planets, but such considerations are beyond the scope of our 1-D modeling.

[81] We have developed 1-D photochemical models for Saturn, Uranus, and Neptune to compare with our results for Jupiter. We adopt the same molecular cross sections and temperature-dependent reaction rate expressions as in the Jupiter modeling. Calculations are for 30° latitude at equinox for low-to-average solar conditions. The background atmospheric structure (*P-T-z* grid) differs for the different models, as does the heliocentric distance and the assumed influx rate of external oxygen compounds. The latter parameters are taken from *Moses* [2001]. The background model atmospheres have been developed by solving the hydrostatic equilibrium equation for the *T-P* profiles shown in Figure 30, using the other physical parameters listed in Table 5. The eddy diffusion coefficient profiles are free parameters in the model and are adjusted until the model CH_4 and C_2H_6 abundances are consistent with observations. For Uranus, C_2H_6 has not been observed, so the C_2H_2 abundance was used to constrain *K* instead. Condensation of C_4H_2, C_4H_{10}, C_6H_6, and H_2O is included in the Saturn model. Condensation of C_2H_2, C_2H_6, C_4H_2, C_4H_{10}, C_6H_6, H_2O, and CO_2 is included in the Uranus and Neptune models. Propane would also condense on Uranus and Neptune, but C_3H_8 condensation was not considered. The Uranus and Neptune models include photolysis from Ly α from the local interplanetary medium.

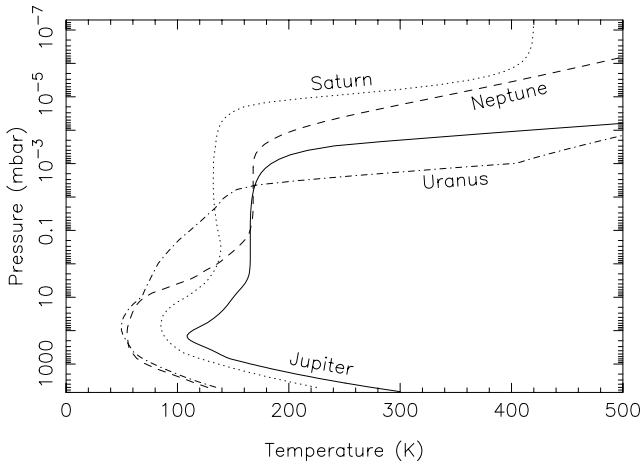

Figure 30. The temperature profiles adopted for all the giant-planet models.

[82] Figure 31 illustrates how Models A and C compare with the observed hydrocarbon abundances on Saturn. Both models do a good job of reproducing the ISO observations of C_2H_6 and CH_3C_2H. The Model C abundances of C_4H_2 and C_2H_2 also compare well with observations, although the 1-mbar C_2H_2 abundance is slightly overpredicted. However, the C_2H_4 abundance is grossly underpredicted with Model C, and the C_2H_2 and C_4H_2 abundances are underpredicted with Model A. Both models slightly overpredict the CH_3 abundance on Saturn.

[83] The models also have mixed success for Neptune (see Figure 32). Both models reproduce the C_2H_6 and CH_3 results. Both models overpredict the C_2H_2 abundance, with Model A resulting in values closer to the observed abundance. For C_2H_4, the abundance predicted by Model A compares well with the Voyager UVS results of *Yelle et al.* [1993] but is higher than that indicated by ISO [*Schulz et al.*, 1999]. Model C underpredicts the abundance of C_2H_4.

[84] For Uranus, the hydrocarbon abundances are affected significantly by the sluggish mixing in the Uranian stratosphere. The eddy diffusion coefficient profile, and probably atmospheric transport in general, have more influence on the results than any particular set of chemical reactions. In addition, different observations taken at different times and/or locations are often inconsistent with each other. Model-data comparisons for Uranus are therefore not very useful in helping constrain the photochemical reaction schemes. During the Voyager era, the UVS occultations [e.g., *Herbert et al.*, 1987; *Bishop et al.*, 1990], which probed the equatorial region, indicated greater hydrocarbon abundances than could be supported from solar ultraviolet reflection observations of the polar regions [e.g., *Yelle et al.*, 1987b, 1989]. Due to the large tilt of Uranus's rotational plane relative to its orbital plane, the polar regions were in constant sunlight at the time of the Voyager encounters, whereas the equatorial regions experienced very low sun angles and much smaller daily insolation values. Seasonal and meridional transport effects likely influence the abundances [e.g., *Yelle et al.*, 1989]. Figure 33 shows our results for five different models for Uranus.

[85] Because the *Yelle et al.* [1989] derived C_2H_2 abundance seems inconsistent with the recent derivation from global-average ISO observations of Uranus [*Encrenaz et al.*, 1998] as well as the UVS occultation results [*Bishop et al.*, 1990], we were required to look at models with two very different eddy diffusion coefficients. A higher value of K = 700 cm^2 s^{-1} is needed to fit the ISO and UVS occultation data, whereas a lower value of 50 cm^2 s^{-1} is consistent with the UVS solar reflection data [*Yelle et al.*, 1989]. In addition, because of the unusual axial tilt and long orbital period of the planet, our 30° latitude equinox model may not be appropriate as a "global average" for recent times, so we ran a couple models with fixed solar zenith angles to compare with specific data sets. The thick solid line in Figure 33 represents a model in which K = 700 cm^2 s^{-1} and the solar zenith angle is fixed at 83°, a value relevant to the UVS occultations [*Herbert et al.*, 1987]. The dot-dashed line represents a model that has K = 50 cm^2 s^{-1} and a solar zenith angle fixed at 21°, an appropriate average for the solar reflection observations [*Yelle et al.*, 1989]. All models are consistent with the CH_4 and C_2H_6 upper limits from ISO [*Encrenaz et al.*, 1998], whereas only the model with the lower eddy diffusion coefficient is consistent with the CH_4 upper limits imposed by *Yelle et al.* [1987b] and *Orton et al.* [1987]. Model C with a K value of 700 cm^2 s^{-1} does the best job of reproducing the new C_2H_2 ISO observations reported by *Encrenaz et al.* [1998], although the total C_2H_2 column abundance in the model ($\sim 8 \times 10^{16}$ cm^{-2}) may be an underestimate. The ISO observations, which are weighted toward middle and high latitudes, suggest that the eddy diffusion coefficient may be increasing in recent years as the Uranian season changes. If so, more hydrocarbons may be

Table 5. Model Parameters for the Giant Planets

	Jupiter	Saturn	Uranus	Neptune
Heliocentric distance, AU	5.203	9.555	19.26	30.11
Equator-orbit inclination, degrees	3.08	26.73	97.92	28.8
Mass, kg	1.890×10^{27}	5.685×10^{26}	8.684×10^{25}	1.024×10^{26}
Equatorial radius at 1 bar, km	71492	60268	25559	24764
30° latitude radius at 1 bar, km	70205	58504	25409	24535
Rotation period at 30° lat, hours	9.92	10.639	16.86	17.64
J_2	0.014697	0.016298	3.3434×10^{-3}	3.411×10^{-3}
J_4	−0.000584	−0.000915	-2.885×10^{-5}	-2.6×10^{-5}
Model C homopause pressure, mbar	2.9×10^{-4}	1.0×10^{-5}	1.7×10^{-1}	1.4×10^{-4}
Model C K_h, cm^2 s^{-1}	1.9×10^6	4.4×10^7	7.0×10^2	2.4×10^6
H_2O influx rate, cm^{-2} s^{-1}	4.0×10^4	1.9×10^6	4.0×10^5	2.6×10^5
CO influx rate, cm^{-2} s^{-1}	4.0×10^6	3.9×10^5	2.2×10^5	3.4×10^5
CO_2 influx rate, cm^{-2} s^{-1}	1.0×10^4	1.4×10^4	2.0×10^4	6.5×10^4

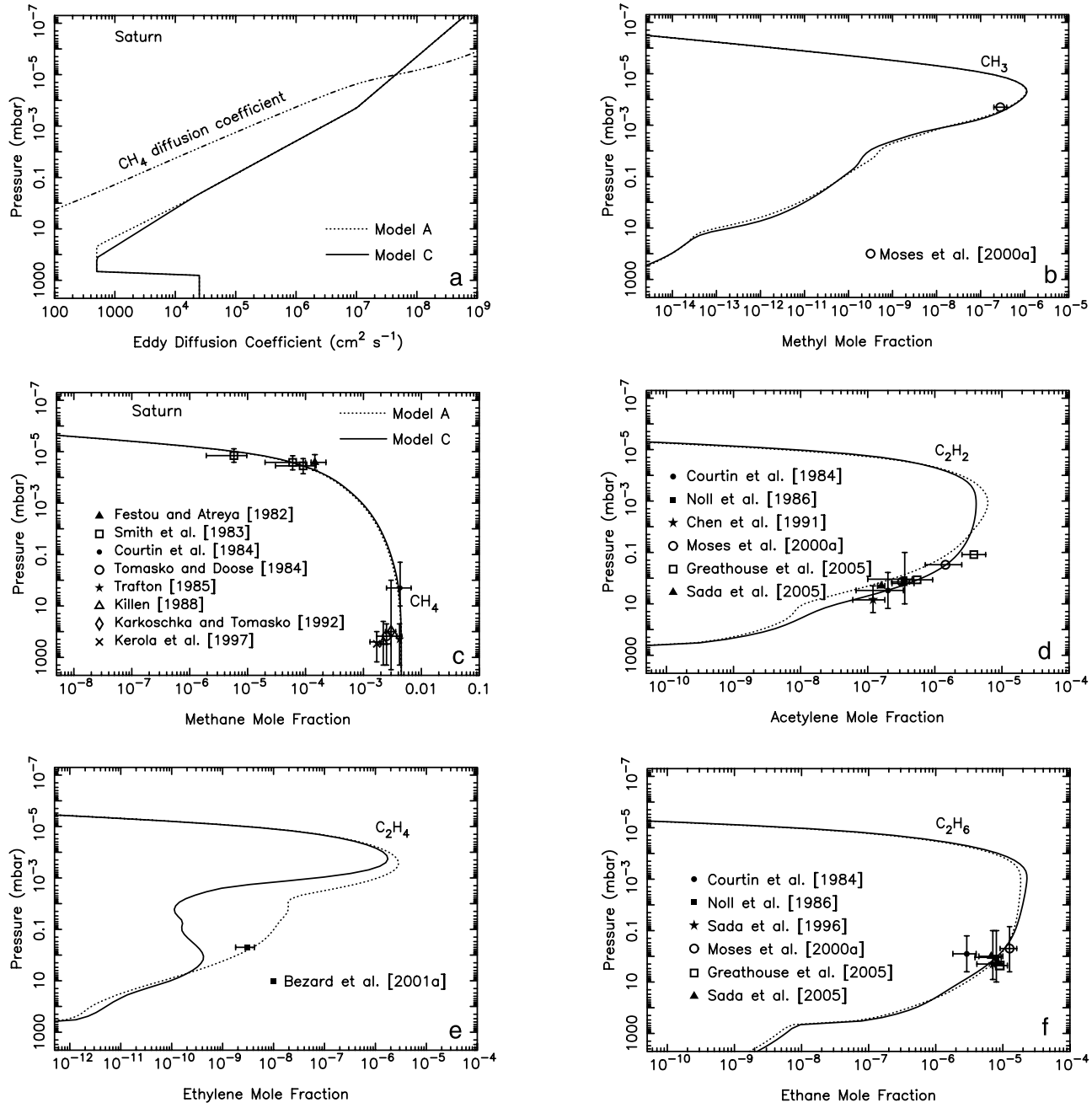

Figure 31. The photochemical model results for the observable hydrocarbons on Saturn: (a) eddy diffusion coefficient profile, and mixing ratio profiles for (b) CH_3, (c) CH_4, (d) C_2H_2, (e) C_2H_4, (f) C_2H_6, (g) CH_3C_2H, (h) C_3H_8, (i) C_4H_2, and (j) C_6H_6. The dotted lines represent a model that has the same chemical reaction list as the Jupiter Models A and B, and the solid lines represent a model that has the same reaction list as Jupiter Model C. The sharp dropoff in the C_4H_2 and C_6H_6 mixing ratios near $\sim$10 mbar is caused by condensation. The various data points with associated error bars represent observational measurements, as labeled. The *Moses et al.* [2000a] points have been scaled from the values provided in that paper to account for an updated temperature profile [e.g., *Lellouch et al.*, 2001]. The CH_3 data point has been scaled by a factor of 2.1 to account for the line-strength updates of *Stancu et al.* [2005].

present in the atmosphere now than were present at the time of the Voyager encounter [see also *Livengood et al.*, 2002; *Hammel et al.*, 2002].

[86] The model-data comparisons for all the giant planets demonstrate that we have not yet devised a photochemical reaction list that can reproduce global average observations from all the giant planets to within the reported error bars. While Models A and C generally provide good first-order estimates, they fall short in several areas, most notably in predicting the C_2H_4 abundance, the C_2H_2/C_2H_4 and $C_2H_6/$

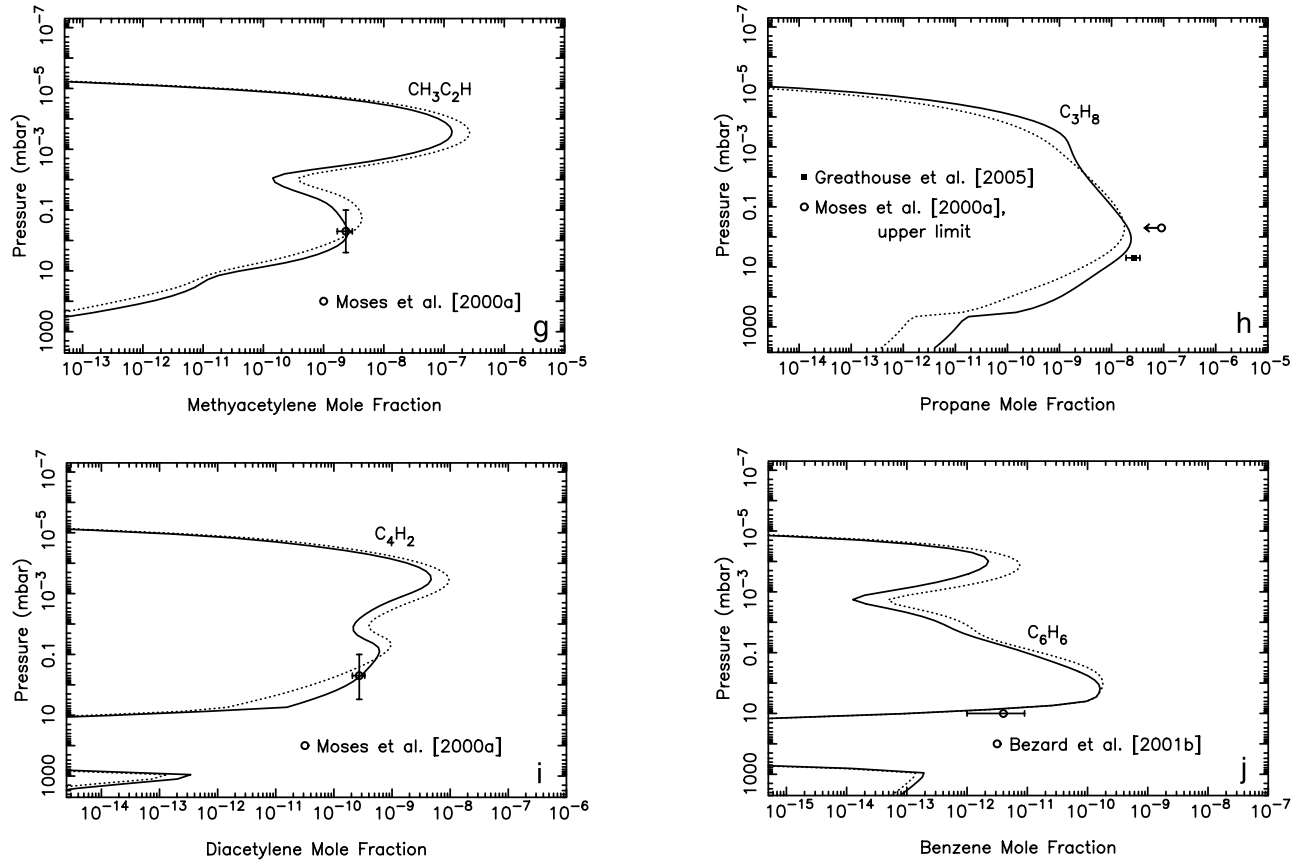

Figure 31. (continued)

C_2H_4 ratios, the C_6H_6 abundances, and the C_2H_6/C_2H_2 ratio. Models A and C bracket the observed values of the C_2H_6/C_2H_2 ratio on Jupiter and Saturn, but both models underpredict the ratio for Neptune. The difficulty in simultaneously reproducing both the C_2H_6 and C_2H_2 abundances for Neptune has long been identified [e.g., *Bézard et al.*, 1991; *Romani et al.*, 1993; *Moses et al.*, 1995; *Bishop et al.*, 1998]. The C_2H_6/C_2H_2 ratio would increase from Jupiter to Neptune if all other parameters such as atmospheric temperatures or the eddy diffusion coefficient profile remained the same. The fact that Jupiter and Saturn have such similar C_2H_6/C_2H_2 ratios ($\sim$11 at 1 mbar on Jupiter and $\sim$10 at 0.5 mbar on Saturn, according to ISO observations) suggests that other factors besides heliocentric distance and photolysis rates play a role.

[87] An even greater problem for the models is the accurate prediction of the C_2H_4 abundances on the giant planets. Models A and C bracket the observed C_2H_6/C_2H_4 and C_2H_2/C_2H_4 ratios on Jupiter, Saturn, and Neptune, with Model C generally producing ratios that are too high, and Model A producing ratios that are too low. Note that the C_2H_2/C_2H_4 ratio decreases progressively from Jupiter (observed ratio of $\sim$410 at 1 mbar), to Saturn (observed ratio of $\sim$220 at 0.5 mbar), to Neptune (observed ratio of $\sim$30 at 0.2 mbar). Similarly, the C_2H_6/C_2H_4 ratio decreases from $\sim$4500 at 1 mbar on Jupiter, to $\sim$2100 at 0.5 mbar on Saturn, to $\sim$770 at 0.2 mbar on Neptune. These trends are largely caused by changes in photolysis rates (and in the corresponding H atom production rates) due to the change in heliocentric distance rather than caused by temperature-dependent reaction rates; the temperature in the upper stratosphere where C_2H_4 is produced from primary reactions does not differ much between Jupiter and Neptune. For Saturn and Neptune, the C_2H_6, C_2H_4, and C_2H_2 abundances are well predicted with the Model C rate coefficients plus the changed values $k_{191} = 3.0 \times 10^{-11}$ cm^3 s^{-1}, $k_{0,192} = 2.0 \times 10^{-27}$ cm^6 s^{-1}, $k_{\infty,192} = 6.0 \times 10^{-11}$ $T^{0.18}$ cm^3 s^{-1}, and k_{194} as in Model A. However, these expressions lead to an overprediction of the C_2H_4 abundance and an underprediction of the C_2H_2 abundance on Jupiter.

[88] We should note that unlike the other main C_2H_x hydrocarbons, the C_2H_4 mole fraction peaks high in the stratosphere at microbar pressure levels. The atmospheric temperature is poorly constrained at these altitudes, and this lack of constraint complicates the observational analysis and quantitative determination of the ethylene abundance.

[89] In summary, while the chemical reaction lists from Models A and C lead to photochemical model results that provide a decent first-order prediction of the hydrocarbon abundances on the giant planets, problems with the current reaction schemes do exist. Model-data comparisons demonstrate that the current schemes cannot reproduce the relative abundances of C_2 hydrocarbons for all the giant planets. In particular, there appears to be a more effective conversion of unsaturated hydrocarbons like C_2H_2 and C_2H_4 to C_2H_6 on Jupiter than on the other giant planets. The models do not reproduce this behavior. Further laboratory chemical kinetics investigations at low temperatures and low pressures are needed to fully understand the reasons

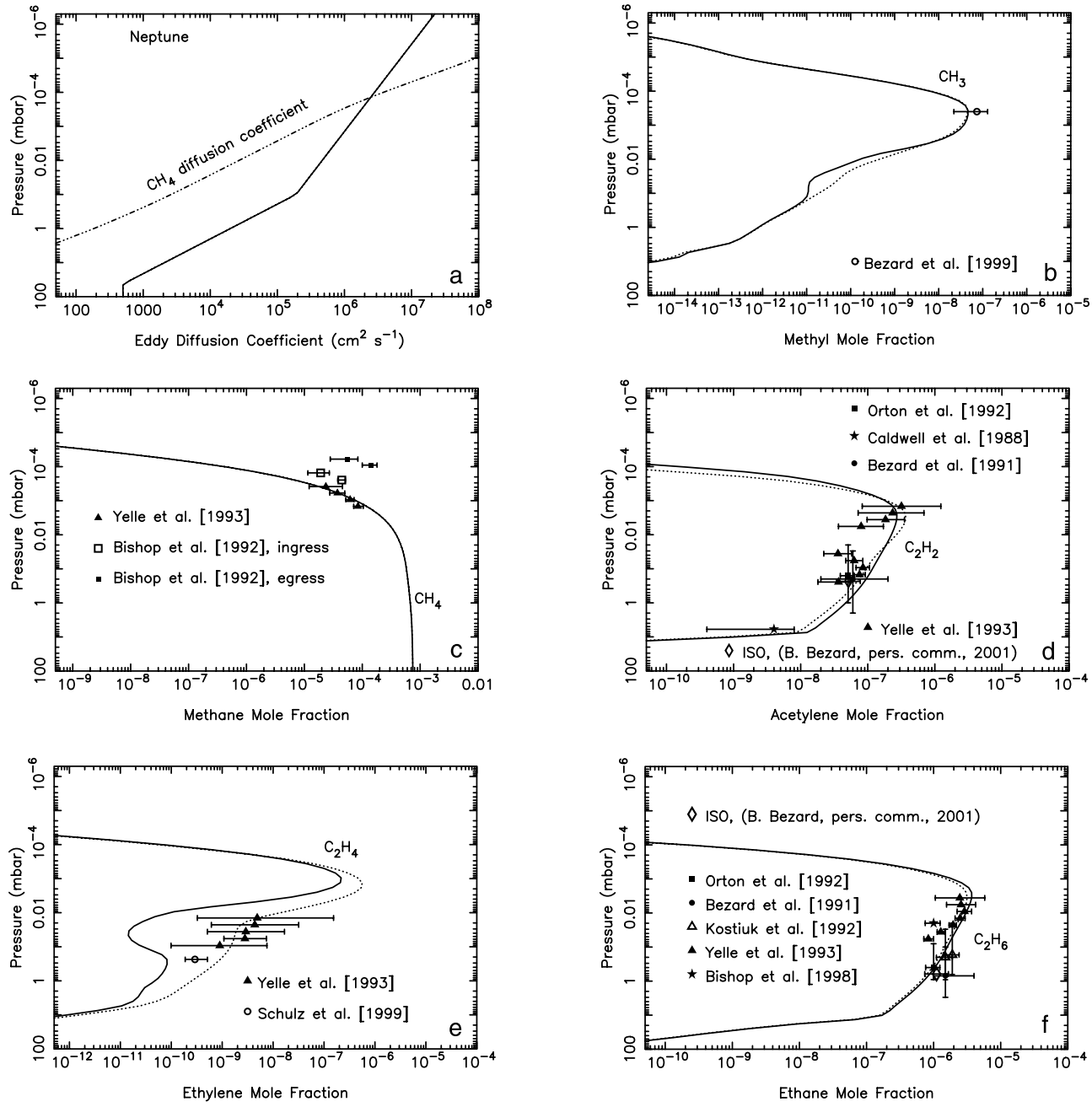

Figure 32. The photochemical model results for some of the hydrocarbons on Neptune: (a) eddy diffusion coefficient profile, and mixing ratio profiles for (b) CH_3, (c) CH_4, (d) C_2H_2, (e) C_2H_4, (f) C_2H_6, (g) CH_3C_2H, (h) C_3H_8, (i) C_4H_2, and (j) C_6H_6. The dotted lines represent a model that has the same chemical reaction list as the Jupiter Models A and B, and the solid lines represent a model that has the same reaction list as Jupiter Model C. The various data points with associated error bars represent observational measurements or upper limits, as labeled. Note that the two Neptune models (called A and C) both have the same eddy diffusion coefficient profile. The data point for CH_3 point has been scaled by a factor of 2.1 to account for the line-strength updates of *Stancu et al.* [2005].

for the shortcomings of the present schemes. The current models also need to incorporate some very recent advances in kinetics calculations and laboratory measurements [e.g., *Miller and Klippenstein*, 2004; *Wu et al.*, 2004; G. P. Smith, personal communication, 2004]. For example, we have not yet incorporated the new low-temperature photoabsorption cross sections of *Wu et al.* [2004] in our models, and the effects of these more physically realistic cross sections on our model C_2H_x abundances have yet to be investigated.

7. Conclusions and Future Work

[90] To investigate the details of hydrocarbon and oxygen chemistry in Jupiter's stratosphere, we have constructed a

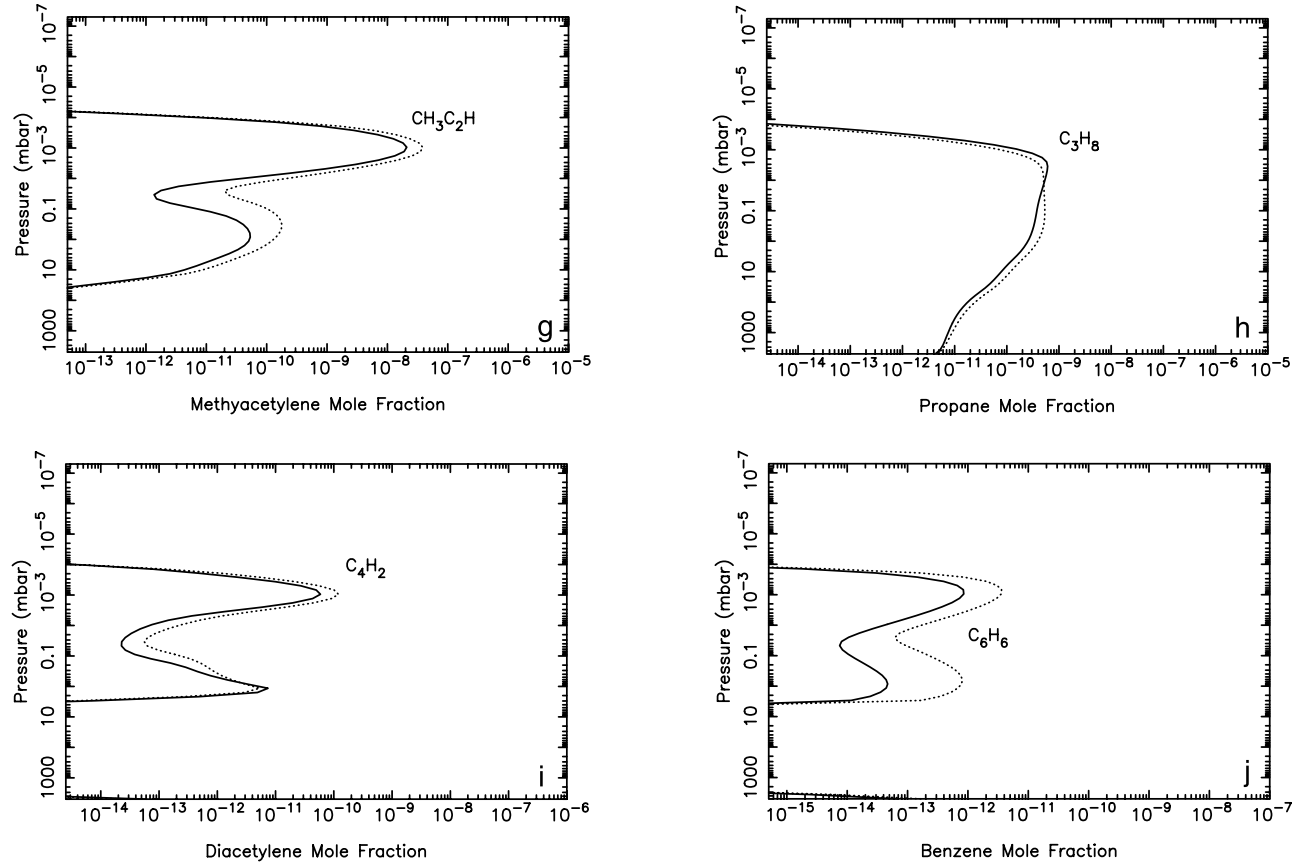

Figure 32. (continued)

one-dimensional, diurnally averaged, photochemical model that considers chemical kinetics, vertical diffusion, photodissociation, and radiative transfer processes. Our chemical reaction list is an updated and expanded version of the ones presented in the Saturn study of *Moses et al.* [2000a, 2000b] and in the Jupiter study of *Gladstone et al.* [1996]. The predictions regarding the vertical profiles of various hydrocarbons are compared with ISO observations to provide constraints for and tests of various aspects of the model. Our main goals of the modeling are to better constrain the eddy diffusion coefficient profile in Jupiter's stratosphere and to better understand the chemical reaction schemes that produce and destroy the observed constituents CH_4, C_2H_2, C_2H_4, C_2H_6, CH_3C_2H, C_6H_6, CO, CO_2, and H_2O (note that information on C_2H_4 and CO is from ground-based infrared observations rather than ISO). One strength of the ISO data that make them particularly useful for investigating photochemistry is that stratospheric temperatures can be obtained from the CH_4 and H_2 emissions observed simultaneously with the hydrocarbon emissions [e.g., *Fouchet et al.*, 2000b; *Lellouch et al.*, 2001]; therefore some of the ambiguities commonly associated with abundance analyses from infrared observations can be reduced. The wide wavelength coverage of the ISO-SWS allows the detection of several molecular constituents during the same observational sequence; the simultaneous detection eliminates potential problems due to temporal variability or inconsistent analysis techniques. In addition, the ISO data have high enough spectral resolution that information on the vertical slope of the C_2H_2 and C_2H_6 mixing ratio profiles can be retrieved; such information provides excellent constraints on the eddy diffusion coefficient profile and on important hydrocarbon reaction schemes. One weakness of the ISO data is the low spatial resolution: the retrieved abundances are effectively global averages. Information on horizontal (latitudinal) variations is limited and is only available for CO_2 and C_6H_6 [e.g., *Bézard et al.*, 2001b; *Lellouch et al.*, 2002].

[91] We have developed three photochemical models that all reproduce the ISO emission from the ν_9 band of ethane and the ν_5 band of acetylene. One difference between the models is the eddy diffusion coefficient in the upper stratosphere. The homopause location on Jupiter is currently uncertain, with information from the *Yelle et al.* [1996] analysis of the Voyager UVS occultation data and from the *Vervack et al.* [1995] and *Gladstone et al.* [1995] analyses of the Voyager and EUVE He 584 Å emission data appearing mutually inconsistent. The *Yelle et al.* [1996] analysis requires higher eddy diffusion coefficients and a homopause at higher altitudes (lower pressures) than can be supported by the observed He 584 Å brightnesses. The location of the methane homopause is an important parameter for photochemical modeling because it affects the efficiency of competing reaction schemes, including the overall effectiveness of methane recycling versus the production of higher-order hydrocarbons. New data from (1) ultraviolet occultations observed from spacecraft at Jupiter, (2) Earth-orbiting telescope ultraviolet observations of Jupiter occulting UV-bright stars, or (3) high-spectral-resolution infrared observations of Jupiter either during the occultation of an infrared-bright star [e.g., *Drossart et al.*, 2000] or more

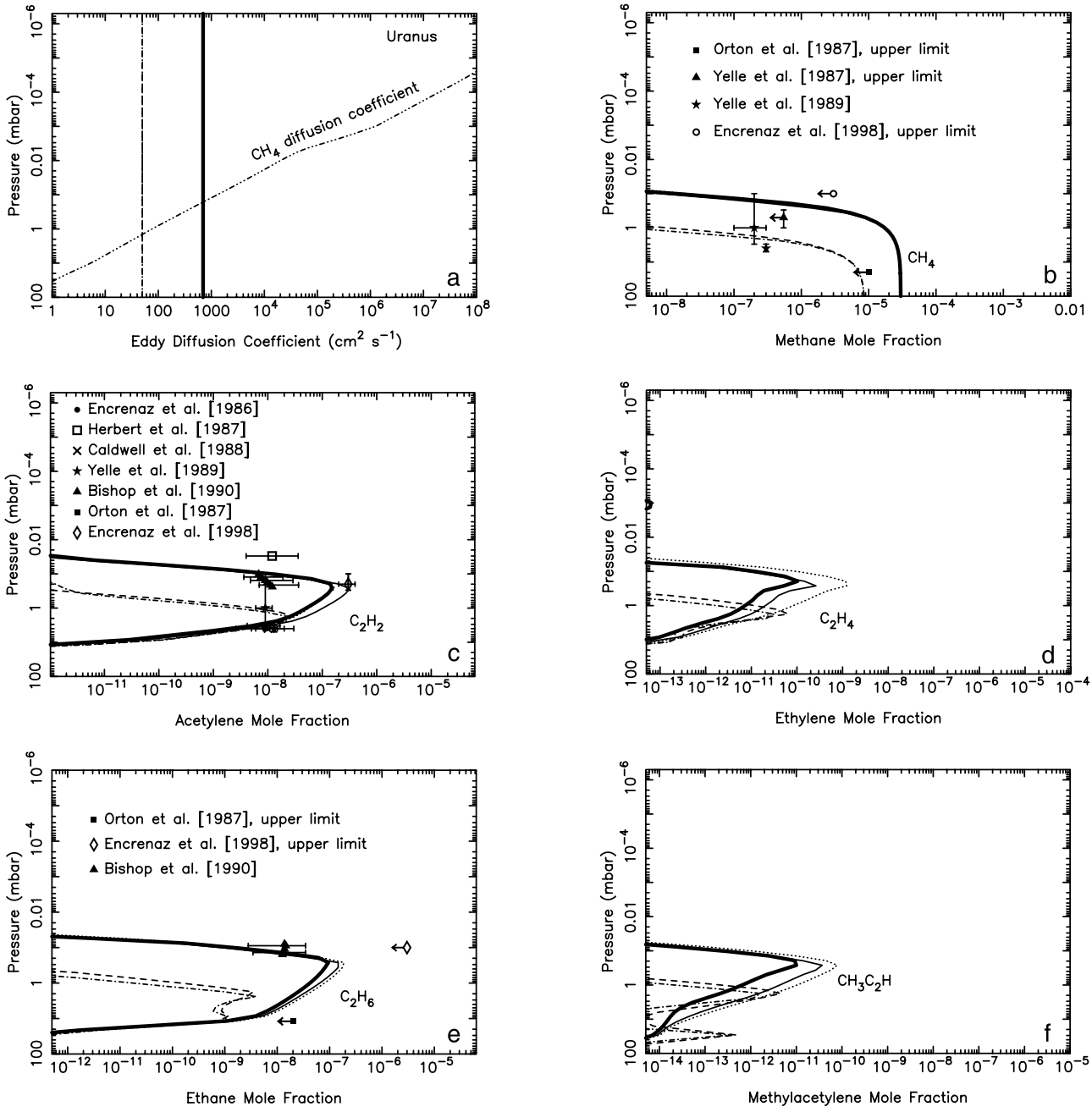

Figure 33. The photochemical model results for some of the hydrocarbons on Uranus: (a) eddy diffusion coefficient profile, and mixing ratio profiles for (b) CH_4, (c) C_2H_2, (d) C_2H_4, (e) C_2H_6, and (f) CH_3C_2H. The dotted lines represent a model that has the same chemical reaction list as the Jupiter Models A and B and an eddy diffusion coefficient of 700 $cm^2\ s^{-1}$, the thin solid lines represent a model that has the same reaction list as Jupiter Model C and an eddy diffusion coefficient of 700 $cm^2\ s^{-1}$, and the dotted lines represent a model that has the same reaction list as Jupiter Models A and B and an eddy diffusion coefficient of 50 $cm^2\ s^{-1}$. The model represented by dot-dashed lines is the same as that for the dotted lines, except the solar zenith angle has been fixed at 21°. The model represented by the thick solid line is the same as that for the thin solid line, except the solar zenith angle has been fixed at 83°. The various data points with associated error bars represent observational measurements or upper limits, as labeled.

standard observations in the $\nu_3 + \nu_4 - \nu_4$ band at ~3.3 μm [e.g., *Drossart et al.*, 2001] could help resolve the ambiguity in the methane homopause level. In the meantime, forward modeling techniques using the results of new photochemical models like the ones presented here could be applied to various existing data sets (e.g., UVS occultations, CH_4 ν_3 fluorescence data, He 584 Å emission) to check whether the models are consistent with the data. The

Table 6. Chemical Kinetics Needs

Number	Reaction	Comments
R5–R9	$CH_4 \xrightarrow{h\nu}$ products	Need quantum yields (especially for CH) and branching ratios, especially at Ly α.
R10–R21	$C_2H_x \xrightarrow{h\nu}$ products	Need quantum yields and branching ratios, especially in the 1500–2200 Å region.
R22–R80	C_3H_x, $C_4H_x \xrightarrow{h\nu}$ products	Need low-temperature absorption cross sections and information on quantum yields/branching ratios as a function of wavelength.
R89–R93	$C_6H_6 \xrightarrow{h\nu}$ products	Need low-temperature absorption cross sections, quantum yields, information on the pressure and temperature dependence of photolysis, and fate of the photolysis products.
R181	$2\ H \xrightarrow{M} H_2$	Need rate coefficient at low temperatures.
R186	$H + CH_3 \xrightarrow{M} CH_4$	Need laboratory measurements of rate constant at low temperatures and low pressures.
R190	$H + C_2H_2 \xrightarrow{M} C_2H_3$	Need laboratory measurements of rate constant at low temperatures and low pressures.
R191–R192	$H + C_2H_3 \longrightarrow$ products	Need to understand the relative efficiency of these two reactions at lower temperatures and lower pressures than has currently been investigated. Note that theoretical predictions differ from laboratory measurements.
R194	$H + C_2H_4 \xrightarrow{M} C_2H_5$	Need laboratory measurements of the rate constant at low temperatures and low pressures.
R199–R217	$H + C_3H_x \longrightarrow$ products	Need information on the relative efficiencies of different reaction pathways, as well as the rate coefficient at low temperature, pressure.
–	$H + CH_3CCH_2 \longrightarrow$ products	Need information on products and rate at low temperatures and pressures.
R258–R259	$^1CH_2 + H_2 \longrightarrow$ products	Need information on relative efficiencies of different pathways at low temperatures and pressures.
R328	$C_2H_3 + H_2 \longrightarrow C_2H_4 + H$	Need laboratory measurements of the rate coefficient at low temperatures. Note that a wide discrepancy in room-temperature values exists from both experiments and theory.

assumptions involved in the analyses of the various data sets also need to be critically reviewed.

[92] Regardless of the homopause level, the ISO C_2H_6 observations can be used to place suitable constraints on the eddy diffusion coefficient profile in Jupiter's stratosphere. The information on the slope of the C_2H_6 mixing ratio derived by ISO greatly aids this analysis, although nonuniqueness problems still hamper the modeling. Ethane is produced primarily near the methane homopause region at high altitudes. Once produced, C_2H_6 is fairly stable photochemically, and its vertical profile depends to a large extent on the eddy diffusion coefficient profile. The slope and magnitude of the K profile in the upper stratosphere can be constrained from both the inferred C_2H_6 abundance at 3.5 mbar and the homopause level derived from either the He 584 Å data or the UVS CH_4 data. The C_2H_6 mixing ratio in the 10-mbar region is very sensitive to K_{min}, the minimum value of the eddy diffusion coefficient profile near the tropopause, as well as to the overall K profile in the lower stratosphere. Given the uncertainties in the chemical reaction scheme and the homopause level, as well as the nonuniqueness of the model fit, we cannot place fully robust constraints on the diffusion coefficient profile. For instance, we find it necessary to put a break in the slope of our K profiles near 1 mbar, and again at pressures below 0.1 mbar, to fit both the altitude-dependent C_2H_6 data from ISO and the homopause level inferences; however, the uncertainties in the homopause level and the reaction scheme are large enough that no concrete conclusions are extracted regarding the overall "shape" of the K profile. Nevertheless, we can say that our modeling suggests that K_{min} must be less than 10^3 cm^2 s^{-1} and K must be less than $\sim 3 \times 10^4$ cm^2 s^{-1} at pressures greater than 1 mbar to remain consistent with the observed C_2H_6 abundance. In addition, lower values of K_h (i.e., a methane homopause level at low altitudes) require smaller values of K in the lower stratosphere to remain consistent with ISO C_2H_6 observations.

[93] Although our models represent an improvement over many of the previous models in terms of their fit to ISO and other observations, not all the predicted hydrocarbon abundances are consistent with the observations to within the stated observational uncertainties. Methylacetylene is underpredicted in all models by a factor of $\sim$3. Benzene is underpredicted by factors of $\sim$2 (Model A) to $\sim$7 (Model C). Ethylene is overpredicted by Model A (factor of $\sim$2.8), Model B (factor of $\sim$2.1), and Model C (factor of $\sim$1.5) as compared with the observations of *Bézard et al.* [2002b]. The models suggest that we are missing some ways to convert C_2H_2 and (especially) C_2H_4 to C_2H_6 on Jupiter. We have attempted to change particular uncertain reaction rate coefficients to help lower the C_2H_4 abundance in our models; however, in doing so, we always altered the C_2H_2 profile in such a way that the models were no longer consistent with observations. Model C provides the best overall fit to the ISO data and has a reaction list that is the most consistent with theoretical data for certain reactions such as R190, R191, and R192. However, the adopted rate coefficient for R328 in Model C is at the high end of theoretical/laboratory measurements, and the C_2H_4 abundance is still overpredicted. More importantly, both the Model A and C reaction lists that were tested in this paper have some difficulties when applied to photochemical models of the other giant planets; that is, we again find some inconsistencies in the predicted abundances as compared with observations (especially in the case of C_2H_4 and C_2H_2). Our model-data comparisons lead us to believe that we do not yet completely understand the photochemistry of C_2H_x hydrocarbons at low temperatures and pressures in hydrogen-dominated atmospheres.

[94] Further progress in our understanding of hydrocarbon photochemistry on the outer planets hinges on the acquisition of high-quality kinetics data for several key reactions at low temperatures and pressures. Table 6 identifies some of these critical reactions. Although recent investigations have extended our knowledge of low-temperature rates in high-pressure regimes, information on the low-pressure limiting rate constant k_0 for termolecular reactions is often not available, especially at low temperatures. This information is critical to studies of giant-planet photochemistry because much of the activity occurs at low stratospheric pressures. Although theoretical calculations are very helpful, the predicted rates calculated using differ-

ent techniques often diverge at low temperatures, and independent confirmation from laboratory measurements is desirable. Our knowledge of low-temperature ultraviolet photoabsorption cross sections for relevant hydrocarbons has improved greatly in the past decade or so [e.g., *Wu et al.*, 2001, 2004; *Chen and Wu*, 2004; *Chen et al.*, 2000; *Bénilan et al.*, 2000; *Smith et al.*, 1998; *Fahr and Nayak*, 1994, 1996; *Smith et al.*, 1991]. However, the photolysis branching ratios and quantum yields are often poorly known or have been investigated only at a few specific wavelengths. Sensitivity studies and "uncertainty" studies such as those presented by *Smith et al.* [2003] and *Dobrijevic et al.* [2003] are very useful in identifying the key reactions at different altitudes and in evaluating the robustness of the models as a whole.

[95] Current and future spacecraft observations (e.g., Cassini) and high-spectral-resolution Earth-based infrared observations [e.g., *Greathouse et al.*, 2005; *Kostiuk et al.*, 2003; *Bézard et al.*, 2001a, 2002b] can also improve our understanding of hydrocarbon photochemistry on the giant planets. Information on the altitude profiles of major constituents will be particularly useful for constraining the photochemical models. Mapping the latitude distribution of both short-lived and long-lived hydrocarbons will also provide important tests of the 1-D seasonal/latitudinal photochemical models [e.g., *Moses and Greathouse*, 2005], and will indicate whether 2-D models that include meridional transport are needed to explain the observations. Note that photochemical model comparisons with observations from Jupiter [*Kunde et al.*, 2004; Nixon et al., submitted manuscript, 2005], Saturn [*Greathouse et al.*, 2005; *Moses and Greathouse*, 2005], and Titan [e.g., *Lebonnois et al.*, 2001; *Luz et al.*, 2003] indicate that stratospheric circulation and meridional transport can affect the latitudinal distribution of hydrocarbons on these planets. For the giant planets, the meridional transport time scales appear to be long enough that only the most photochemically stable species (e.g., C_2H_6) are affected by meridional circulation. Photochemical models would also benefit from the acquisition of data that help pinpoint the methane homopause location across the giant planets (e.g., Cassini UVIS occultation observations) with an altitude resolution of 20 km; such observations would be important for constraining both the eddy diffusion coefficient profile and the production efficiency of higher-order hydrocarbons.

[96] Our model-data comparisons for the giant planets illustrate the importance of testing a proposed reaction scheme against available global-average data from all low-temperature, hydrogen-dominated planets for which we have hydrocarbon abundance observations. A single reaction scheme that works well for one planet may fail for another, indicating that some problems exist with the proposed scheme. Applying the hydrocarbon reaction scheme to photochemical models of Titan's stratosphere would also be illuminating. Titan's hydrocarbon photochemistry is similar in many respects to that of the giant planets, but H_2 is no longer the background gas, and reactions with H_2 and even H decline in importance. Recent studies applying the same reaction schemes to Titan and the giant planets [e.g., *Lebonnois*, 2005; *Lee et al.*, 2000] have highlighted several key similarities and differences in the hydrocarbon chemistry between these different classes of objects. The comparative planetology approach to the problem provides fundamental information that may help identify the weaknesses and strengths of the proposed reaction schemes.

[97] **Acknowledgments.** The Caltech/JPL KINETICS code was developed by Yuk L. Yung and Mark Allen, with assistance from many people over the years. We are grateful to them for allowing the first author to use this powerful and adaptable code. Fruitful discussions with Greg Smith, Askar Fahr, and Tommy Greathouse improved the quality the investigation and are greatly appreciated. We thank Robert Wu and Long Lee for providing cross-section data in digital form. This work was supported by NASA Planetary Atmospheres grants NAG5-11032 and NNG05GA42G and by the Lunar and Planetary Institute, which is operated by the Universities Space Research Association under a NASA contract. This paper represents LPI contribution 1253.

References

Alkemade, U., and K. H. Homann (1989), Formation of C_6H_6 isomers by recombination of propynyl in the system sodium vapour/propynylhalide, *Z. Phys. Chem. Neue Folge*, *161*, 19–34.

Allara, D. L., and R. Shaw (1980), A compilation of kinetic parameters for the thermal degradation of *n*-alkane molecules, *J. Phys. Chem. Ref. Data*, *9*, 523–559.

Allen, M., J. P. Pinto, and Y. L. Yung (1980), Titan: Aerosol photochemistry and variations related to the sunspot cycle, *Astrophys. J.*, *242*, L125–L128.

Allen, M., Y. L. Yung, and J. W. Waters (1981), Vertical transport and photochemistry in the terrestrial mesosphere and lower thermosphere (50–120 km), *J. Geophys. Res.*, *86*, 3617–3627.

Allen, M., Y. L. Yung, and G. R. Gladstone (1992), The relative abundance of ethane to acetylene in the Jovian stratosphere, *Icarus*, *100*, 527–533.

Atkinson, D. B., and J. W. Hudgens (1999), Rate coefficients for the propargyl self-reaction and oxygen addition reaction measured using ultraviolet ring-down spectroscopy, *J. Phys. Chem. A*, *103*, 4242–4252.

Atreya, S. K. (1986), *Atmospheres and Ionospheres of the Outer Planets and Their Satellites*, 224 pp., Springer, New York.

Atreya, S. K., and T. M. Donahue (1979), Models of the Jovian upper atmosphere, *Rev. Geophys.*, *17*, 388–396.

Atreya, S. K., Y. L. Yung, T. M. Donahue, and E. S. Barker (1977), Search for Jovian auroral hot spots, *Astrophys. J.*, *218*, L83–L87.

Atreya, S. K., T. M. Donahue, and M. C. Festou (1981), Jupiter: Structure and composition of the upper atmosphere, *Astrophys. J.*, *247*, L43–L47.

Baulch, D. L., et al. (1994), Evaluated kinetic data for combustion modeling, *J. Phys. Chem. Ref. Data*, *23*, 847–1033. (Errata, *J. Phys. Chem. Ref. Data*, *24*, 1609–1630, 1995.)

Becker, K. H., R. Kurtenbach, and P. Wiesen (1991), Temperature and pressure dependence of the reaction CH + H_2, *J. Phys. Chem.*, *95*, 2390–2394.

Bénilan, Y., N. Smith, A. Jolly, and F. Raulin (2000), The long wavelength range temperature variations of the mid-UV acetylene absorption coefficient, *Planet. Space Sci.*, *48*, 463–471.

Ben Jaffel, L., C. Magnan, and A. Vidal-Madjar (1988), The Lyman alpha albedo of Jupiter, *Astron. Astrophys.*, *204*, 319–326.

Ben Jaffel, L., J. T. Clarke, R. Prangé, G. R. Gladstone, and A. Vidal-Madjar (1993), The Lyman alpha bulge of Jupiter: Effects of non-thermal velocity field, *Geophys. Res. Lett.*, *20*, 747–750.

Bergin, E. A., et al. (2000), Submillimeter Wave Astronomy Satellite observations of Jupiter and Saturn: Detection of 557 GHz water emission from the upper atmosphere, *Astrophys. J.*, *539*, L147–L150.

Berman, M. R., and M. C. Lin (1984), Kinetics and mechanisms of the reactions of CH and CD with H_2, and D_2, *J. Chem. Phys.*, *81*, 5743–5750.

Bézard, B., P. N. Romani, B. J. Conrath, and W. C. Maguire (1991), Hydrocarbons in Neptune's stratosphere from Voyager infrared observations, *J. Geophys. Res.*, *96*, 18,961–18,975.

Bézard, B., H. Feuchtgruber, J. I. Moses, and T. Encrenaz (1998), Detection of methyl radicals (CH_3) on Saturn, *Astron. Astrophys.*, *334*, L41–L44.

Bézard, B., P. N. Romani, H. Feuchtgruber, and T. Encrenaz (1999), Detection of the methyl radical on Neptune, *Astrophys. J.*, *515*, 868–872.

Bézard, B., J. I. Moses, J. Lacy, T. Greathouse, M. Richter, and C. Griffith (2001a), Detection of ethylene C_2H_4 on Jupiter and Saturn in non-auroral regions, *Bull. Am. Astron. Soc.*, *33*, 1079–1080.

Bézard, B., P. Drossart, T. Encrenaz, and H. Feuchtgruber (2001b), Benzene on the giant planets, *Icarus*, *154*, 492–500.

Bézard, B., E. Lellouch, D. Strobel, J.-P. Maillard, and P. Drossart (2002a), Carbon monoxide on Jupiter: Evidence for both internal and external sources, *Icarus*, *159*, 95–111.

Bézard, B., T. Greathouse, J. Lacy, M. J. Richter, J. Moses, and C. Griffith (2002b), High spectral resolution observations of Jupiter and Saturn near 10 micron: Ethylene and the CH_3D/CH_4 ratio, paper presented at Jupiter after Galileo and Cassini, Lisbon, 17–21 June.

Bishop, J., S. K. Atreya, F. Herbert, and P. Romani (1990), Reanalysis of Voyager 2 UVS solar occultations at Uranus: Hydrocarbon mixing ratios in the equatorial stratosphere, *Icarus*, *88*, 448–464.

Bishop, J., S. K. Atreya, P. N. Romani, B. R. Sandel, and F. Herbert (1992), Voyager 2 ultraviolet spectrometer solar occultations at Neptune: Constraints on the abundance of methane in the stratosphere, *J. Geophys. Res.*, *97*, 11,681–11,694.

Bishop, J., P. N. Romani, and S. K. Atreya (1998), Voyager 2 ultraviolet spectrometer solar occultations at Neptune: Photochemical modeling of the 125–165 nm lightcurves, *Planet. Space Sci.*, *46*, 1–20.

Blitz, M. A., M. J. Pilling, and P. W. Seakins (2001), Collision induced intersystem crossing in methylene on reactive surfaces: Application of a new technique to CH_2 (a^1A_1) + H_2, *Phys. Chem. Chem. Phys.*, *3*, 2241–2244.

Borysow, A., and L. Frommhold (1986), Theoretical collision induced rototranslational absorption spectra for the outer planets: H_2-CH_4 pairs, *Astrophys. J.*, *304*, 849–865.

Borysow, J., L. Trafton, L. Frommhold, and G. Birnbaum (1985), Modeling of pressure-induced far-infrared absorption spectra: Molecular hydrogen pairs, *Astrophys. J.*, *296*, 644–654.

Borysow, J., L. Frommhold, and G. Birnbaum (1988), Collision-induced rototranslational absorption spectra of H_2-He pairs at temperatures from 40 to 3000 K, *Astrophys. J.*, *326*, 509–515.

Braun, W., A. M. Bass, and M. Pilling (1970), Flash photolysis of ketene and diazomethane: The production and reaction kinetics of triplet and singlet methylene, *J. Chem. Phys.*, *52*, 5131–5143.

Broadfoot, A. L., B. R. Sandel, D. E. Shemansky, J. C. McConnell, G. R. Smith, J. B. Holberg, S. K. Atreya, T. M. Donahue, D. F. Strobel, and J. L. Bertaux (1981), Overview of the Voyager ultraviolet spectrometry results through Jupiter encounter, *J. Geophys. Res.*, *86*, 8259–8284.

Brooke, T. Y., R. F. Knacke, T. Encrenaz, P. Drossart, D. Crisp, and H. Feuchtgruber (1998), Models of the ISO 3-μm reflection spectrum of Jupiter, *Icarus*, *136*, 1–13.

Brouard, M., M. T. MacPherson, and M. J. Pilling (1989), Experimental and RRKM modeling study of the CH_3 + H and CH_3 + D reactions, *J. Phys. Chem.*, *93*, 4047–4059.

Caldwell, J., R. Wagener, and K.-H. Fricke (1988), Observations of Neptune and Uranus below 2000 Å with the IUE, *Icarus*, *74*, 133–140.

Callear, A. B., and G. B. Smith (1986), Recurring chains following addition of atomic hydrogen to acetylene, *J. Phys. Chem.*, *90*, 3229–3237.

Carlson, R. W., and D. L. Judge (1971), The extreme ultraviolet dayglow of Jupiter, *Planet. Space Sci.*, *19*, 327–343.

Carlson, R. W., and D. L. Judge (1974), Pioneer 10 ultraviolet photometer observations at Jupiter encounter, *J. Geophys. Res.*, *79*, 3623–3633.

Chen, F. Z., and C. Y. R. Wu (2004), Temperature-dependent photoabsorption cross sections in the VUV-UV region. I. Methane and ethane, *J. Quant. Spectrosc. Radiat. Transfer*, *85*, 195–209.

Chen, F., D. L. Judge, C. Y. R. Wu, J. Caldwell, H. P. White, and R. Wagener (1991), High-resolution low-temperature photoabsorption cross sections of C_2H_2, PH_3, AsH_3, and GeH_4, with application to Saturn's atmosphere, *J. Geophys. Res.*, *96*, 17,519–17,527.

Chen, F. Z., D. L. Judge, and C. Y. R. Wu (2000), Temperature dependent photoabsorption cross sections of allene and methyl-acetylene in the VUV-UV region, *Chem. Phys.*, *260*, 215–223.

Clarke, J. T., H. A. Weaver, P. D. Feldman, H. W. Moos, W. G. Fastie, and C. B. Opal (1980), Spatial imaging of hydrogen Lyman α emission from Jupiter, *Astrophys. J.*, *240*, 696–701.

Clarke, J. T., G. R. Gladstone, and L. Ben Jaffel (1991), Jupiter's dayglow H Ly alpha emission line profile, *Geophys. Res. Lett.*, *18*, 1935–1938.

Cody, R. J., W. A. Payne Jr., R. P. Thorn Jr., F. L. Nesbitt, M. A. Iannone, D. C. Tardy, and L. J. Stief (2002), Rate constant for the recombination reaction $CH_3 + CH_3 \rightarrow C_2H_6$ at T = 298 and 202 K, *J. Phys. Chem. A*, *106*, 6060–6067.

Cody, R. J., P. N. Romani, F. L. Nesbitt, M. A. Iannone, D. C. Tardy, and L. J. Stief (2003), Rate constant for the reaction $CH_3 + CH_3 \rightarrow C_2H_6$ at T = 155 K and model calculation of the CH_3 abundance in the atmospheres of Saturn and Neptune, *J. Geophys. Res.*, *108*(E11), 5119, doi:10.1029/2002JE002037.

Conrath, B. J., and D. Gautier (2000), Saturn helium abundance: A reanalysis of Voyager measurements, *Icarus*, *144*, 124–134.

Conrath, B. J., D. Gautier, R. A. Hanel, and J. S. Hornstein (1984), The helium abundance of Saturn from Voyager measurements, *Astrophys. J.*, *282*, 807–815.

Courtin, R., D. Gautier, A. Marten, B. Bézard, and R. Hanel (1984), The composition of Saturn's atmosphere at northern temperate latitudes from Voyager IRIS spectra: NH_3, PH_3, C_2H_2, C_2H_6, CH_3D, CH_4, and the Saturnian D/H isotopic ratio, *Astrophys. J.*, *287*, 899–916.

Dang-Nhu, M., and J. Pliva (1989), Intensities in the ν_4, ν_{12}, ν_{13}, and ν_{14} bands of benzene, *J. Mol. Spectrosc.*, *138*, 423–429.

de Graauw, T., et al. (1996), Observing with the ISO Short-Wavelength Spectrometer, *Astron. Astrophys.*, *315*, L49–L52.

DeMore, W. B., S. P. Sander, D. M. Golden, R. F. Hampson, M. J. Kurylo, C. J. Howard, A. R. Ravishankara, C. E. Kolb, and M. J. Molina (1992), *Chemical kinetics and photochemical data for use in stratospheric modeling, evaluation number 10*, *JPL Publ. 92-20*, Jet Propul. Lab., Pasadena, Calif.

Dobrijevic, M., J. L. Ollivier, F. Billebaud, J. Brillet, and J. P. Parisot (2003), Effect of chemical kinetic uncertainties on photochemical modeling results: Application to Saturn's atmosphere, *Astron. Astrophys.*, *398*, 335–344.

Drossart, P., T. Fouchet, J. Crovisier, E. Lellouch, T. Encrenaz, H. Feuchtgruber, and J. P. Champion (1999), Fluorescence in the 3 micron bands of methane on Jupiter and Saturn from ISO/SWS observations, in *The Universe as Seen by ISO*, edited by P. Cox and M. F. Kessler, *Eur. Space Agency Spec. Publ.*, *ESA SP-427*, 169–172.

Drossart, P., B. Sicardy, F. Roques, T. Widemann, G. R. Gladstone, J. H. Waite, and M. Vincent (2000), The methane homopause of Jupiter as seen in IR spectroscopy from the occultation of star HIP9369, *Bull. Am. Astron. Soc.*, *32*, 1013.

Drossart, P., T. Fouchet, E. Raynaud, B. Sicardy, T. Widemann, J. H. Waite, and G. R. Gladstone (2001), The upper atmosphere of Jupiter from VLT/ISAAC observations, *Bull. Am. Astron. Soc.*, *33*, 1026.

Durán, R. P., V. T. Amorebieta, and A. J. Colussi (1988), Is the homogeneous thermal dimerization of acetylene a free-radical chain reaction? Kinetic and thermochemical analysis, *J. Phys. Chem.*, *92*, 636–640.

Edgington, S. G., S. K. Atreya, L. M. Trafton, J. J. Caldwell, R. F. Beebe, A. A. Simon, R. A. West, and C. Barnet (1998), On the latitude variation of ammonia, acetylene, and phosphine altitude profiles on Jupiter from HST Faint Object Spectrograph observations, *Icarus*, *133*, 192–209.

Edgington, S. G., S. K. Atreya, L. M. Trafton, J. J. Caldwell, R. F. Beebe, A. A. Simon, and R. A. West (1999), Ammonia and eddy mixing variations in the upper troposphere of Jupiter from HST Faint Object Spectrograph observations, *Icarus*, *142*, 342–356.

Emerich, C., L. Ben Jaffel, and R. Prangé (1993), On the analysis of the H Lyman-α dayglow of Jupiter, Saturn and Uranus, *Planet. Space Sci.*, *41*, 363–371.

Emerich, C., L. Ben Jaffel, J. T. Clarke, R. Prangé, G. R. Gladstone, J. Sommeria, and G. Ballester (1996), Evidence for supersonic turbulence in the upper atmosphere of Jupiter, *Science*, *273*, 1085–1087.

Encrenaz, T. (2003), ISO observations of the giant planets and Titan: What have we learnt?, *Planet. Space Sci.*, *51*, 89–103.

Encrenaz, T., et al. (1986), A study of the upper atmosphere of Uranus using the IUE, *Astron. Astrophys.*, *162*, 317–322.

Encrenaz, T., et al. (1996), First results of ISO-SWS observations of Jupiter, *Astron. Astrophys.*, *315*, L397–L400.

Encrenaz, T., H. Feuchtgruber, S. K. Atreya, B. Bézard, E. Lellouch, J. Bishop, S. Edgington, T. de Graauw, M. Griffin, and M. F. Kessler (1998), ISO observations of Uranus: The stratospheric distribution of C_2H_2 and the eddy diffusion coefficient, *Astron. Astrophys.*, *333*, L43–L46.

Encrenaz, T., P. Drossart, H. Feuchtgruber, E. Lellouch, B. Bézard, T. Fouchet, and S. K. Atreya (1999), The atmospheric composition and structure of Jupiter and Saturn from ISO observations: A preliminary review, *Planet. Space Sci.*, *47*, 1225–1242.

Fahr, A. (1995), Rate constant and a detailed error analysis for C_2H_3 + H reaction, *Int. J. Chem. Kinet.*, *27*, 769–776.

Fahr, A., and A. K. Nayak (1994), Temperature dependent ultraviolet absorption cross sections of 1,3-butadiene and butadiyne, *Chem. Phys.*, *189*, 725–731.

Fahr, A., and A. Nayak (1996), Temperature dependent ultraviolet absorption cross sections of propylene, methylacetylene and vinylacetylene, *Chem. Phys.*, *203*, 351–358.

Fahr, A., and A. Nayak (2000), Kinetics and products of propargyl (C_3H_3) radical self-reactions and propargyl-methyl cross-combination reactions, *Int. J. Chem. Kinet.*, *32*, 118–124.

Fahr, A., P. S. Monks, L. J. Stief, and A. H. Laufer (1995), Experimental determination of the rate constant for the reaction of C_2H_3 with H_2 and implications for the partitioning of hydrocarbons in atmospheres of the outer planets, *Icarus*, *116*, 415–422.

Festou, M. C., and S. K. Atreya (1982), Voyager ultraviolet stellar occultation measurements of the composition and thermal profiles of the Saturnian upper atmosphere, *Geophys. Res. Lett.*, *9*, 1147–1150.

Festou, M. C., S. K. Atreya, T. M. Donahue, B. R. Sandel, D. E. Shemansky, and A. L. Broadfoot (1981), Composition and thermal profiles of the Jovian upper atmosphere determined by the Voyager

ultraviolet stellar occultation experiment, *J. Geophys. Res.*, *86*, 5715–5725.

Feuchtgruber, H., E. Lellouch, T. de Graauw, B. Bézard, T. Encrenaz, and M. Griffin (1997), External supply of oxygen to the atmospheres of the giant planets, *Nature*, *389*, 159–162.

Feuchtgruber, H., E. Lellouch, T. Encrenaz, B. Bézard, A. Coustenis, P. Drossart, A. Salama, T. de Graauw, and G. R. Davis (1999), Oxygen in the stratospheres of the giant planets and Titan, in *The Universe as Seen by ISO*, edited by P. Cox and M. F. Kessler, *Eur. Space Agency Spec. Publ.*, *ESA SP-427*, 133–136.

Flasar, F. M., and the Cassini CIRS Investigation Team (2004), Early results on the Saturn system from Cassini CIRS, *Bull. Am. Astron. Soc.*, *36*, abstract 1.05.

Forst, W. (1991), Microcanonical variational theory of radical recombination by inversion of interpolated partition function, with examples: CH_3 + H, CH_3 + CH_3, *J. Phys. Chem.*, *95*, 3612–3620.

Fouchet, T., E. Lellouch, B. Bézard, T. Encrenaz, P. Drossart, H. Feuchtgruber, and T. de Graauw (2000a), ISO-SWS observations of Jupiter: Measurement of the ammonia tropospheric profile and of the $^{15}N/^{14}N$ isotopic ratio, *Icarus*, *143*, 223–243.

Fouchet, T., E. Lellouch, B. Bézard, H. Feuchtgruber, P. Drossart, and T. Encrenaz (2000b), Jupiter's hydrocarbons observed with ISO-SWS: Vertical profiles of C_2H_6 and C_2H_2, detection of CH_3C_2H, *Astron. Astrophys.*, *355*, L13–L17.

Fouchet, T., E. Lellouch, and H. Feuchtgruber (2003), The hydrogen ortho-to-para ratio in the stratospheres of the giant planets, *Icarus*, *161*, 127–143.

Friedson, A. J., A.-S. Wong, and Y. L. Yung (2002), Models for polar haze formation in Jupiter's stratosphere, *Icarus*, *158*, 389–400.

Giles, J. W., H. W. Moos, and W. R. McKinney (1976), The far ultraviolet (1200–1900 Å) spectrum of Jupiter obtained with a rocket-borne multichannel spectrometer, *J. Geophys. Res.*, *81*, 5797–5806.

Gladstone, G. R. (1988), UV resonance line dayglow emissions on Earth and Jupiter, *J. Geophys. Res.*, *93*, 14,623–14,630.

Gladstone, G. R., and Y. L. Yung (1983), An analysis of the reflection spectrum of Jupiter from 1500 Å to 1740 Å, *Astrophys. J.*, *266*, 415–424.

Gladstone, G. R., D. T. Hall, and J. H. Waite Jr. (1995), EUVE observations of Jupiter during the impact of comet Shoemaker-Levy 9, *Science*, *268*, 1595–1597.

Gladstone, G. R., M. Allen, and Y. L. Yung (1996), Hydrocarbon photochemistry in the upper atmosphere of Jupiter, *Icarus*, *119*, 1–52.

Gladstone, G. R., W. R. Pryor, W. K. Tobiska, A. I. F. Stewart, K. E. Simmons, and J. M. Ajello (2004), Constraints on Jupiter's hydrogen corona from Galileo UVS observations, *Planet. Space Sci.*, *52*, 415–421.

Greathouse, T. K., J. H. Lacy, B. Bézard, J. I. Moses, C. A. Griffith, and M. J. Richter (2005), Meridional variations of temperature, C_2H_2 and C_2H_6 abundances in Saturn's stratosphere at southern summer solstice, *Icarus*, in press.

Hammel, H. B., D. K. Lynch, R. W. Russell, M. K. Sitko, and E. Polomski (2002), Neptune's ethane abundance and Uranus' lack thereof, *Bull. Am. Astron. Soc.*, *34*, 850.

Hanning-Lee, M. A., and M. J. Pilling (1992), Kinetics of the reaction between H atoms and allyl radicals, *Int. J. Chem. Kinet.*, *24*, 271–278.

Harding, L. B., and S. J. Klippenstein (2000), Theoretical kinetic estimates for the recombination of hydrogen atoms with propargyl and allyl radicals, *Proc. Combust. Inst.*, *28*, 1503–1509.

Herbert, F., B. R. Sandel, R. V. Yelle, J. B. Holberg, A. L. Broadfoot, D. E. Shemansky, S. K. Atreya, and P. N. Romani (1987), The upper atmosphere of Uranus: EUV occultations observed by Voyager 2, *J. Geophys. Res.*, *92*, 15,093–15,109.

Hippler, H., K. Luther, A. R. Ravishankara, and J. Troe (1984), High-pressure effects in the recombination reaction CH_3 + CH_3 → C_2H_6, *Z. Phys. Chem. (Neue Folge)*, *142*, 1–12.

Howe, P.-T., and A. Fahr (2003), Pressure and temperature effects on product channels of the propargyl (HC ≡ CCH_2) combination reaction and the formation of the "first ring," *J. Phys. Chem. A*, *107*, 9603–9610.

Hubbard, W. B., V. Haemmerle, C. C. Porco, G. H. Rieke, and M. Rieke (1995), The occultation of SAO 78505 by Jupiter, *Icarus*, *113*, 103–109.

Hunten, D. M. (1969), The upper atmosphere of Jupiter, *J. Atmos. Sci.*, *26*, 826–834.

Jacquinet-Husson, N., et al. (1999), The 1997 spectroscopic GEISA databank, *J. Quant. Spectrosc. Radiat. Transfer*, *62*, 205–254.

Karkoschka, E., and M. G. Tomasko (1992), Saturn's upper atmospheric hazes observed by the Hubble Space Telescope, *Icarus*, *106*, 428–441.

Kerola, D. X., H. P. Larson, and M. G. Tomasko (1997), Analysis of the near-IR spectrum of Saturn: A comprehensive radiative transfer model of its middle and upper troposphere, *Icarus*, *127*, 190–212.

Kessler, M. F., et al. (1996), The Infrared Space Observatory (ISO) mission, *Astron. Astrophys.*, *315*, L27–L30.

Killen, R. M. (1988), Longitudinal variations in the Saturnian atmosphere. I. Equatorial region, *Icarus*, *73*, 227–247.

Klippenstein, S. J., and L. B. Harding (1999a), A direct transition state theory based study of methyl radical recombination kinetics, *J. Phys. Chem. A*, *103*, 9388–9398.

Klippenstein, S. J., and L. B. Harding (1999b), A theoretical study of the kinetics of C_2H_3 + H, *Phys. Chem. Chem. Phys.*, *1*, 989–997.

Knyazev, V. D., and I. R. Slagle (1996), Experimental and theoretical study of the $C_2H_3 \rightleftharpoons H + C_2H_2$ reaction: Tunneling and the shape of falloff curves, *J. Phys. Chem.*, *100*, 16,899–16,911.

Knyazev, V. D., and I. R. Slagle (2001), Kinetics of the reactions of allyl and propargyl radicals with CH_3, *J. Phys. Chem. A*, *105*, 3196–3204.

Knyazev, V. D., A. Bencsura, S. I. Stoliarov, and I. R. Slagle (1996), Kinetics of the $C_2H_3 + H_2 \rightleftharpoons H + C_2H_4$ and $CH_3 + H_2 \rightleftharpoons H + CH_4$ reactions, *J. Phys. Chem.*, *100*, 11,346–11,354.

Kostiuk, T., F. Espenak, M. J. Mumma, D. Deming, and D. Zipoy (1987), Variability of ethane on Jupiter, *Icarus*, *72*, 394–410.

Kostiuk, T., P. Romani, F. Espenak, and B. Bézard (1992), Stratospheric ethane on Neptune: Comparison of groundbased and Voyager IRIS retrievals, *Icarus*, *99*, 353–362.

Kostiuk, T., P. Romani, F. Espenak, T. A. Livengood, and J. J. Goldstein (1993), Temperature and abundances in the Jovian auroral stratosphere. 2. Ethylene as a probe of the microbar region, *J. Geophys. Res.*, *98*, 18,823–18,830.

Kostiuk, T., K. Fast, T. A. Livengood, F. Schmuelling, T. Hewagama, D. Buhl, P. Romani, and H. U. Kaufl (2003), Ethane on Saturn: Spatial and temporal variation, *Bull. Am. Astron. Soc.*, *35*, abstract 50.05.

Kunde, V. G., et al. (2004), Jupiter's atmospheric composition from the Cassini thermal infrared spectroscopy experiment, *Science*, *305*, 1582–1586.

Landry, B., M. Allen, and Y. L. Yung (1991), Troposphere-stratosphere interactions in a one-dimensional model of Jovian photochemistry, *Icarus*, *89*, 377–383.

Langford, A. O., H. Petek, and C. B. Moore (1983), Collisional removal of CH_2 ($^1A_1$): Absolute rate constants for atomic and molecular collisional partners at 295 K, *J. Chem. Phys.*, *78*, 6650–6659.

Lara, L. M., E. Lellouch, J. J. López-Moreno, and R. Rodrigo (1996), Vertical distribution of Titan's atmospheric neutral constituents, *J. Geophys. Res.*, *113*, 2–26.

Lara, L.-M., B. Bézard, C. A. Griffith, J. H. Lacy, and T. Owen (1998), High-resolution 10-micronmeter spectroscopy of ammonia and phosphine lines on Jupiter, *Icarus*, *131*, 317–333.

Laufer, A. H., E. P. Gardner, T. L. Kwok, and Y. L. Yung (1983), Computations and estimates of rate coefficients for hydrocarbon reactions of interest to the atmospheres of the outer solar system, *Icarus*, *56*, 560–567.

Lebonnois, S. (2005), Benzene and aerosol production in Titan and Jupiter's atmospheres: A sensitivity study, *Planet. Space Sci.*, *53*, 486–497.

Lebonnois, S., D. Toublanc, F. Hourdin, and P. Rannou (2001), Seasonal variations in Titan's atmospheric composition, *Icarus*, *152*, 384–406.

Lebonnois, S., E. L. O. Bakes, and C. P. McKay (2003), Atomic and molecular hydrogen budget in Titan's atmosphere, *Icarus*, *161*, 474–485.

Lee, A. Y. T., Y. L. Yung, and J. Moses (2000), Photochemical modeling of CH_3 abundances in the outer solar system, *J. Geophys. Res.*, *105*, 20,207–20,225.

Lellouch, E., B. Bézard, T. Fouchet, H. Feuchtgruber, T. Encrenaz, and T. de Graauw (2001), The deuterium abundance in Jupiter and Saturn from ISO-SWS observations, *Astron. Astrophys.*, *370*, 610–622.

Lellouch, E., B. Bézard, J. I. Moses, G. R. Davis, P. Drossart, H. Feuchtgruber, E. A. Bergin, R. Moreno, and T. Encrenaz (2002), The origin of water vapor and carbon dioxide in Jupiter's stratosphere, *Icarus*, *159*, 112–131.

Lellouch, E., D. F. Strobel, B. Bézard, G. L. Bjoraker, F. M. Flasar, and P. N. Romani (2005), The HCN and CO_2 distribution on Jupiter, *Bull. Am. Astron. Soc.*, *36*, abstract 30.01.

Lightfoot, P. D., and M. J. Pilling (1987), Temperature and pressure dependence of the rate constant for the addition of H to C_2H_4, *J. Phys. Chem.*, *91*, 3373–3379.

Lindal, G. F. (1992), The atmosphere of Neptune: An analysis of radio occultation data acquired with Voyager 2, *Astron. J.*, *103*, 967–982.

Lindemayer, J., U. Magg, and H. Jones (1988), Diode laser spectroscopy of the ν_4 band of benzene, *J. Mol. Spectrosc.*, *128*, 172–175.

Lindzen, R. S. (1981), Turbulence and stress owing to gravity wave and tidal breakdown, *J. Geophys. Res.*, *86*, 9707–9714.

Livengood, T. A., H. B. Hammel, T. Kostiuk, J. N. Annen, K. E. Fast, T. Hewagama, F. Schmülling, and D. Buhl (2002), A new infrared heterodyne search for ethane in the stratosphere of Uranus, *Bull. Am. Astron. Soc.*, *34*, 851.

Luz, D., F. Hourdin, P. Rannou, and S. Lebonnois (2003), Latitudinal transport by barotropic waves in Titan's stratosphere. II. Results from a coupled dynamics-microphysics-photochemistry GCM, *Icarus*, *166*, 343–358.

McConnell, J. C., B. R. Sandel, and A. L. Broadfoot (1981), Voyager U. V. spectrometer observations of He 584 Å dayglow at Jupiter, *Planet. Space Sci.*, *29*, 283–292.

McGrath, M. A. (1991), An unusual change in the Jovian Lyman-alpha bulge, *Geophys. Res. Lett.*, *18*, 1931–1934.

McGrath, M. A., and J. T. Clarke (1992), HI Lyman alpha emission from Saturn (1980–1990), *J. Geophys. Res.*, *97*, 13,691–13,703.

Mebel, A. M., K. Morokuma, and M. C. Lin (1995), Ab initio molecular orbital study of potential energy surface for the reaction of C_2H_3 with H_2 and related reactions, *J. Chem. Phys.*, *103*, 3440–3449.

Mebel, A. M., S. H. Lin, X. M. Yang, and Y. T. Lee (1997), Theoretical study on the mechanism of the dissociation of benzene: The C_5H_3 + CH_3 product channel, *J. Phys. Chem. A*, *101*, 6781–6789.

Medvedev, A. S., and G. P. Klassen (1995), Vertical evolution of gravity wave spectra and the parameterization of associated wave drag, *J. Geophys. Res.*, *100*, 25,841–25,853.

Michelangeli, D. V., M. Allen, Y. L. Yung, R.-L. Shia, D. Crisp, and J. Eluszkiewicz (1992), Enhancement of atmospheric radiation by an aerosol layer, *J. Geophys. Res.*, *97*, 865–874.

Miller, J. A., and S. J. Klippenstein (2004), The H + C_2H_2 (+M) $\rightleftharpoons$ C_2H_3 (+M) and H + C_2H_4 (+M) $\rightleftharpoons$ C_2H_5 (+M) reactions: Electronic structure, variational transition-state theory, and solutions to a two-dimensional master equation, *Phys. Chem. Chem. Phys.*, *6*, 1192–1202.

Monks, P. S., F. L. Nesbitt, W. A. Payne, M. Scanlon, L. J. Stief, and D. E. Shallcross (1995), Absolute rate constant and product branching ratios for the reaction between H and C_2H_3 at T = 213 and 298 K, *J. Phys. Chem.*, *99*, 17,151–17,159.

Moreno, R., A. Marten, H. E. Matthews, and Y. Biraud (2003), Long-term evolution of CO, CS and HCN in Jupiter after the impacts of comet Shoemaker-Levy 9, *Planet. Space Sci.*, *51*, 591–611.

Morrissey, P. F., P. D. Feldman, M. A. McGrath, B. C. Wolven, and H. W. Moos (1995), The ultraviolet reflectivity of Jupiter at 3.5 Å resolution from Astro-1 and Astro-2, *Astrophys. J.*, *454*, L65–L68.

Morter, C. L., S. K. Farhat, J. D. Adamson, G. P. Glass, and R. F. Curl (1994), Rate constant measurements of the recombination reaction C_3H_3 + C_3H_3, *J. Phys. Chem.*, *98*, 7029–7035.

Moses, J. I. (1996), SL9 impact chemistry: Long-term photochemical evolution, in *The Collision of Comet Shoemaker-Levy 9 and Jupiter*, edited by K. S. Noll, H. A. Weaver, and P. D. Feldman, pp. 243–268, Cambridge Univ. Press, New York.

Moses, J. I. (2001), Meteoroid ablation on the outer planets, *Lunar Planet. Sci.*, *XXXII*, abstract 1161.

Moses, J. I., and T. K. Greathouse (2005), The variation of hydrocarbon abundances with latitude and season in Saturn's stratosphere, *Proc. Lunar Planet. Sci. Conf. 36th*, abstract 1342.

Moses, J. I., K. Rages, and J. B. Pollack (1995), An analysis of Neptune's stratospheric haze using high-phase-angle Voyager images, *Icarus*, *113*, 232–266.

Moses, J. I., B. Bézard, E. Lellouch, G. R. Gladstone, H. Feuchtgruber, and M. Allen (2000a), Photochemistry of Saturn's atmosphere. I. Hydrocarbon chemistry and comparisons with ISO observations, *Icarus*, *143*, 244–298.

Moses, J. I., E. Lellouch, B. Bézard, G. R. Gladstone, H. Feuchtgruber, and M. Allen (2000b), Photochemistry of Saturn's atmosphere. II. Effects of an influx of external material, *Icarus*, *145*, 166–202.

Moses, J. I., T. Fouchet, R. V. Yelle, A. J. Friedson, G. S. Orton, B. Bézard, P. Drossart, G. R. Gladstone, T. Kostiuk, and T. A. Livengood (2004), The stratosphere of Jupiter, in *Jupiter: Planet, Satellites and Magnetosphere*, edited by F. Bagenal, W. McKinnon, and T. Dowling, pp. 129–157, Cambridge Univ. Press, New York.

Nakashima, N., and K. Yoshihara (1982), Laser photolysis of benzene. V. Formation of hot benzene, *J. Chem. Phys.*, *77*, 6040–6050.

Niemann, H. B., et al. (1998), The composition of the Jovian atmosphere as determined by the Galileo probe mass spectrometer, *J. Geophys. Res.*, *103*, 22,831–22,845.

Noll, K. S., R. F. Knacke, A. T. Tokunaga, J. H. Lacy, S. Beck, and E. Serabyn (1986), The abundances of ethane and acetylene in the atmospheres of Jupiter and Saturn, *Icarus*, *65*, 257–263.

Orton, G. S., D. K. Aitken, C. Smith, P. F. Roche, J. Caldwell, and R. Snyder (1987), The spectra of Uranus and Neptune at 8–14 and 17–23 microns, *Icarus*, *70*, 1–12.

Orton, G. S., J. H. Lacy, J. M. Achtermann, P. Parmar, and W. E. Blass (1992), Thermal spectroscopy of Neptune: The stratospheric temperature, hydrocarbon abundances, and isotopic ratios, *Icarus*, *100*, 541–555.

Pantos, E., J. Philis, and A. Bolovinos (1978), The extinction coefficient of benzene vapor in the region 4.6 to 36 eV, *J. Mol. Spectrosc.*, *72*, 36–43.

Parkinson, C. D., E. Griffioen, J. C. McConnell, G. R. Gladstone, and B. R. Sandel (1998), He 584 Å dayglow at Saturn: A reassessment, *Icarus*, *133*, 210–220.

Payne, W. A., and L. J. Stief (1976), Absolute rate constant for the reaction of atomic hydrogen with acetylene over an extended pressure and temperature range, *J. Chem. Phys.*, *56*, 1150–1155.

Prasad, S. S., L. A. Capone, and L. J. Schneck (1975), Photochemistry of hydrocarbons in the Jovian upper atmosphere, *Geophys. Res. Lett.*, *2*, 161–164.

Romani, P. N. (1996), Recent rate constant and product measurements of the reactions C_2H_3 + H_2 and C_2H_3 + H—Importance for photochemical modeling of hydrocarbons on Jupiter, *Icarus*, *122*, 233–241.

Romani, P. N., and S. K. Atreya (1988), Methane photochemistry and haze production on Neptune, *Icarus*, *74*, 424–445.

Romani, P. N., J. Bishop, B. Bézard, and S. Atreya (1993), Methane photochemistry on Neptune: Ethane and acetylene mixing ratios and haze production, *Icarus*, *106*, 442–463.

Rottman, G. J., H. W. Moos, and C. S. Freer (1973), The far-ultraviolet spectrum of Jupiter, *Astrophys. J.*, *184*, L89–L92.

Sada, P. V., G. H. McCabe, G. L. Bjoraker, D. E. Jennings, and D. C. Reuter (1996), ^{13}C-ethane in the atmospheres of Jupiter and Saturn, *Astrophys. J.*, *472*, 903–907.

Sada, P. V., G. L. Bjoraker, D. E. Jennings, G. H. McCabe, and P. N. Romani (1998), Observations of CH_4, C_2H_6, and C_2H_2 in the stratosphere of Jupiter, *Icarus*, *136*, 192–201.

Sada, P. V., G. L. Bjoraker, D. E. Jennings, P. N. Romani, and G. H. McCabe (2005), Observations of C_2H_6 and C_2H_2 in the stratosphere of Saturn, *Icarus*, *173*, 499–507.

Sandel, B. R., A. L. Broadfoot, and D. F. Strobel (1980), Discovery of a longitudinal asymmetry in the H Lyman-alpha brightness of Jupiter, *Geophys. Res. Lett.*, *7*, 5–8.

Schulz, B., T. Encrenaz, B. Bézard, P. N. Romani, E. Lellouch, and S. K. Atreya (1999), Detection of C_2H_4 in Neptune from ISO/PHT-S observations, *Astron. Astrophys.*, *350*, L13–L17.

Seakins, P. W., S. H. Robertson, M. J. Pilling, D. M. Wardlaw, F. L. Nesbitt, R. P. Thorn, W. A. Payne, and L. J. Stief (1997), Temperature and isotope dependence of the reaction of methyl radicals with deuterium, *J. Phys. Chem. A*, *101*, 9974–9987.

Seiff, A., D. B. Kirk, T. C. D. Knight, R. E. Young, J. D. Mihalov, L. A. Young, F. S. Milos, G. Schubert, R. C. Blanchard, and D. Atkinson (1998), Thermal structure of Jupiter's atmosphere near the edge of a 5-μm hot spot in the north equatorial belt, *J. Geophys. Res.*, *103*, 22,857–22,889.

Shemansky, D. E. (1985), An explanation for the H Ly α longitudinal asymmetry in the equatorial spectrum of Jupiter: An outcrop of paradoxical energy deposition in the exosphere, *J. Geophys. Res.*, *90*, 2673–2694.

Shemansky, D. E., and D. L. Judge (1988), Evidence for change in particle excitation of Jupiter's atmosphere 1968–1979, *J. Geophys. Res.*, *93*, 21–28.

Skinner, T. E., M. T. DeLand, G. E. Ballester, K. A. Coplin, P. D. Feldman, and H. W. Moos (1988), Temporal variation of the Jovian H I Lyman alpha emission (1979–1986), *J. Geophys. Res.*, *93*, 29–34.

Slagle, I. R., D. Gutman, J. W. Davies, and M. J. Pilling (1988), Study of the recombination reaction CH_3 + CH_3 → C_2H_6. 1. Experiment, *J. Phys. Chem.*, *92*, 2455–2462.

Smith, G. P. (2003), Rate theory of methyl recombination at the low temperatures and pressures of planetary atmospheres, *Chem. Phys. Lett.*, *376*, 381–388.

Smith, G. P., D. L. Huestis, and D. Nash (2003), Photochemical model sensitivity analysis for Jovian planets, *Bull. Am. Astron. Soc.*, *35*, 999.

Smith, G. R., D. E. Shemansky, J. B. Holberg, A. L. Broadfoot, B. R. Sandel, and J. C. McConnell (1983), Saturn's upper atmosphere from the Voyager 2 EUV solar and stellar occultations, *J. Geophys. Res.*, *88*, 8667–8678.

Smith, N., Y. Bénilan, and P. Bruston (1998), The temperature dependent absorption cross sections of C_4H_2 at mid ultraviolet wavelengths, *Planet. Space Sci.*, *46*, 1215–1220.

Smith, P. L., K. Yoshino, W. H. Parkinson, K. Ito, and G. Stark (1991), High-resolution, VUV (147–201 nm) photoabsorption cross sections for C_2H_2 at 195 and 295 K, *J. Geophys. Res.*, *96*, 17,529–17,533.

Stancu, G. D., J. Röpcke, and P. B. Davies (2005), Line strengths and transition dipole moment of the ν_2 fundamental band of the methyl radical, *J. Chem. Phys.*, *122*, 014306.

Stoliarov, S. I., V. D. Knyazev, and I. R. Slagle (2000), Experimental study of the reaction between vinyl and methyl radicals in the gas phase: Temperature and pressure dependence of overall rate constants and product yields, *J. Phys. Chem. A*, *104*, 9687–9697.

Strobel, D. F. (1969), The photochemistry of methane in the Jovian atmosphere, *J. Atmos. Sci.*, *26*, 906–911.

Strobel, D. F. (1973), The photochemistry of hydrocarbons in the Jovian atmosphere, *J. Atmos. Sci.*, *30*, 489–498.

Strobel, D. F. (1975), Aeronomy of the major planets: Photochemistry of ammonia and hydrocarbons, *Rev. Geophys.*, *13*, 372–382.

Strobel, D. F. (1983), Photochemistry of the reducing atmospheres of Jupiter, Saturn, and Titan, *Int. Rev. Phys. Chem.*, *3*, 145–176.
Strobel, D. F., J. P. Apruzese, and M. R. Schoeberl (1985), Energy balance constraints on gravity wave induced diffusion in the mesosphere and lower thermosphere, *J. Geophys. Res.*, *90*, 13,067–13,072.
Sugawara, K., K. Okazaki, and S. Sato (1981), Temperature dependence of the rate constants of H and D-atom additions to C_2H_4, C_2H_3D, C_2D_4, C_2H_2, and C_2D_2, *Bull. Chem. Soc. Jpn.*, *54*, 2872–2877.
Summers, M. E., and D. F. Strobel (1989), Photochemistry of the atmosphere of Uranus, *Astrophys. J.*, *346*, 495–508.
Suto, M., X. Wang, J. Shan, and L. C. Lee (1992), Quantitative photoabsorption and fluorescence spectroscopy of benzene, naphthalene, and some derivatives at 106–295 nm, *J. Quant. Radiat. Transfer*, *48*, 79–89.
Takahashi, J., T. Momose, and T. Shida (1994), Thermal rate constants for $SiH_4 = SiH_3 + H$ and $CH_4 = CH_3 + H$ by Canonical Variational Transition State Theory, *Bull. Chem. Soc. Jpn.*, *67*, 74–85.
Tomasko, M. G., and L. R. Doose (1984), Polarimetry and photometry of Saturn from Pioneer 11: Observations and constraints on the distribution and properties of cloud and aerosol particles, *Icarus*, *63*, 1–34.
Torr, M. R., D. G. Torr, R. A. Ong, and H. E. Hinteregger (1979), Ionization frequencies for major thermospheric constituents as a function of solar cycle 21, *Geophys. Res. Lett*, *6*, 771–774.
Toublanc, D., J. P. Parisot, J. Brillet, D. Gautier, F. Raulin, and C. P. McKay (1995), Photochemical modeling of Titan's atmosphere, *Icarus*, *113*, 2–26.
Trafton, L. (1985), Long-term changes in Saturn's troposphere, *Icarus*, *63*, 374–405.
Tsai, S.-T., C.-K. Lin, Y. T. Lee, and C.-K. Ni (2000), Dissociation rate of hot benzene, *J. Chem. Phys.*, *113*, 67–70.
Tsai, S.-T., C.-L. Huang, Y. T. Lee, and C.-K. Ni (2001), Ring opening dissociation of d_6-benzene, *J. Chem. Phys.*, *115*, 2449–2455.
Tsang, W. (1991), Chemical kinetic data base for combustion chemistry. Part 5. Propene, *J. Phys. Chem. Ref. Data*, *20*, 221–274.
Tsang, W., and R. F. Hampson (1986), Chemical kinetic data base for combustion chemistry. Part 1. Methane and related compounds, *J. Phys. Chem. Ref. Data*, *15*, 1087–1279.
Vervack, R. J., Jr., B. R. Sandel, G. R. Gladstone, J. C. McConnell, and C. D. Parkinson (1995), Jupiter's He 584 Å dayglow: New results, *Icarus*, *114*, 163–173.
von Zahn, U., D. M. Hunten, and G. Lehmacher (1998), Helium in Jupiter's atmosphere: Results from the Galileo probe Helium Interferometer Experiment, *J. Geophys. Res.*, *103*, 22,815–22,829.
Wagener, R., J. Caldwell, T. Owen, S.-J. Kim, T. Encrenaz, and M. Combes (1985), The Jovian stratosphere in the ultraviolet, *Icarus*, *63*, 222–236.
Wagner, H. G., and R. Zellner (1972), Reaktionen von wasserstoffatoman mit ungesättigten C_3-kohlenwasserstoffen. II. Die reaktion von H-atomen mit methylacetylen, *Ber. Bunsenges. Phys. Chem.*, *76*, 518–525.
Wallace, L., and D. M. Hunten (1973), The Lyman-alpha albedo of Jupiter, *Astrophys. J.*, *182*, 1013–1031.
Walter, D., H.-H. Grotheer, J. W. Davies, M. J. Pilling, and A. F. Wagner (1990), Experimental and theoretical study of the recombination reaction $CH_3 + CH_3 \rightarrow C_2H_6$, *Proc. Combust. Inst.*, *23*, 107–114.
Wang, B., H. Hou, and Y. Gu (2000), Mechanism and rate constant of the reaction of atomic hydrogen with propyne, *J. Chem. Phys.*, *112*, 8458–8465.
Wang, J.-H., K. Liu, Z. Min, H. Su, R. Bersohn, J. Preses, and J. Larese (2000), Vacuum ultraviolet photochemistry of CH_4 and isotopomers. II. Product channel fields and absorption spectra, *J. Chem. Phys.*, *113*, 4146–4152.
Waschull, J., Y. Heiner, B. Sumpf, and H.-D. Kronfeldt (1998), Diode laser spectroscopy in the 9.8-μm ν_{14} band of benzene. II. Self-, air-, and noble-gas broadening coefficients, *J. Mol. Spectrosc.*, *190*, 140–149.
Weissman, M. A., and S. W. Benson (1988), Rate parameters for the reactions of C_2H_3 and C_4H_5 with H_2 and C_2H_2, *J. Phys. Chem.*, *92*, 4080–4084.
West, R. A., D. F. Strobel, and M. G. Tomasko (1986), Clouds, aerosols, and photochemistry in the Jovian atmosphere, *Icarus*, *65*, 161–217.
Westmoreland, P. R., A. M. Dean, J. B. Howard, and J. P. Longwell (1989), Forming benzene in flames by chemically activated isomerization, *J. Phys. Chem.*, *93*, 8171–8180.
Whytock, D. A., W. A. Payne, and L. J. Stief (1976), Rate of the reaction of atomic hydrogen with propyne over and extended pressure and temperature range, *J. Chem. Phys.*, *65*, 191–195.
Wilson, E. H., and S. K. Atreya (2004), Current state of modeling the photochemistry of Titan's mutually dependent atmosphere and ionosphere, *J. Geophys. Res.*, *109*, E06002, doi:10.1029/2003JE002181.
Wilson, E. H., S. K. Atreya, and A. Coustenis (2003), Mechanisms for the formation of benzene in the atmosphere of Titan, *J. Geophys. Res.*, *108*(E2), 5014, doi:10.1029/2002JE001896.
Wong, A.-S., A. Y. T. Lee, Y. L. Yung, and J. M. Ajello (2000), Jupiter: Aerosol chemistry in the polar atmosphere, *Astrophys. J.*, *534*, L215–L217.
Wong, A.-S., Y. L. Yung, and A. J. Friedson (2003), Benzene and haze formation in the polar atmosphere of Jupiter, *Geophys. Res. Lett.*, *30*(8), 1447, doi:10.1029/2002GL016661.
Woods, T. N., W. K. Tobiska, G. J. Rottman, and J. R. Worden (2000), Improved solar Lyman α irradiance modeling from 1947 through 1999 based on UARS observations, *J. Geophys. Res.*, *105*, 27,195–27,215.
Wu, C. H., and R. D. Kern (1987), Shock-tube study of allene pyrolysis, *J. Phys. Chem.*, *91*, 6291–6296.
Wu, C. Y. R., F. Z. Chen, and D. L. Judge (2001), Measurement of temperature-dependent absorption cross sections of C_2H_2 in the VUV-UV region, *J. Geophys. Res.*, *106*, 7629–7636.
Wu, C. Y. R., F. Z. Chen, and D. L. Judge (2004), Temperature-dependent photoabsorption cross sections in the VUV-UV region: Ethylene, *J. Geophys. Res.*, *109*, E07S15, doi:10.1029/2003JE002180.
Yelle, R. V., and S. Miller (2004), Jupiter's thermosphere and ionosphere, in *Jupiter: Planet, Satellites and Magnetosphere*, edited by F. Bagenal, W. McKinnon, and T. Dowling, pp. 185–218, Cambridge Univ. Press, New York.
Yelle, R. V., J. C. McConnell, B. R. Sandel, and A. L. Broadfoot (1987a), The dependence of electroglow on the solar flux, *J. Geophys. Res.*, *92*, 15,110–15,124.
Yelle, R. V., L. R. Doose, M. G. Tomasko, and D. F. Strobel (1987b), Analysis of Raman scattered Ly-alpha emissions from the atmosphere of Uranus, *Geophys. Res. Lett.*, *14*, 483–486.
Yelle, R. V., J. C. McConnell, and D. F. Strobel (1989), The far ultraviolet reflection spectrum of Uranus: Results from the Voyager encounter, *Icarus*, *77*, 439–456.
Yelle, R. V., F. Herbert, B. R. Sandel, R. J. Vervack Jr., and T. M. Wentzel (1993), The distribution of hydrocarbons in Neptune's upper atmosphere, *Icarus*, *104*, 38–59.
Yelle, R. V., L. A. Young, R. J. Vervack Jr., R. Young, L. Pfister, and B. R. Sandel (1996), The structure of Jupiter's upper atmosphere: Predictions for Galileo, *J. Geophys. Res.*, *101*, 2149–2161.
Yelle, R. V., C. A. Griffith, and L. A. Young (2001), Structure of the Jovian stratosphere at the Galileo probe entry site, *Icarus*, *152*, 331–346.
Yokoyama, A., X. Zhao, E. J. Hintsa, R. E. Continetti, and Y. T. Lee (1990), Molecular beam studies of the photodissociation of benzene at 193 and 248 nm, *J. Chem. Phys.*, *92*, 4222–4233.
Young, L. A., R. V. Yelle, R. Young, A. Seiff, and D. B. Kirk (2005), Gravity waves in Jupiter's stratosphere, as measured by the Galileo ASI experiment, *Icarus*, *173*, 185–199.
Yung, Y. L., and W. B. DeMore (1999), *Photochemistry of Planetary Atmospheres*, 456 pp., Oxford Univ. Press, New York.
Yung, Y. L., and D. F. Strobel (1980), Hydrocarbon photochemistry and Lyman alpha albedo of Jupiter, *Astrophys. J.*, *239*, 395–402.
Yung, Y. L., M. Allen, and J. P. Pinto (1984), Photochemistry of the atmosphere of Titan: Comparison between model and observations, *Astrophys. J. Suppl. Ser.*, *55*, 465–506.

B. Bézard, T. Fouchet, and E. Lellouch, LESIA, Observatoire de Paris, 5 place Jules Janssen, F-92195 Meudon Cedex, France. (bruno.bezard@obspm.fr; thierry.fouchet@obspm.fr; emmanuel.lellouch@obspm.fr)

H. Feuchtgruber, Max-Planck-Institut für Extraterrestrische Physik, D-85740 Garching, Germany. (fgb@mpe.mpg.de)

G. R. Gladstone, Space Sciences Department, Southwest Research Institute, 6220 Culebra Road, San Antonio, TX 78228-0510, USA. (randy.gladstone@swri.org)

J. I. Moses, Lunar and Planetary Institute, 3600 Bay Area Boulevard, Houston, TX 77058-1113, USA. (moses@lpi.usra.edu)